DYNAMIC AND WIDEBAND MICROWAVE PHOTONIC SIGNAL PROCESSING

by

JIA GE

(Under the Direction of Mable P. Fok)

ABSTRACT

Radio frequency (RF) signal processing is ubiquitous in various fields, where dynamic and wideband processing capabilities are increasingly desired in modern systems. The inherent limitations of electronics make conventional RF signal processing technique lack of tunability, which cannot fulfill the functionalities required in modern systems. Microwave photonics (MWP) – a hybrid signal processing technique, which takes advantages from the unique properties of photonics, making it possible to remove the bottlenecks of electronic system. Here, we draw inspiration from photonics and bring breakthrough functionalities and great improvements to conventional signal processing technique. Various microwave photonic systems are developed and experimentally demonstrated, with great operating flexibility, wide bandwidth, and fast processing speed. The demonstrated systems include gigahertz-speed tunable MWP filters, highly reconfigurable MWP multiband filters, broadband and reconfigurable RF spectral shaper, and RF equalizer. The wideband operation range and extraordinary system flexibility make them suitable for a variety of applications in RF/microwave signal processing and emerging communication systems.

INDEX WORDS: Microwave photonics, Radio frequency signal processing, Optical signal processing, Radio frequency filter, Finite impulse response filter, Microwave photonic filter, Radio frequency multiband filter, Radio frequency spectrum shaping, Radio frequency equalizer.

DYNAMIC AND WIDEBAND MICROWAVE PHOTONIC SIGNAL PROCESSING

by

JIA GE

B.Eng., Shandong University, China, 2010

M.Eng., Jinan University, China, 2013

A Dissertation Submitted to the Graduate Faculty of The University of Georgia in Partial Fulfillment of the Requirements for the Degree

DOCTOR OF PHILOSOPHY

ATHENS, GEORGIA

2017

DYNAMIC AND WIDEBAND MICROWAVE PHOTONIC SIGNAL PROCESSING

by

JIA GE

Major Professor:	Mable P. Fok
Committee:	Lawrence A. Hornak
	Peter Kner
	Luke J. Mortensen

Electronic Version Approved:

Suzanne Barbour
Dean of the Graduate School
The University of Georgia
December 2017

ACKNOWLEDGEMENTS

Here, I would like to thank a number of people for their help with this work. First and foremost, my major advisor Dr. Mable P. Fok, she leads me to the field and provides huge support along my study, from the well-equipped lab and fun lab culture, to her exquisite experimental skill and great patience. I feel so lucky to have such an amazing researcher, mentor, and friend as my major advisor, who cares both my career and life. Without her help, there is no way I can accomplish so much and become so confident at my graduation.

I'm grateful to have many advisors who also provide great guidance along my study. I would like to thank my committee members -- Dr. Peter Kner, Dr. Lawrence A. Hornak and Dr. Luke J. Mortensen for their time and effort in improving this work. Their knowledge and experience have helped me to keep on track and broadened my scope. I also want to thank Dr. Gee-Kung Chang from Georgia Tech for serving as an external reader of my dissertation, Dr. Lawrence Chen from McGill University and his student Ms. Zifei Wang for their generous help on the system integration, as well as Dr. Jesse Simsarian from Nokia Bell Labs for his guidance during the internship. This work would not have been possible without the effort from everyone above.

Furthermore, I would also like to thank the students working together with me in the lab. Graduate students: Hanlin Feng, Marry Locke, Qi Zhou, Ryan Toole, Li Xu, Ruizhe Lin, Qidi Liu, Mei Yang, and undergraduate students: Alex Matthews, Aneek James, William Nguyen, Phiet Do, Luis Perea, Jay Patel, Matthew Miller, Daniel Garon, Allen Spain, also played an critical role in lab. Their assistance on experiments and companion as friends, are unimaginable important to a smooth pace of this work. In addition, I would like to express my appreciation to the staff in the College of Engineering, in particular Ms. Clodagh Miller and Ms. Margaret J. Sapp, for their assistance along my study.

Last, I would like to express my deepest gratitude to my parents, Ms. Yan Wang and Dr. Peijin Ge. As a Ph.D. candidate in Engineering, I am definitely the outcome from an engineer and a doctor. Their countless and unconditional support over the past 30 years, both financial and emotional, provides me the opportunity to pursue what I really want without worrying about anything. I love you so much and I will spend more time with you.

TABLE OF CONTENTS

LIST OF TABLES

LIST OF FIGURES

Page

CHAPTER 1

INTRODUCTION

Radio frequency (RF) signals refer to the electromagnetic waves with frequencies between 3 kHz to 300 GHz, which are widely used in a number of fields and can be found almost everywhere. Applications of RF signals include wireless and optical communications, radar and satellite systems, sensing, computing, instrumentation and medical treatment. Thus, the generation, processing and transmission of RF signals are of great interest, and numerous related research have been performed for decades. RF signals are usually processed by electronic circuits, which are based on resistors and capacitors (RC circuits) with particular transfer functions. With the rapid development of electronics industry, tons of devices and systems for RF signal processing have been developed and widely applied. In recent years, due to the huge data explosion from new Internet based technologies such as cloud storage and computing, big data, artificial intelligence and virtual reality, there is an ever-increasing demand of high-speed and wide bandwidth data transmission. To fulfill the functionalities, wideband systems and multiband communications over a wider RF range are implemented to increase the available spectral resource. On the other side, adaptive systems are developed to dynamically allocate the spectral resource to improve the spectrum usage efficiently. Although RF electronics offers compact and cost-effective designs, the design of RC circuit usually results in limited operation bandwidth, hinder its application in wideband operations. Furthermore, the inherent nature of electronics makes it lack of tunability, which is extremely desired in modern dynamic systems. Thus, conventional RC circuits gradually meet their bottleneck and their performance in modern RF systems are limited, mainly in terms of the wideband and dynamic operation capabilities.

In recent 20 years, photonic technologies are intensively developed for high-speed data transmission. Different from RF signals, optical signals are at a higher frequencies (in the order of THz) which results in relative wider operation bandwidth compared with RF signals. With the rapid development and mature fabrication process of optical fibers, optical communication has been widely implemented worldwide and the data transmission speed and bandwidth have been dramatically increased. The capability of photonics for signal transmission has been well developed, meanwhile, its huge potential for RF signal processing comes to people's sight. The unique features of photonics, such as low loss, ultra-wide bandwidth, fast transmission and response speed, polarization diversity, special nonlinear effects and immunity to electromagnetic interference, making it a power tool for RF signal processing. Thanks to the fast development of wideband electro-optic (EO) and optic-electro (OE) conversion devices, such as EO modulators and photo diodes which have been widely used in optical communications, RF signals can be easily converted between electrical domain and optical domain. Thus, the processing of the original RF signal can be done by all kinds of photonic techniques in the optical domain and then converted back, which is a hybrid signal processing technique – microwave photonics (MWP). Figure 1.1 shows an illustration of a microwave photonic system [1], instead of directly processing the input RF signal (f_{RF}) in electrical domain (①-④), an EO modulator is used to up-converted the RF signal to the frequency an optical carrier (v), this process is called modulation. Then the modulated signal ($v + f_{RF}$ and $v - f_{RF}$) is processed by a designed transfer function through optical signal processing techniques, and at last converted back to an electrical signal through a photo diode. The extra process (①-②-③-④) allows powerful optical techniques to be used, resulting in unique properties and functions that cannot be achieved with RF electronics.

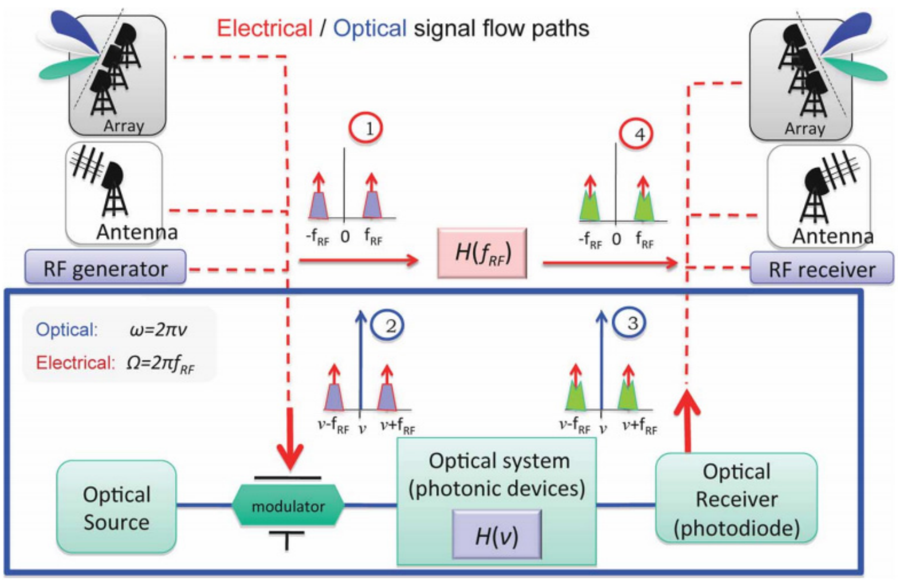

Figure 1.1. Illustration of a microwave photonic signal processing system [1]. Red line: electrical signal, blue line: optical signal.

Some of the MWP systems are designed to carry the equivalent tasks of conventional RF systems but with better performance, and bring unique advantages from photonics to enhance the functionalities that are very complex or even impossible with traditional technologies [1-6]. It opens up new possibilities for overcoming inherent limitations of conventional electronics, in particular on the wideband and dynamic capabilities. During the past decades, a considerable amount of work for MWP signal processing has been carried out [7,8], the implemented functionalities include RF signal generation and filtering, beam-forming, frequency measurement and scanning, arbitrary waveform generation, analog-to-digital conversion, and radio over fiber. Almost all the functions demonstrated by conventional RF electronics can also be achieved through MWP, meanwhile, optical signal processing techniques greatly enables dynamic reconfiguration of the achieved functions. Furthermore, since the modulated RF frequency range is only a very small fraction of the optical frequency, usually MWP signal processing supports an ultra-wide operation bandwidth in term of the RF range. For example, a 100 GHz range is already a huge bandwidth for RF systems, however it only consumes ~2.2% of the C band in optical communication (C band is about 4.4 THz from 1530 nm to 1565 nm). This is a fundamental advantage compared with RF electronics. As the spectral scarcity is becoming the major hurdle of RF systems and wideband operation at higher frequency is inevitable (such as the situation of 5G wireless network), MWP is becoming a promising solution for a number of essential RF processing tasks and functionality.

In this dissertation, we draw inspiration from photonics for achieving high-speed, wideband and dynamic RF signal processing. Since RF filters are the most essential and widely used components in RF systems, and they are the key to implement various signal processing functions, we start our study by developing several MWP filters. In Chapter 2, we develop a MWP notch filter with gigahertz tuning capability. The notch filter can be used as an ultrafast RF switch with only hundreds of picoseconds response time. In Chapter 3, a MWP dual-band bandpass filter also with gigahertz switching speed is developed. The MWP bandpass filter is based on finite impulse response, which is first introduced in the chapter 3. These two high-speed tunable MWP filters are the first demonstrations of tunable RF filter operating at gigahertz level, which are extremely desired in high-speed switching and scanning applications. In Chapter 4, several MWP multiband filters are developed also based on finite impulse response. The maximum passband number of RF multiband filters has been significantly increased to 13, meanwhile, generated passbands are both tunable and reconfigurable. Based on these powerful MWP multiband filters, two potential applications are demonstrated in Chapter 5, which are RF spectral shaper and equalizer. Arbitrary RF spectrum shaping and equalization are successfully achieved. In Chapter 6, we discuss the potential integration of the demonstrated systems, and conclude this dissertation.

CHAPTER 2

HIGH-SPEED TUNABLE MWP BANDSTOP FILTER

2.1 RF Bandstop Filter

RF bandstop filter (or notch filter) is a key component in RF signal processing, it is designed for removing undesired signals at certain frequencies, and passing most other frequencies unaltered. RF bandstop filter is widely used for interference mitigation, and has been successfully demonstrated based on conventional electronic techniques. Generally the RF bandstop filter is constructed by combining a low-pass filter and a high-pass filter in series, with their pass-bands not overlapping. Typically, a desired RF bandstop filter should have a high rejection ratio, narrow rejection bandwidth, wide operation range, flat passband response, and good operation flexibility. The last characteristic becomes increasingly important in modern RF systems where dynamic operation are commonly found, which requires rapid changing of the operating frequency of the notch filter [5]. Unfortunately, it is very difficult to make an electronics based RF notch filter to be tuned over a wide frequency range at high speed, due to the fact that they are basically resistor inductor capacitor circuits.

In recent years, microwave photonics brings great improvements on RF notch filter design, especially on the operating tunability and reconfigurability [7,8]. Various MWP approaches have been reported to demonstrate tunable and reconfigurable MWP notch filters. Examples include the use of stimulated Brillouin scattering in optical fiber to achieve good selectivity and tunable performance [9-11], microring resonators for a high rejection ratio and is potentially integrable

[12-15], and delay line based MWP filters with tunable filter frequency [16-18]. Although the above approaches have successfully achieved tunable MWP notch filters, they either require high operation optical power due to the nonlinearity in fiber involved, or are based on complex tuning mechanisms and have a limited tuning range, or have a significant undesired change in free spectral range during tuning. Fast frequency tuning is essential in a dynamic environment where frequency and bandwidth of the unwanted signal may change over time. However, most tuning mechanisms in exiting approaches are based on thermal [19-21] or mechanical [22,24] tuning, that have slow tuning speeds of around kHz range [23]; or require complex tuning mechanism, i.e., simultaneously adjusting multiple parameters during tuning.

In this chapter, frequency and bandwidth tunable MWP notch filters based on phase modulator incorporated Lyot loop filter (PM-Lyot) and loop mirror filter (PM-LMF) for high-speed tunable optical filtering is proposed and demonstrated. Gigahertz notch frequency tuning speed is experimentally achieved by varying the birefringence of the phase modulator through electro-optics Pockels effect, and the tuning mechanism is also simple that solely rely on the applied voltage to the phase modulator for continuously notch frequency tuning. Moreover, sharper filter profile and bandwidth tuning is also achieved by the unique PM-Lyot filter, the 10-dB bandwidth of the MWP notch filter is experimentally tuned from 0.81 to 1.85 GHz through polarization adjustment. The high-speed tunable MWP notch filter is then tested as a RF/microwave frequency switch, that on/off switch and two-channel switch at gigahertz switching speed are experimentally demonstrated.

As such, the following work is drawn from our paper published on Optics Letters (vol. 40, pp. 48-51, Jan. 2015) by Jia Ge, Hanlin Feng, Guy Scott, and Mable P. Fok, entitled “High-speed tunable microwave photonic notch filter based on phase modulator incorporated Lyot filter”, and paper published on Scientific Reports (vol. 5, p. 17263, Nov. 2015) by Jia Ge and Mable P. Fok, entitled "Ultra high-speed radio frequency switch based on photonics".

2.2 Implementation of the MWP Notch Filter

2.2.1 Single-sideband modulation through SOA-polarizer structure

Experimental setup of the proposed MWP notch filter is shown in Figure 2.1. Input microwave signal is modulated onto an optical carrier through a 10-GHz standard Mach-Zehnder modulator (MZM). The modulated signal is then fed into a SOA at 45 degrees with respect to the orientation layers, which is driven at 350 mA for SSB generation and followed by a polarizer (P1) for further suppressing the lower sideband. The power of the modulated optical signal launching into the SOA is 7 dBm and polarizer P1 is adjusted to obtain the best SSR. The generated SSB signal is then launched into the PM-Lyot filter through an optical circulator (C1) for spectrum filtering. As a result, a portion of optical spectrum is chopped out by the optical PM-Lyot filter, as

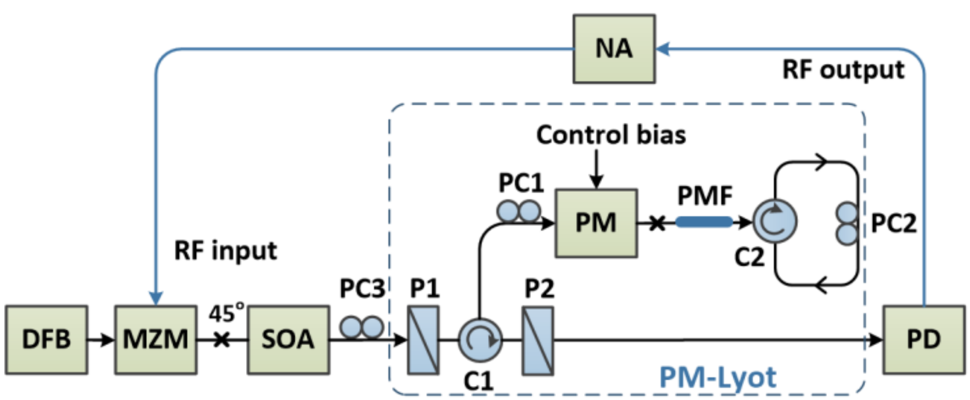

Figure 2.1. Experimental setup of the proposed tunable MWP notch filter. DFB: distributed feedback laser; MZM: Mach-Zehnder modulator; SOA: semiconductor optical amplifier; PC1-PC3: polarization controllers; P1-P2: polarizers; C1-C2: circulators; PM: phase modulator; PMF: polarization maintaining fiber; PD: photo detector; NA: network analyzer.

illustrated in Figure 2.2(a). The filtered optical signal is then converted back to an electrical signal with a photodetector and measured by a network analyzer (Keysight E5071C).

Rejection ratio of MWP notch filter is mainly determined by the peak-to-notch extinction ratio of the optical filter and the sideband suppression ratio (SSR) of the SSB signal. Most existing approaches have good peak-to-notch extinction ratio for the optical filter, thus, the SSR of the SSB signal becomes the limiting factor of achieving high rejection ratio in MWP notch filter. SSB signal is usually generated by a dual-drive Mach-Zehnder modulator (DDMZM) together with a RF phase shifter and 90 degree hybrid coupler [9-11]. The sideband suppression is not uniform over a wide frequency range (e.g. 10 GHz) due to the non-uniform phase shift and frequency response of the phase shifter and hybrid coupler, resulting in an inconsistent and relative low rejection ratio in the MWP notch filter. To improve and maintain the rejection ratio during tuning, a broadband SSB modulation scheme with good and uniform sideband suppression is desired.

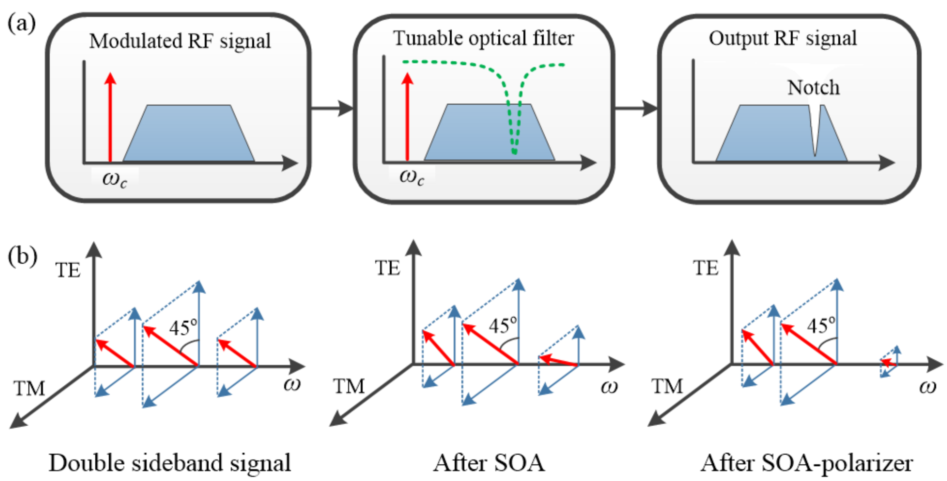

Figure 2.2. Principle of the (a) tunable MWP notch filter and (b) SOA-polarizer based SSB signal generation.

The SOA-polarizer based SSB generation scheme was developed in [20] as illustrated in Figure 2.2(b), which is based on self-phase modulation and self-gain modulation differences between the transverse-electric (TE) and transverse-magnetic (TM) axis in the SOA. By properly adjusting the polarizer angle after the SOA and the input optical power of the SOA, complete suppression of lower sideband can be achieved. Figure 2.3 shows the SOA-polarizer based SSB signal spectra at different modulation frequencies, measured by an optical spectrum analyzer with resolution of 0.8 pm. As shown, the lower sideband is completely suppressed to the noise level, over 40 dB SSR is achieved from 1 to 10 GHz with minimal polarization adjustment. Compared with conventional SSB modulation schemes such as using DDMZM together with a 90 degree RF

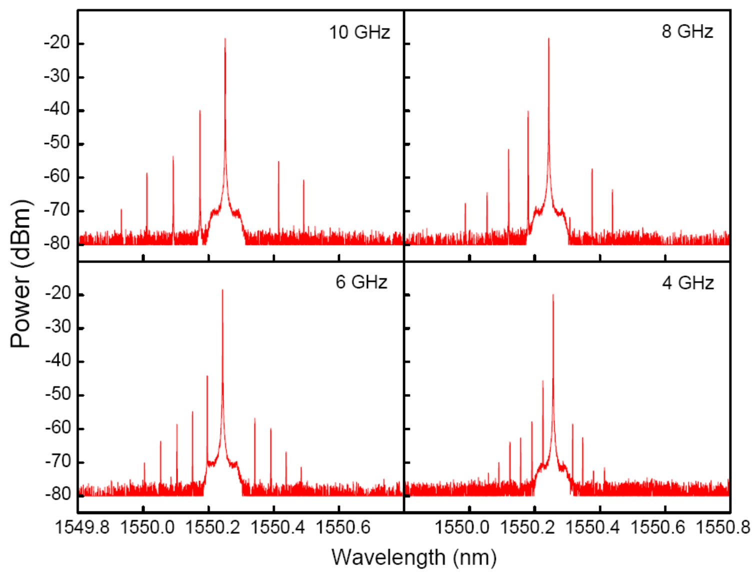

Figure 2.3. Measured SOA-polarizer based SSB modulation spectra at different modulation frequencies.

hybrid coupler [11], sideband suppression is uniform and improved significantly when SOA-polarizer based SSB generation scheme is used.

The use of a SOA-polarizer based structure for SSB generation eliminates the bottleneck of broadband RF hybrid coupler and RF phase shifter, with better sideband suppression and uniform frequency response. Due to the high sideband suppression achieved over a wide range of frequency, the proposed MWP notch filter has an ultrahigh rejection ratio over 60 dB and is well maintained throughout the entire tuning range.

2.2.2 Implementation through the PM-Lyot structure

As shown in Figure 2.2(a), the implementation of the MWP notch filter is based on optical spectral filtering method, where the key component is an optical filter with flexible tunability (the green curve in Figure 2.2(a)). In this section, a PM-Lyot filter is first introduced which works as the spectral filtering device to remove unwanted frequency components from input RF signals. As illustrated inside the dotted box in Figure 2.1, the PM-Lyot consists of a phase modulator (PM), a piece of polarization maintaining fiber (PMF), two polarizers (P1 and P2), and two optical circulators (C1 and C2). The generated SSB signal is launched into the filter and propagates through the PM and PMF twice via the optical circulator loop formed by circulator C2. Polarizer P2 is aligned with the polarizer P1 as a classic Lyot filter [21]. A phase difference is acquired between the two fields propagating along the fast and slow axis of the PM and PMF, which is determined by Eq. (2.1),

$$\Delta\varphi(\lambda) = \frac{2\pi}{\lambda}(B_{PMF} \cdot L_{PMF} + B_{PM} \cdot L_{PM}) \tag{2.1}$$

where B_{PMF}, L_{PMF}, B_{PM} and L_{PM} are the birefringence and length of the PMF and the PM, respectively. The total phase difference depends on whether the TE axis of the PM is aligned with the fast or slow axis of the PMF. In our setup, the TE axis of the PM is set to align with the fast axis of the PMF, resulting in an addition of the total phase difference. Free spectral range of the PM-Lyot filter is determined by Eq. (2.2), which also represents the free spectral range of the MWP notch filter.

$$\Delta\lambda = \frac{\lambda^2}{B_{PMF} \cdot L_{PMF} + B_{PM} \cdot L_{PM}} \tag{2.2}$$

The transfer function of the PM-Lyot filter can be described by the following Jones matrix (Eq. (2.3) - Eq. (2.6)),

$$E_{out} = P_2 R(-\theta_1) F(\Delta\varphi) R(\theta_2) F(\Delta\varphi) R(\theta_1) P_1 \cdot E_{in} \tag{2.3}$$

$$R(\theta) = \begin{bmatrix} \cos\theta & -\sin\theta \\ \sin\theta & \cos\theta \end{bmatrix} \tag{2.4}$$

$$P_{1,2} = \begin{bmatrix} 1 & 0 \\ 0 & 0 \end{bmatrix} \tag{2.5}$$

$$F(\varphi) = \begin{bmatrix} e^{-\frac{i\Delta\varphi}{2}} & 0 \\ 0 & e^{\frac{i\Delta\varphi}{2}} \end{bmatrix} \tag{2.6}$$

where $R(\theta)$, $P_{1,2}$, and $F(\varphi)$ represent the transfer matrix of the polarization controllers, polarizers and birefringence device (PM and PMF), respectively. The polarization rotation angle θ is with respect to the polarizer's transmission angle. The aligned PM-PMF structure works as a birefringence device in which the birefringence can be slightly but rapidly tuned through electro-optic effect. Notch position of the PM-Lyot filter can be continuously tuned by changing the birefringence (B_{PM}) through applying different voltages to the PM [22]. In the experiment, a phase modulator together with a piece of 37.5-m PMF with birefringence of 6.6×10^{-4} are used, and a MWP notch filter with free spectral range of 10 GHz is generated. The tuning speed can be as fast as tens of gigahertz and is governed by the modulation bandwidth of the phase modulator.

The notch sharpness of a MWP notch filter is determined by the profile of the optical filter, i.e. the PM-Lyot filter. In most application, a sharper notch is more desirable due to its better selectivity. Different from classic Lyot filters with a standard interferometric profile [23], by setting the polarization rotation angles of PC1 (θ_1) and PC2 (θ_2) to 30° in Eq. (3), an unique filter profile with sharper notch is achieved, as shown by the red solid curve in Figure 2.4. Compare with standard interferometric optical filters [16-19], the proposed PM-Lyot filter provides a much sharper notch and flatter peak. Figure 2.4 shows the comparison between a standard MZI and the proposed PM-Lyot filter with the same free spectral range of 80 pm. The PM-Lyot filter has a sharper notch profile, flatter transmission peak, and a significant narrower bandwidth of 6.3 pm (10-dB), while that of the MZI is 18.6 pm. Since the optical spectrum and RF spectrum has a direct correspondent, the above characteristics result in a MWP notch filter with a better bandstop selectivity and a flatter bandpass response.

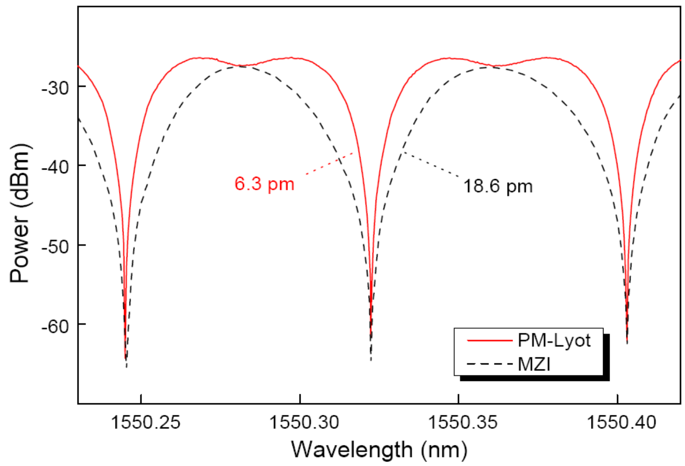

Figure 2.4. Comparison between the proposed PM-Lyot filter and standard interferometric filter (e.g. MZI).

Transmission spectrum of the PM-Lyot filter is tunable by applying different voltages to the PM for changing the waveguide birefringence. Figure 2.5(a) shows the measured transmission spectra of the PM-Lyot filter at different applied voltages, both the spectral shape and the peak-to-notch extinction ratio are maintained throughout the whole tuning range. Free spectral range of the PM-Lyot filter is 80 pm, corresponding to a MWP notch filter with free spectral range of 10 GHz. The free spectral range is determined by the length of the PMF, as in Eq. (2), which can be adjusted to meet specific application requirement (e.g. several MHz with longer PMF). Correspondingly, the measured RF frequency spectra of the MWP notch filter at different applied voltages are shown in Figure 2.5(b). Frequency response is measured by a RF network analyzer with an intermediate frequency bandwidth of 5 kHz. As shown, the MWP notch position is continuously tunable over the 10 GHz range with a filter rejection ratio of over 60 dB. Both the filter shape and rejection ratio are uniform, with a 10-dB bandwidth of 0.8 GHz. The 60 dB rejection ratio and sharp filter profile offer good bandstop selectivity, while a flat transmission response with power difference of <2 dB is also observed. The fast electro-optic based tuning capability not only enables fast notch frequency tuning, it also allows fast compensation of any wavelength drifting in the Lyot filter or the laser source.

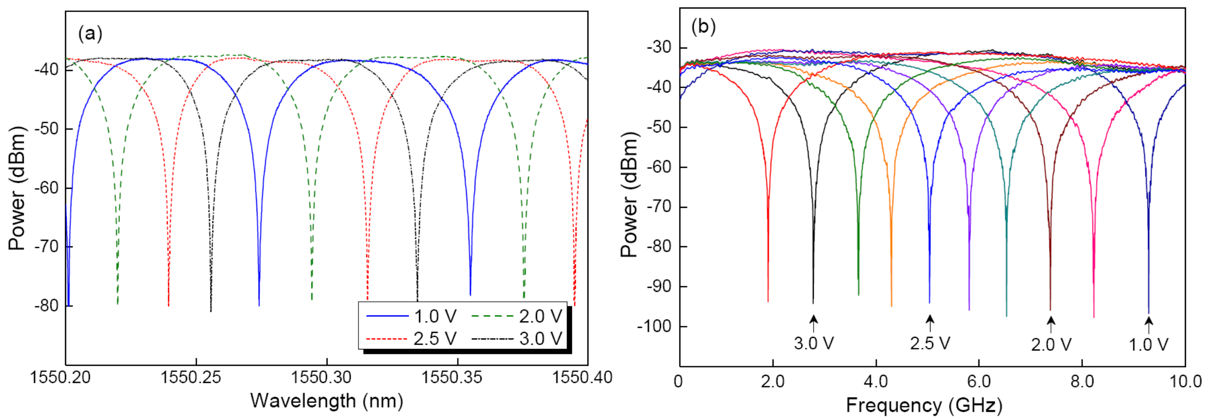

Figure 2.5. (a) Measured transmission spectra of the PM-Lyot filter at different applied voltages. (b) Measured frequency tuning spectra of the MWP notch filter.

Figure 2.6 shows the notch position of the MWP filter (black square curve) and the amount of notch frequency shift (red circle curve) in response to different tuning voltages, respectively. Frequency tuning range of 8 GHz is obtained with the applied voltage being tuned from 1.0 to 3.3 V, resulting in an average tuning efficiency of 3.48 GHz/V. The notch shift is not obvious under 1.0 V because the birefringence change in PM is not significant at relatively low applied voltage. The notch can be continuously tuned over two free spectral ranges. In principle, frequency tuning range is limited by how much the birefringence can be changed in the PM. A 0.24 nm wavelength shift in optical domain is experimentally achieved with a driving voltage of 6.0 V, corresponding to a frequency tuning of 30 GHz in RF domain.

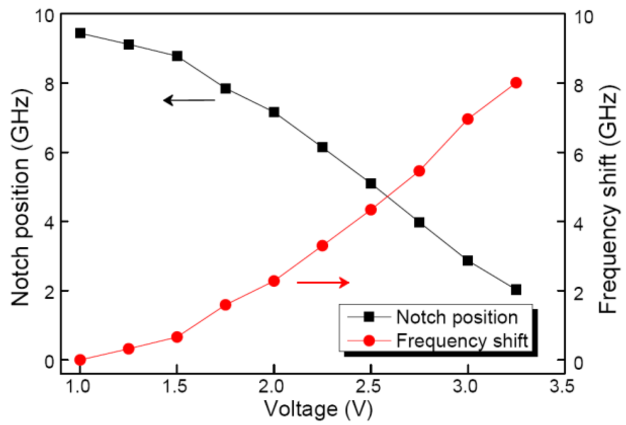

Figure 2.6. Notch position and frequency shift of the MWP filter in response to different tuning voltages.

Besides high-speed notch frequency tuning, the bandwidth of the proposed MWP notch filter is also tunable. Through polarization adjustment at PC1 inside the PM-Lyot filter, filter profile can be adjusted between the unique narrow profile and standard interferometric profile. Figures 2.7(a) and 2.7(b) show the measured bandwidth tuning spectra of the PM-Lyot filter in optical domain and that of the MWP notch filter in RF domain, respectively. The 10-dB optical bandwidth is tuned from 6.3 pm to 16.4 pm with stable peak-to-notch extinction ratio during tuning. Figure 2.7(b) shows the RF transmission spectra of the MWP notch filter with tunable bandwidth (10-dB) from 0.81 GHz to 1.85 GHz. A rejection ratio of 60 dB is observed during the entire tuning process.

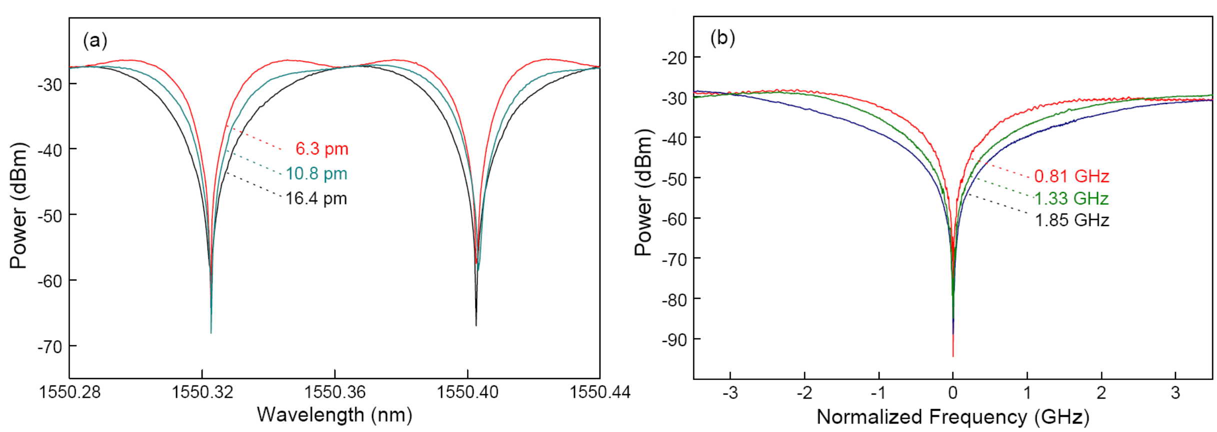

Figure 2.7. (a) Measured bandwidth tuning optical spectra of the PM-Lyot filter. (b) Corresponding bandwidth tuning RF spectra of the MWP notch filter.

2.2.3 Implementation through the PM-LMF structure

The PM-Lyot structure demonstrated in the previous section shows its unique second-order optical spectrum and correspondingly, resulting in narrower 3-dB bandwidth of the MWP notch filter and bandwidth tuning capability. However, the use of a Lyot loop structure requires polarization adjustment and a relative complex system, which is not favored in many applications. In this section, we proposed a different scheme based on phase modulator incorporated loop mirror filter (PM-LMF), which has simpler system setup and more stable performance. The PM-LMF structure also has gigahertz speed tunability, however, the cost is the bandwidth of the MWP notch filter is no longer tunable. The choice of using PM-Lyot or PM-LMF structure depends on whether the application requires bandwidth tuning capability, or favors a more simpler and stable performance.

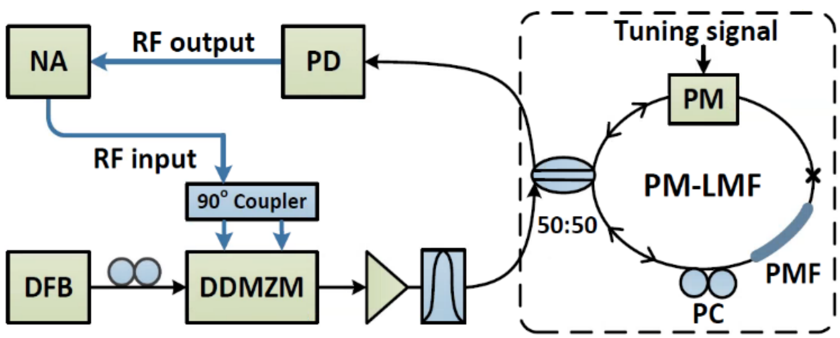

Figure 2.8. Experimental setup of the PM-LMF based MWP notch filter. DFB: distributed feedback laser; DDMZM: dual drive Mach-Zehnder modulator; PM: phase modulator; PMF: polarization maintaining fiber; PC: polarization controller; PD: photo detector; NA: network analyzer.

Just like the operating principle of the PM-Lyot structure shown in Figure 2.2(a), the system is also based on single sideband modulation and optical spectral filtering. Here, the spectrum filtering device becomes the proposed PM-LMF to remove unwanted frequency components from the RF signal, which has shown its fast and wide tunability in various applications previously [22,23]. As illustrated in the dotted box in Figure 2.8(a), the PM-LMF consists of a coupler, a piece of PMF, a PM and a PC. The transmission function is described by the following Eq. (2.5),

$$T(\lambda) = \frac{1}{2}\left[1 - cos\big(\varphi(\lambda)\big)\right] \tag{2.5}$$

where $\varphi(\lambda)$ depicts the phase difference between the two counter-propagating beams of the LMF. The total phase difference is an addition of the PM and PMF when the transverse-electric (TE) axis of the PM is aligned with the fast axis of the PMF, which is determined by Eq. (2.6),

$$\varphi(\lambda) = \frac{2\pi}{\lambda}\,(B_{PMF} \cdot L_{PMF} + B_{PM} \cdot L_{PM}) \tag{2.6}$$

where B_{PMF}, L_{PMF}, B_{PM} and L_{PM} are the birefringence and length of the polarization maintaining fiber and phase modulator, respectively. The transmission function is determined by the birefringence and length of the PMF and the PM. Only B_{PM} is tuned during the operation by applying different DC or AC voltages to the PM based on electro-optics Pockels effect. Since electro-optics Pockels effect has a fast response time, tens of gigahertz tuning speed of the PM-LMF can be achieved and is mainly governed by the modulation bandwidth of the phase modulator.

The free spectral range of the PM-LMF is determined by Eq. (2.7), which also represents the FSR of the tunable MWP notch filter. In the experimental setup, the same 10-GHz phase modulator is used as the tuning device, and a MWP notch filter with FSR of 10 GHz is achieved. The FSR can be adjusted to meet specific application requirement by changing the length of the PMF, i.e. a longer piece of PMF results in a MWP filter with smaller FSR.

$$\Delta\lambda = \frac{\lambda^2}{B_{PMF} \cdot L_{PMF} + B_{PM} \cdot L_{PM}} \tag{2.7}$$

The transmission spectra of the PM-LMF at different tuning voltages are shown in Figure 2.9. An optical comb filter with a FSR of 80 pm is observed. The peak-to-notch extinction ratios are over 35 dB, with both the spectral shape and extinction ratio remain unchanged during the entire tuning process. The PM-LMF is continuously tuned by applying different DC voltages to the PM, wavelength tuning over one FSR is observed at an applied voltage of 3.5 V and up to three FSR frequency tuning range is recorded at an applied voltage of 5.5 V. The change in comb spacing as a consequence of frequency tuning effect is less than 2 pm, thus, its influence to MWP notch filter can be neglected. Figure 2.10(a) shows the frequency tuning spectra of the MWP notch filter at different voltages. The RF filter notch position is continuously tuned from 1.5 to 10 GHz with a 10-dB bandwidth of 1.7 GHz. The notch rejection ratios are over 50 dB, which provide good filter selectivity. Stable filter profiles and uniform notch rejection ratios are observed throughout the entire tuning range. The amount of notch frequency tuning in response to different tuning voltages is shown in Figure 2.10(b), notch frequency is tuned by 8 GHz with a tuning voltage of 3.3 V. The notch frequency tuning is not obvious when applied voltage is under 1.0 V due to the insignificant change of birefringence in the PM. The total tuning range is determined by how much the birefringence can be changed in the PM, up to three FSR total frequency tuning can be experimentally achieved.

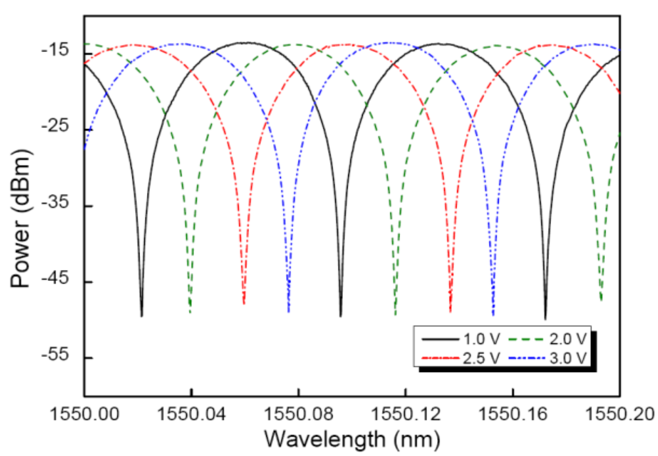

Figure 2.9. Measured optical spectra of the PM-LMF under different tuning voltages.

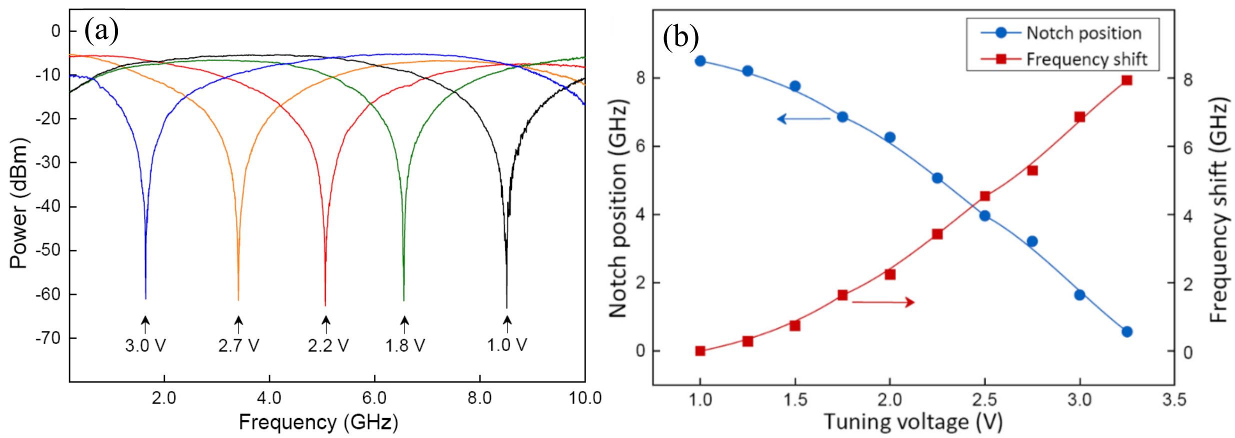

Figure 2.10. (a) Measured frequency tuning spectra of the MWP notch filter. (b) Notch frequency shift in response to different tuning voltages.

2.3 Gigahertz Speed Tuning Through Pockels Effect

The most significant improvement of the proposed MWP notch filter is the gigahertz tuning speed of the notch position, which is achieved by applying different control voltages to the phase modulator inside the PM-Lyot or PM-LMF structure through Pockels Effect. The phase modulator used in the system is made of $LiNbO_3$, which is a commonly used material to build high-speed electro-optic modulators. Up to 40 GHz modulators are already commercially available, meaning the response time of the modulator is shorter than 25 ps. This ultrafast electro-optic devices has been widely used in high-speed optical communication applications, but its potential in high-speed RF signal processing is not fully developed. The proposed MWP notch filter takes advantage from this ultrafast electro-optic device and up to gigahertz tuning of the MWP notch filter is experimentally demonstrated.

According to Pockels effect, the refractive index of the $LiNbO_3$ waveguide is changed linearly with the applied electric field [24]. With a "z-cut" phase modulator, the refractive index change in the transverse-magnetic (TM) mode is larger than that in the TE mode. Although the change in birefringence (B_{PM}) is small, the birefringence tuning speed is in the order of GHz due to the fast electro-optics Pockels effect [23]. With different value of B_{PM}, the phase difference $\varphi(\lambda)$ of the two interfering branches, the comb spacing $\Delta\lambda$, and the transmission function $T(\lambda)$ are changed, depending on the applied electric signal to the phase modulator. According to Eq. (2.2) and Eq. (2.7) in previous sections, the change in birefringence in phase modulator results in a change in comb spacing in the PM-Lyot and PM-LMF. Since the change in comb spacing is extremely small, i.e. <2 pm, a wavelength shift in the comb position is observed instead when focusing at certain wavelength range (e.g., C-band) due to the sinusoidal nature of the transmission spectrum. As a result, an electro-optic wavelength tunable comb filter is achieved.

In the experiment, a 10 GHz phase modulator (EOSPACE PM-0K5-10) is used as the tuning device, which consists of a 71-mm $LiNbO_3$ crystal with birefringence of 7.4×10^{-3} and ~1-m of PMF pigtails with birefringence of 3.0×10^{-4}. The response time is shorter than 100 ps since the modulator is designed for 10 GHz phase modulation. The optical spectra of the corresponding PM-Lyot or PM-LMF shift as fast as the rate of change of the applied electrical voltage and tuning speed is limited by the modulation bandwidth of the modulator. Since the phase modulator is a high-speed device, tuning speed of the PM-LMF can be as fast as several tens of GHz, enabling high-speed tuning and switching applications.

To investigate the center frequency tuning speed of the MWP notch filter, a 9 GHz sinusoidal signal is launched into the DDMZM as the input signal, as shown in Figure 2.11(a). The notch filter is first aligned at 9 GHz when no tuning signal is applied, i.e. the 9 GHz signal is blocked by the MWP notch filter. 1 GHz and 4.5 GHz sinusoidal signals are used in turn to tune the MWP notch filter, corresponding output signals are measured by a 30-GHz oscilloscope. The peak voltages of the tuning signals are set to 2.5 V (i.e. the tuning signal is changing from 0 to 2.5

V in a sinusoidal manner). When the tuning signal is between 0-1 V, the notch shift is insignificant (MWP notch filter is blocking the 9 GHz input signal), resulting in the zero level in Figure 2.11(b). As the voltage of the tuning signal increases from 1.0 V to 2.5 V, frequency shift in the notch frequency is observed such that the notch is tuned far away from the 9 GHz signal when the voltage reaches 2.5 V, allowing the 9 GHz input signal to completely pass through. As a result, the 9 GHz input signal starts to show up in Figure 2.11(b) and reaches its peak value when the tuning signal is at 2.5 V, indicated by the sinusoidal envelope of the output signal. If a square wave is used as the tuning signal, the 9 GHz input signal will be turned on and off. Similar phenomenon is observed when a 4.5 GHz sinusoidal signal is used for tuning, such that every other cycle of the input signal is passed through the MWP notch filter, as shown in Figure 2.11(c). The measurement results prove that the proposed MWP notch filter is able to work at GHz tuning speed with stable performance. The above frequencies are chosen due to the synchronization requirement of the

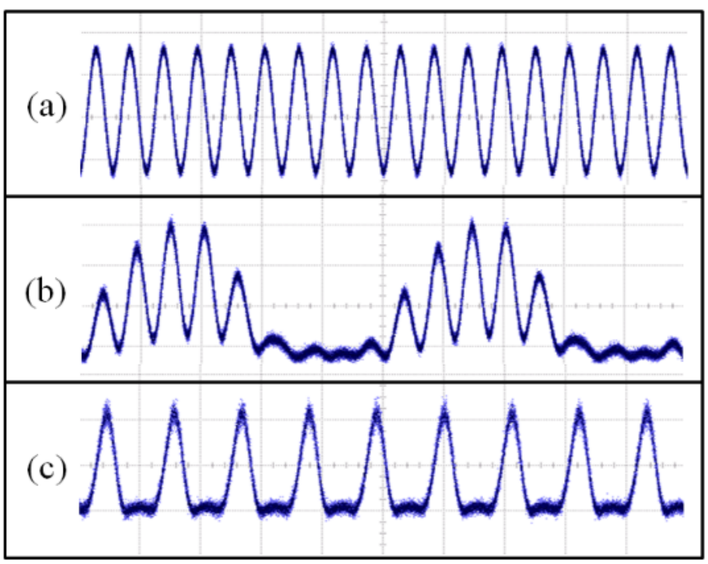

Figure 2.11. Tuning speed measurement of the MWP notch filter. (a) 9 GHz sinusoidal input signal without tuning. (b) Tune at 1 GHz with a sinusoidal signal. (c) Tune at 4.5 GHz with a sinusoidal signal. Scale: 200 ps/div.

equipment used for the experiment. In principle, any frequency within the modulation bandwidth of the PM can be used for filter tuning.

2.4 Application - Ultrafast RF Switch

A RF switch, also called a microwave switch, is a device to route high frequency signals between different transmission channels or devices, which is an essential component in a wide range of applications including wireless communications, radar systems, satellite communications, and microwave test systems. Switching speed is a key parameter to define a RF switch, which is the time needed to change the state of a switch from ON to OFF or from OFF to ON. In conventional RF switches, the switching speed is limited to microsecond range for both electromechanical switches and micro-electromechanical systems (MEMS) switches and nanosecond range for solid-state switches [25-28]. The speed is either limited by the physical properties of the materials and switching mechanisms of the electrical devices or the limited tuning capability of the resistor-capacitor (RC) circuits that is being utilized in the switch.

With the demonstrated high-speed tunability, the proposed MWP notch filter can be used for fast switching between different frequency channels – working as an ultrafast RF switch. The MWP notch filter is set to rapidly switch out different inputs by blocking an unwanted signal frequency and passing the desired signal frequency. The experimental setup for testing the MWP RF switch is shown in Figure 2.12(a), and corresponding operating principle is illustrated in Figure 2.12(b). An input RF signal with frequencies at f_1 and f_2 is launched to the RF input of the MWP RF switch, while a square wave with two voltage levels (V_1 and V_2) is used as the control signal for switching out one of the input RF signal at a time. The voltage levels ($V_{control}$) are set such that the MWP notch filter is aligned with frequency f_1 when $V_{control} = V_1$, resulting in the blocking of signal f_1 and allowing f_2 to pass through; while the MWP notch filter is aligned with f_2 when $V_{control} = V_2$, resulting in the blocking of signal f_2 and allowing f_1 to pass through. When the control signal is switching between V_1 and V_2, the output is also switching between f_2 and f_1. The MWP RF switch can also serve as an ON/OFF switch when only one input RF signal is provided, such that the input RF signal is blocked when the notch position is located at the signal frequency, while it passes through the switch when the MWP notch filter is tuned away from the signal frequency by the control signal.

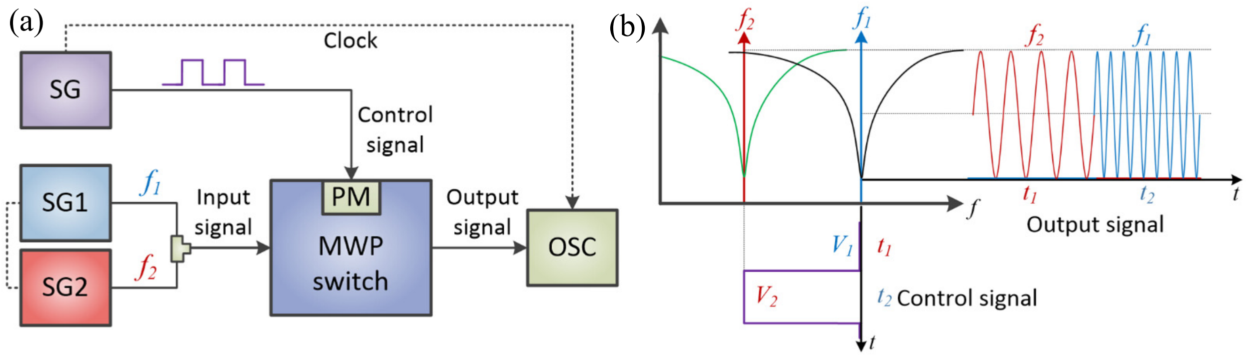

Figure 2.12. Schematic illustration of the proposed ultrafast RF switch. (a) Experimental test setup of the RF switch. SG: signal generator; PM: phase modulator; OSC: oscilloscope. (b) Operating principle of the RF switch based on a high-speed tunable MWP notch filter.

Figure 2.13 shows the ON/OFF switching performance of the proposed MWP RF switch, measured by a 30 GHz oscilloscope. A 0.5 GHz square wave is used as the control signal and a 9 GHz sinusoidal signal is launched into the DDMZM as the input RF signal, as shown in Figure. 2.13(a) and 2.13(b), respectively. The MWP notch filter is first aligned at 9 GHz when no control signal is applied, i.e., the 9 GHz sinusoidal signal is blocked by the notch filter. The peak voltage of the control signal is set to 2.5 V such that the filter notch is tuned away from 9 GHz during the high voltage period of the square wave, allowing the input RF signal to completely pass through the RF switch. As a result of applying a 0.5 GHz square control signal to the RF switch, the input

9 GHz RF signal is switched ON and OFF periodically with an ON-state and OFF-state duration of 1000 ps, as shown in Figure. 2.13(c). A closer look of the switching performance is shown in Figure 2.13(d). As shown, the input 9 GHz signal is completely blocked during the OFF state and is recovered and well maintained during the ON state. The switch has an ON-OFF transition time of ~140 ps and an OFF-ON transition time of ~190 ps, as shown by the dotted lines in Figure 2.13(d). Since the switching time is measured by taking the temporal separation of the closest signal peak of a fully recovered sinusoidal signal and an OFF state of the switch, thus, the real response time should be shorter than the measured value due to the "sampling" effect of the sinusoidal RF signal. Furthermore, the control signal itself has a rise and fall time of ~100 ps, which proposes a limitation in measuring the actual switching speed of the RF switch. Therefore, a shorter switching time could be obtained if a control signal with shorter rise/fall time is used. The power fluctuation during the ON/OFF transition period is caused by the significant high frequency ripples around the rising and falling edges of the control signal, while the weak residual input signal found during off state is due to misalignment between the filter notch and the input signal resulted from the non-flat low-level region in the control signal, as shown in Figure 2.13(a). Thus, a better square control signal with stable rising/falling edges and flat low-level region can be used to get better switching performance and suppression of the unwanted frequency.

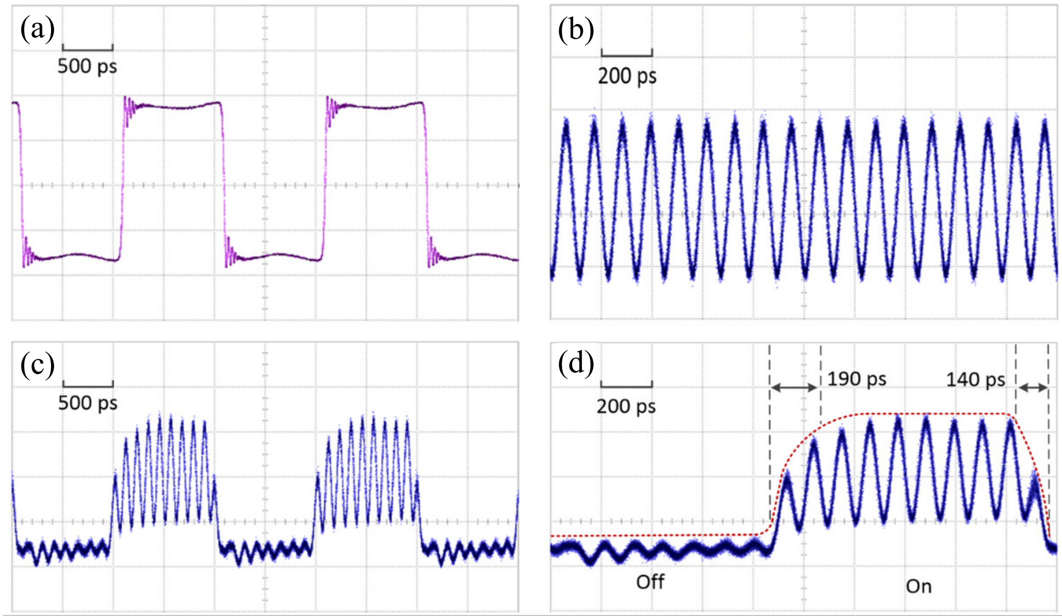

Figure 2.13. Measured on/off switching performance of the proposed MWP switch. (a) 0.5 GHz square tuning signal. (b) 9 GHz sinusoidal input signal without tuning. (c) 9 GHz input signal is switched by the 0.5 GHz square tuning signal. (d) Close-up of the on/off output signal.

To demonstrate the capability to switch between two frequency channels, a set of 6 GHz and 12 GHz sinusoidal signals are used as the two input signals. Power of the 12 GHz signal is intentionally set to be weaker to enable an easy identification of the switching process. The switching performance is shown in Figure 2.14. The two frequency signals are combined with a power combiner and launched into the MWP RF switch through the input port. The same 0.5 GHz square wave as shown in Figure 2.13(a) is used as the control signal. The voltage levels of the square wave are set to 0 V and 2.8 V such that the MWP notch filter is blocking the 6 GHz signal at low voltage level and allowing the 12 GHz signal to pass through; while it is blocking the 12 GHz signal at high level and allowing the 6 GHz signal to pass through. At the output of the MWP RF switch, a RF signal that is switching between the two input RF signals (6 GHz and 12 GHz) is obtained as shown in Figure. 2.14(a). As shown in the closer look in Figure. 2.14(b), the output signal is a periodical signal switching between the 6 GHz and 12 GHz input RF signals. Similar to the on/off switch performance, the switching times between different channels are ~170 ps (switching from 12 GHz to 6 GHz) and ~80 ps (switching from 6 GHz to 12 GHz). The above frequencies are chosen due to the synchronization requirement of the equipment used for the measurement. In principle, any frequency within the modulation bandwidth of the DDMZM can be used as the input signals, resulting in broadband operation. The presented results prove that the proposed MWP RF switch has a gigahertz switching speed, which is governed by the bandwidth of the phase modulator. The tens of picoseconds switching speed demonstrated above is based on a 10 GHz phase modulator, and can be potentially increased with the use of a larger bandwidth modulator.

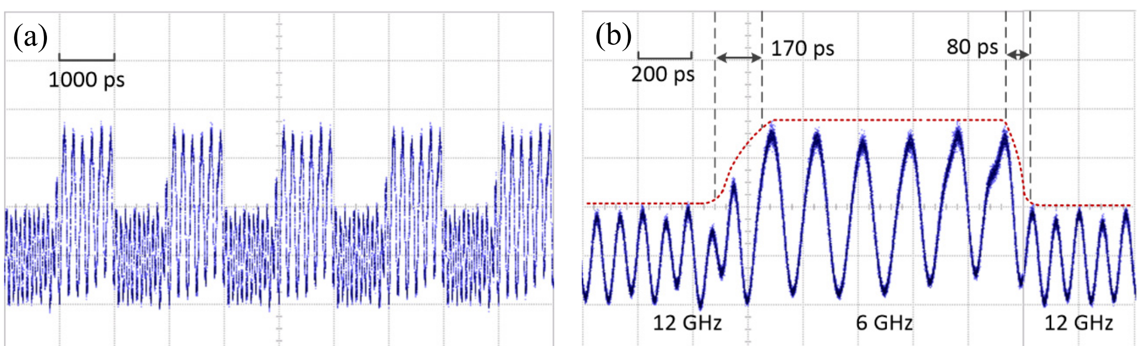

Figure 2.14. Measured two-channel switching performance of the proposed RF switch. (a) Switching between 6 GHz and 12 GHz signals, tuned by a 0.5 GHz square tuning signal. (b) Close-up of the two-channel output signal.

Figure 2.15 shows the dynamic range measurement of the RF switch. The system has a spurious free dynamic range (SFDR) of 96 dBm*Hz$^{2/3}$, and the input third-order intercept point (IIP3) is at 25 dBm. A good linear response is observed between the input and output power, with a 1-dB compression point at 5 dBm, which is mainly governed by the RF amplifier used before the DDMZM. Insertion loss of the system is 6 dB during ON state. Figure 2.15(b) shows the measured frequency spectra at the switch output. The 9 GHz input signal found at the switch output is -12 dBm during ON state and is -70 dBm during OFF state, resulting in a switch isolation of 58 dB.

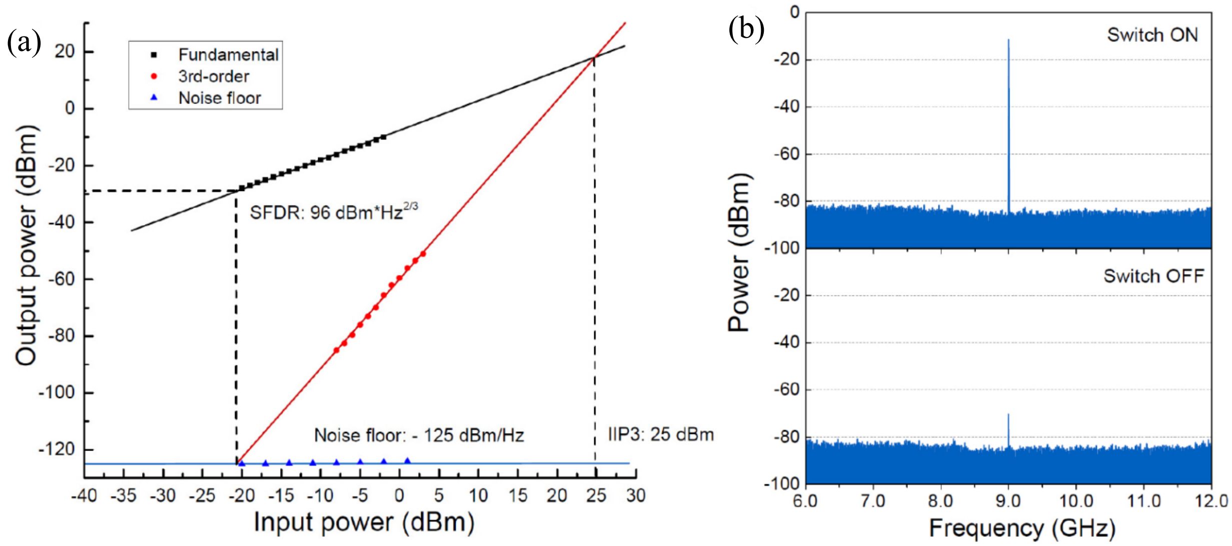

Figure 2.15. Performance metrics measurement of the ultrafast RF switch. (a) Dynamic range measurement of the system, with a SFDR of 96 dBm*Hz$^{2/3}$ and IIP3 at 25 dBm. (b) Measured isolation between ON and OFF states, with an isolation of 58 dB.

2.5 Summary

In summary, in this chapter we developed and experimentally demonstrated MWP notch filters with gigahertz frequency tuning speed. Both the PM-Lyot and PM-LMF based structures are continuously tunable over 10 GHz by adjusting, with stable filter shapes and over 60 dB rejection ratio over the entire tuning range. The center frequency of the proposed MWP notch filters are able to be tuned at gigahertz speed, which is achieved by the ultra-fast electro-optics Pockels effect in a phase modulator. The proposed MWP notch filter is tested as an ultrafast RF switch with fast switching speed and ultra-short ON/OFF transition time. Both the ON/OFF switch and the two-channel switch have been experimentally demonstrated and shown switching times of tens of picosecond with stable and repeatable switching performance. This design significantly improves the tuning speed of the MWP notch filter and has practical value for dynamic systems and high-speed signal processing applications.

CHAPTER 3

HIGH-SPEED SWITCHABLE MWP DUAL-BAND BANDPASS FILTER

3.1 RF Bandpass Filter

In the previous section, high-speed tunable MWP bandstop filters are developed. Although gigahertz tunability is demonstrated and the filter is successfully used as an ultrafast RF switch, the inherent limitation of the bandstop response hinders its application. The reason is a RF bandstop filter can only block one of input signal at a time, the demonstrated RF switch is only suitable for special scenarios when there is only one or two input signals. An ideal device which only selects one particular signal at a time is more desired in common applications – a bandpass filter. In this chapter, we will focus on the photonic implementation of MWP bandpass filters and bring high-speed tuning capability to bandpass filter design.

RF bandpass filters are essential components for selecting desired frequency signals and removing unwanted interference signals, they only allow signals which lie within the specified frequencies to pass through. An ideal RF bandpass filter should perform good frequency selectivity – high main-to-sidelobe suppression ratio (MSSR), sharp passband profile, high out-of-band rejection ratio, and high Q factor (quality factor). In the past several decades, various types of RF bandpass filter have been demonstrated through different electronic techniques, including microstrip [29,30], low-temperature cofired ceramic (LTCC) [31], and stepped impedance resonator [32]. These techniques are already very mature and related products can be found in various of RF systems. Although conventional RF electronics approaches offer on-chip, compact and low-cost design, the performance and functionality of conventional RF bandpass filters already meet the bottleneck, in particular on the operating flexibility, wideband and multiband capability. In recent years, researchers have been actively trying to add tunability on RF bandpass filter design which is extremely desired in modern dynamic systems. The center frequency of the RF bandpass filter is required to be changed over a wide range of frequency to meet the requirement of dynamic systems. Possible electronics based solutions include adding adjustable trimmer capacitor or varactor to microstrip [29,30], using defected ground structure on microstrip [33] and RF MEMS [34]. These approaches allow slight adjustment of the RC value of the circuit design, which in turn change the center frequency of the generated RF filter. However, the resulted tunability is very limited in terms of the tuning range (i.e., only several MHz to at most a few GHz) and tuning speed (i.e., kHz to MHz range) [30], at the same time undesired changes on other characteristics of the RF filter are observed during the tuning process.

Microwave photonics techniques have received great attention and brought a number of significant performance enhancements to RF devices and systems, especially on the operating flexibility. Various studies for designing MWP bandpass RF filters with tunable passbands have been intensively reported in recently years, mainly including multi-tap delay line based schemes [35,36], optical comb based schemes [37-41], and stimulated Brillouin scattering (SBS) based schemes [42-44]. The first two categories are based on finite impulse response filter, which is the most commonly used method to implement a RF bandpass filter, and the center frequency of the passbands can be continuously tuned through an optical tunable delay line [37]. While the SBS based approaches are implemented through nonlinear optics effect, which usually result in extremely narrow bandwidth of the RF filter. The center frequency of generated passbands can be adjusted by controlling the wavelength of the pump laser, which could support a wide tuning range of the RF filter. Although photonics brings exceptional operation flexibility to RF filter design, most of the existing tuning mechanisms are based on thermal tuning or mechanical tuning [41,44], e.g., adjusting polarization controllers, optical delay lines, heaters or laser wavelengths, which can only support slow tuning speed of kilohertz range, limiting their application in high-speed dynamic microwave systems.

In this chapter, we developed an optically controlled reconfigurable MWP dual-band filter with gigahertz tuning speed. The filter is based on finite impulse response, which is a widely used method to generate RF bandpass filters and introduced in this chapter. A Lyot loop filter is used to slice the broadband light source, and generate an optical comb with four different frequency spacing combinations. Correspondingly, four different operation states in the MWP bandpass filter is obtained, i.e., all-block state, dual-band state and single-band state with two different frequencies. The switching between four different operation states is achieved by the ultrafast nonlinear polarization rotation effect (NPR) in an SOA, gigahertz reconfiguration speed between different states is experimentally demonstrated through the control of the optical pump power. To the best of our knowledge, this is the first demonstration of an optically controlled RF filter with such high-speed reconfigurable capability. Furthermore, good passband quality and good filter selectivity are achieved, which are indicated by the 40 dB sidelobe suppression, as well as the clean and sharp filter profiles.

As such, the following work is drawn from our paper published on IEEE Transactions on Microwave Theory and Techniques (vol. 65, pp. 253-259, Jan. 2017) by Jia Ge and Mable P. Fok, entitled “Optically controlled fast reconfigurable microwave photonic dual-band filter based on nonlinear polarization rotation”.

3.2 Finite Impulse Response Filter

The most widely applied approach for implementing RF bandpass filter is based on discrete-time signal processing, where a number of weighted and delayed replicas of the original RF signal are processed and then combined upon detection. In particular, finite impulse response (FIR) filters combine a finite set of samples (or taps) of the input signal, which are usually implemented through arrayed lasers and delay lines. While if the number of the replicas of the RF signal is infinite, an infinite impulse response (IIR) filter can be obtained. IIR filters are usually implemented through recirculating devices or systems, such as ring resonators or loop structure. In general, FIR filters are much easier to be implemented than IIR filter, and usually have more stable performance, while IIR filters usually perform better Q factor since there is an infinite number of filter taps. It is worth mentioning that FIR and IIR filter can be implemented by both electronic and optical techniques, meaning that the generation of replicas of the original signal can either in RF domain or optical domain. This make it possible to build RF filters using optical signal processing techniques – MWP filter.

For an FIR based MWP filter, the frequency response can be expressed as the addition of a series of weighted and delayed replicas of the RF input signal, as illustrated in Eq. (3.1),

$$H(\Omega) \propto \sum_{n=1}^{N} P_n \cdot e^{-j\Omega nT} \tag{3.1}$$

where Ω is the microwave frequency, N is the total tap number, P_n is the power of the *nth* tap, and T is the differential time delay between each adjacent tap. The tap number N governs the order of the filter response, for the design of a bandpass filter, a large tap number is desired to get a high MSSR and a high passband quality factor (Q factor). In the experiment, usually tens or up to a hundred total tap number is desired for a good bandpass filter performance. The center frequency of the generated passband is governed by the time delay T between each tap. As can be seen in Eq.

(3.1), the overall response is periodic in frequency domain, the period, known as the free spectral range, is given by

$$FSR = 1/T \tag{3.2}$$

In order to build a MWP filter with tunable passband, the FSR of the frequency response needs to be changed, meaning that flexibly control of time delay *T* in the setup is required. The values of P_n govern the overall amplitude profile of the multiple taps, which in turn determines the profile of the generated passband in RF domain. An inverse Fourier transform can be performed to precisely tailor the amplitude and phase of each filter tap for generating desired passband profiles, which could be done in an optical wave shaper [45]. Gaussian, flat-top and chirped passband profiles have been demonstrated for different applications [46]. These parameters in Eq. (3.1) provide flexibility on FIR filter designs, for both electronics based on photonics based approaches.

Photonic implementation of FIR filters (MWP FIR filter) is first implemented by a classic delay line array based scheme, as illustrated by the top part of Figure 3.1. A continuous-wave (CW) laser is used as the optical carrier, and the input RF signal is modulated onto the CW laser through an electro-optic modulator. Then the modulated signal is divided into *N* parallel branches through a 1 by N divider, working as the *N* taps of the FIR filter. Each of the replica of the input RF signal is weighted by an attenuator, and delayed by an optical delay line with a constant delay difference of *T*. Then the weighted and delayed taps are combined in an N by 1 combiner, and then converted back to an electric signal in a photo diode. A MWP FIR filter response in RF domain is then formed and can be measured by a vector network analyzer. This multiple delay line based approach is straightforward in terms of generating multiple taps of the FIR filter, however, it has several limitations. First, the total number of filter tap is limited by the complexity of the delay line array, which will in turn result in low quality of the filter. Usually a larger number of filter tap will result in a higher quality (Q factor) of the generated bandpass filter. In this scheme, the system complexity and cost will significant increase when a large number of filter tap is applied, since each branch requires an optical attenuator and a delay line. Second, this straightforward scheme is not suitable for passband tuning. In order to change the center frequency of the generated passband, the time delay *T* between each adjacent tap needs to be tuned. This requires the adjustment of the

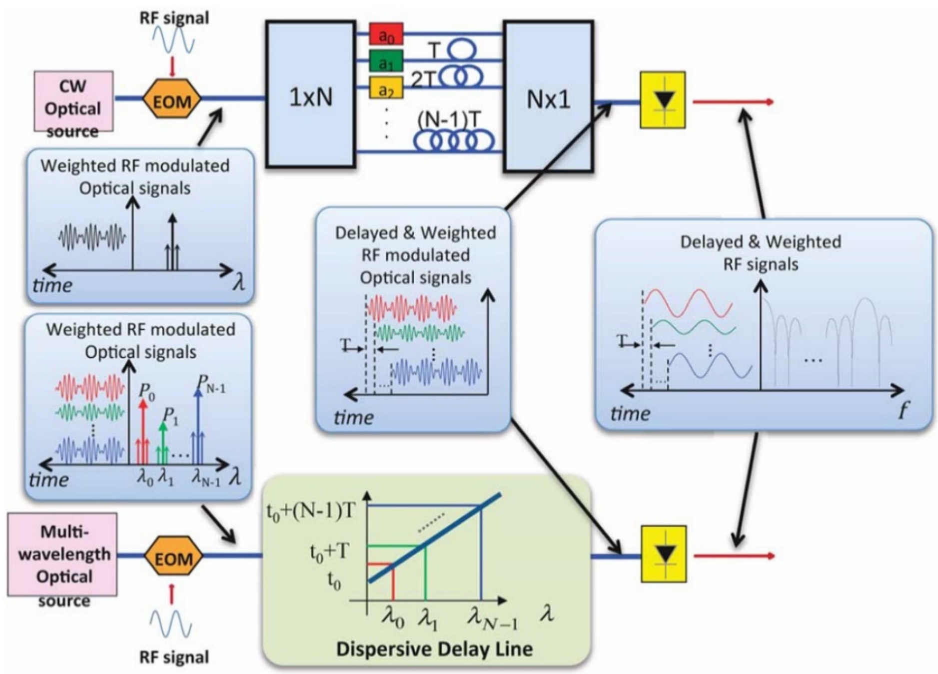

Figure 3.1. Schematic diagram of a photonic implemented FIR filter [1]. Upper scheme: delay line array based structure, Bottom scheme: Multi-wavelength source based structure.

values of all the delay lines in the setup, which is extremely inconvenient and impractical. Because of these limitations, the delay line array based scheme is not preferred in large tap number and tunable MWP filter design.

The bottom scheme shown in Figure 3.1 is a more compact and low cost structure, which is based on a multi-wavelength optical source and a dispersive medium. A relative larger amount of filter tap can be implemented through the multi-wavelength optical source, and the time delays between each filter tap are obtained through a dispersive medium. Each single wavelength of the multi-wavelength source works as a filter tap, and the input RF signal is modulated and duplicated onto the multiple optical carriers through an electro-optic modulator. The linear dispersive medium has a linear wavelength dependent dispersion, which provides different amount of time delay for different optical carriers. There are two key points to successfully build a FIR filter based on this scheme: (1) The wavelength spacing between each adjacent optical carrier must be the same, and (2) the dispersive medium must have a linearly group velocity dispersion over wavelength. These two requirements are needed to obtain a contact time delay between each adjacent tap of filter, which is required by the FIR filter design and can be expressed by Eq. (3.3)

$$T = \Delta\omega \cdot \beta_2 \cdot L_D \tag{3.3}$$

where β_2 and L_D are the group velocity dispersion and length of the dispersive device, and $\Delta\omega$ is the frequency spacing between each adjacent tap of the optical multi-wavelength source. In this scheme, usually the dispersion and length of the dispersive device are fixed. However, there are

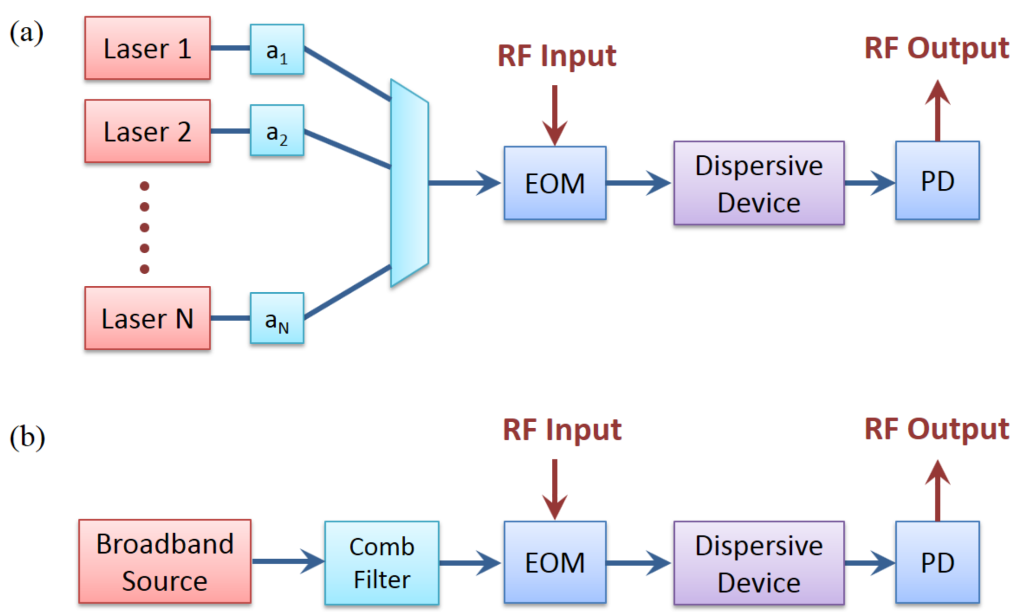

Figure 3.2. Two schemes to implement the multi-wavelength optical source based MWP FIR filter. (a) Based on a laser array. (b) Based on a broadband source and an optical comb filter.

several possible schemes to adjust the center wavelengths of the multi-wavelength optical source, making it suitable for building MWP filter with tunable passband.

Figure 3.2 shows two multi-wavelength optical source based schemes to build MWP FIR filters with tunable passbands. In Figure 3.2(a) the multi-wavelength optical source is implemented by a laser array, which consists a large number of laser diodes with tunable operating wavelengths. The center wavelengths of the laser diodes are set to have an equal wavelength spacing ($\Delta\omega$), such that the time delay difference T between each adjacent filter tap is the same. Time delay T can be adjusted by setting the center wavelengths of the laser diodes with different wavelength spacing ($\Delta\omega$), which will in turn controls the center frequency of the generated passband of the FIR filter, as described in Eq. (3.1). The amplitudes of the filter taps can be adjusted by the output power of each laser diode, or through the optical attenuators in the laser array. Although tunable MWP filters can be achieved through this laser array scheme, tuning process requires simultaneous adjustment of the center wavelengths a large number of laser diodes with different amount. Furthermore, accurate fixing the center wavelengths of the laser diodes is also needed, which required active thermal control of the laser array. These requirement makes the laser array based scheme not favored in practical applications.

Another scheme for implementing MWP FIR filter is shown in Figure 3.2(b), that the multi-wavelength source is generated through an optical broadband source and an optical comb filter. The broadband source is spectrally sliced by the optical comb filter, such that a large number of optical carriers can be easily generated. Usually optical comb filters are based on interferometric structures, such that the generated optical combs have same comb spacings between each adjacent peaks. The transmission function of an interferometric optical comb filter can be described as

$$T(\lambda) = \frac{1}{2}\left[1 - cos\big(\varphi(\lambda)\big)\right] \tag{3.4}$$

where $\varphi(\lambda)$ is the phase difference between the two interfered optical beams. For a classic Mach-Zehnder interferometer (MZI) structure, the phase difference can be calculated by Eq. (3.5)

$$\varphi(\lambda) = \frac{2\pi n_e d}{\lambda} \tag{3.5}$$

where n_e is the refractive index of the fiber used in the MZI, and d is the path difference between the two branches. The comb spacing of the generated optical frequency comb can be written as

$$\Delta\omega = \frac{2\pi\lambda^2}{n_e d} \tag{3.6}$$

When optical comb filter is analyzed within a certain wavelength range (e.g., C-band), the comb spacing of can be regarded as same for each adjacent peaks. With the use of a linear dispersive device, this feature guarantees the time delay difference T between each adjacent filter taps is always the same, fulfilling the requirement of the FIR filter design. Meanwhile, continuously adjustment of the comb spacing can be simply achieved by using an optical delay line in one of the interferometric branch, such that the center frequency of the generated FIR filter can be continuously tuned over a wide range of frequency. The amplitudes of the filter taps in this scheme can be adjusted by using a broadband optical filter or a wave shaper to shape the overall profile of the optical comb. Compared with the laser array based scheme, only two devices are used and a much larger number of taps can be generated through the broadband source and optical comb filter based scheme, which could result in better filter quality and with lower system complexity and cost. Furthermore, this scheme is more practically in term of the tunability of the FIR filter. Based on these reasons, the MWP filters demonstrated in this chapter is based on the broadband source and optical comb filter based scheme.

3.3 Implementation of the Reconfigurable MWP Dual-Band Filter

Figure 3.3 shows the schematic diagram of the optically controlled reconfigurable MWP dual-band filter. A broadband source is used as the light source, which is reshaped by a Gaussian profile optical filter and then spectrally sliced by an optically controlled Lyot loop filter. Polarizer P1 is aligned with P2 like a standard Lyot filter. The Lyot loop filter is an optical comb filter with switchable frequency spacings, which is controlled by the optical pump power from a DFB laser injecting into the SOA. An optical comb is generated after the Lyot loop filter and then modulated by the RF input signal through a phase modulator (PM). Each of the comb lines works as a single tap, which is weighted by the Gaussian optical filter and then delayed by the dispersion compensation fiber (DCF). The Gaussian optical filter is used to apodize the amplitude of the taps such that the passband sidelobes can be significantly suppressed and resulting in a clean bandpass profile with high sidelobe suppression; while the DCF is used to provide linear time delay for different wavelengths (filter taps). Finally the modulated optical signal is fed into a photo-detector and converted back to a RF signal [47]. In the experiment, a swept signal from a network analyzer

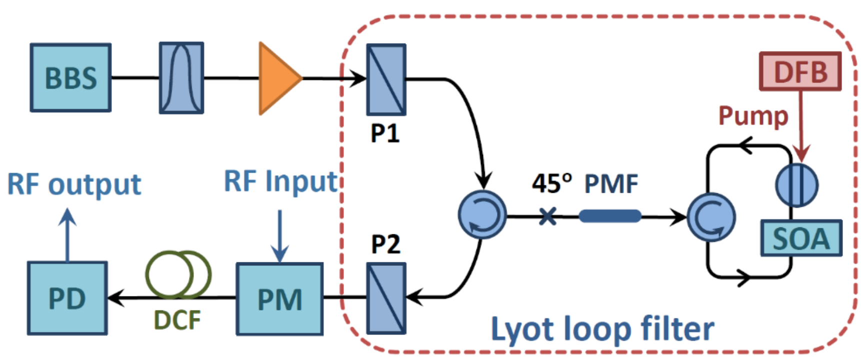

Figure 3.3. Schematic diagram of the optically controlled reconfigurable MWP dual-band filter. BBS: broadband source; Amplifier: Erbium-doped fiber amplifier (EDFA); DFB: distributed feedback laser; SOA: semiconductor optical amplifier; P1-P2: polarizers; PM: phase modulator; PMF: polarization maintaining fiber; PD: photo-detector; DCF: dispersion compensating fiber.

is used as the RF input, while the output of the MWP filter is launched to the input of the network analyzer for measuring the frequency response of the reconfigurable MWP filter.

The optically controlled Lyot loop filter, shown in the dashed box in Figure 3.3, is a modified version of a Lyot loop filter [48][21] (or a Solc filter [49]), which uses a circulator-SOA loop to replace the manual polarization controller for fast optical frequency spacing tuning. The operation principle is shown in Figure 3.4. The circulator-SOA loop allows the light to propagate through a single piece of PMF twice, and the SOA is used for high-speed polarization state adjustment. As shown, the input optical signal is a linear polarized broadband light and is aligned at 45° with respect to the fast axis of the PMF. A phase difference of $\Delta\varphi$ is obtained between the fast and slow axis after the light passes through the PMF, as given in Eq. (3.7). B and L are the birefringence and length of the PMF, and λ is the wavelength of the light. Then the optical signal is launched back to the same PMF through the circulator-SOA loop and propagates in the opposite direction with a polarization rotation angle ($\Delta\theta$). By adjusting the optical power of the pump laser, the polarization rotation angle ($\Delta\theta$) can be changed to 0°, 45° or 90°, and an accumulated phase difference ($\sum\Delta\varphi$) of $2\Delta\varphi$, $\Delta\varphi$ or 0 can be obtained at the output, which corresponds to a piece of PMF with equivalent length (L_e) of $2L$, L and 0, respectively. Different equivalent PMF lengths will result in different frequency spacings ($\Delta\omega$) in the Lyot loop filter, which is determined by Eq. (3.8) below, where c is the speed of light. By controlling the optical power of the pump light, various frequency spacings can be obtained from the Lyot loop filter. As a result, an optically controlled comb filter with switchable frequency spacing is achieved, which is the foundation of the proposed reconfigurable MWP filter.

$$\Delta\varphi = \frac{2\pi BL}{\lambda} \tag{3.7}$$

$$\Delta\omega = \frac{2\pi c}{BL_e} \tag{3.8}$$

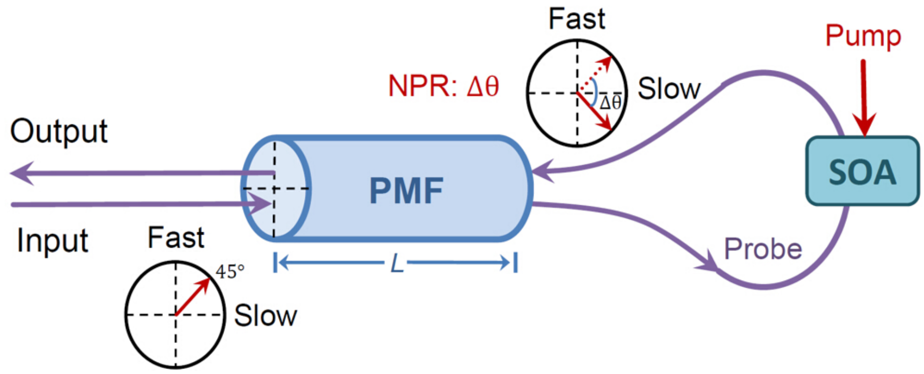

Figure 3.4. Operation principle of the optically controlled Lyot loop filter. The pump laser and semiconductor optical amplifier (SOA) work as an optically controlled polarization controller through ultrafast nonlinear polarization rotation (NPR) effect.

The frequency spacing of the optical comb ($\Delta\omega$) determines the optical carrier frequency separation between taps in the MWP filter, which in turn governs the passband frequencies (Ω_0) of the MWP filter through Eq. (3.9). β_2 and L_D are the group velocity dispersion and length of the DCF, which are fixed in a MWP filter. Therefore, the passband frequency is solely governed by the optical comb frequency spacing, which is optically tunable in the proposed MWP filter by adjusting the pump power being injected into the SOA. With different frequency spacing combinations in the optical comb, an optically controlled reconfigurable MWP filter can be achieved. The 3-dB bandwidth of the passbands is determined by Eq. (3.10) [40], where $\delta\omega$ represents the overall bandwidth of the Gaussian optical comb, which is also fixed in the MWP filter. As a result, the filter passband bandwidth is inversely proportional to the group velocity dispersion and the length of the DCF. With the use of different dispersion medium, bandwidth of the MWP filter can be adjusted correspondingly.

$$\Omega_0 = \frac{2\pi}{\beta_2 L_D \Delta\omega} = \frac{BL_e}{\beta_2 L_D c} \tag{3.9}$$

$$\delta\Omega_{3dB} = \frac{\sqrt{8\ln 2}}{\beta_2 L_D \delta\omega} \tag{3.10}$$

3.4 Gigahertz Speed Switching Through Nonlinear Polarization Rotation

Instead of adjusting the polarization rotation angles through a polarization controller manually, polarization states can be changed rapidly through nonlinear polarization rotation effect. The SOA together with the pump laser work as an optically controlled polarization controller for adjusting the polarization rotation angle inside the Lyot loop filter. With different optical pump powers, the effective birefringence of the SOA is changed, such that the broadband signal (probe) experiences different polarization rotation angles after propagating through the SOA [50]. By adjusting the optical power of the pump signal through an electro-optic intensity modulator, a polarization rotation range up to 180° can be achieved [51], providing enough polarization rotation angle to tune the comb spacing of the Lyot loop filter. Furthermore, NPR effect is an ultrafast optics effect that has been proved to be able to operate at gigahertz rate [52], enable high-speed tuning of the proposed MWP filter. Due to the counter-propagation of the optical pump and the broadband light, the optical pump is blocked by the circulator after NPR in the SOA and will not affect the rest part of the system.

The experimental setup of the proposed system is shown in Figure 3.5. First, we investigated the performance of nonlinear polarization rotation effect in SOA. A laser source at 1550 nm is launched into the SOA as the optical pump, which is counter-propagating with the broadband source (probe signal). The SOA is driving at a constant current of 150 mA, and a polarization controller is used at the DFB laser output to optimize the NPR effect in the SOA.

Figure 3.6(a) shows the measured result of the polarization rotation angles under different pump powers, optical power of the pump laser is adjusted from -13.0 dBm to +12.0 dBm. As shown, NPR effect is not significant when the pump power is relatively low (i.e., below 0 dBm), while the probe polarization starts to rotate significantly when the pump power is above +2.0 dBm. A polarization rotation angle of 45° is obtained at a pump power of +4.9 dBm and a 90° rotation is observed at a pump power of +10.0 dBm, which provides sufficient rotation angle for the optically controlled Lyot loop filter to achieve the desired comb spacings. Operation speed measurement of the NPR effect is shown in Figure 3.6(b), where a 1 Gb/s "10101100" non-return-to-zero (NRZ) bit sequence is modulated onto the pump laser through an electro-optic intensity modulator, as shown by the solid waveform. A polarizer is used after the SOA to translate the polarization rotation into amplitude change by blocking the probe signal when the optical pump is off. Optical pump power for bit "1" is set to +10.2 dBm to let the probe signal rotate by 90° through NPR, such that it can pass the polarizer when the control signal is a bit "1". Corresponding NPR response measured after the polarizer is shown by the dotted waveform in Figure 3.6(b), a 1 Gb/s waveform

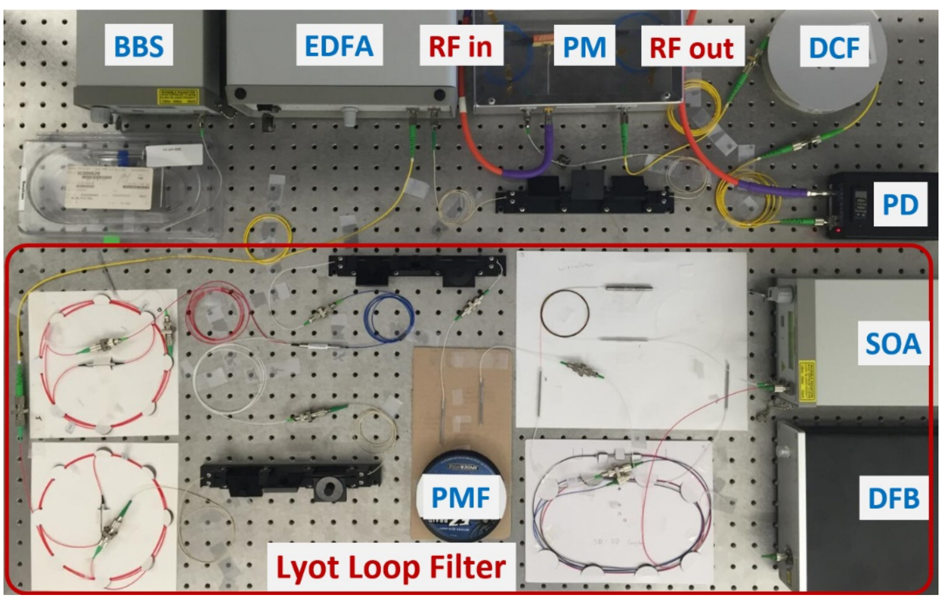

Figure 3.5. Experimental setup of the optically controlled reconfigurable MWP dual-band filter.

with the same bit sequence is observed, proving that the NPR effect can be operated at gigahertz speed. The rise/fall time of the resulted signal is about 200 ps, which is mainly determined by the gain recovery time of SOA [53].

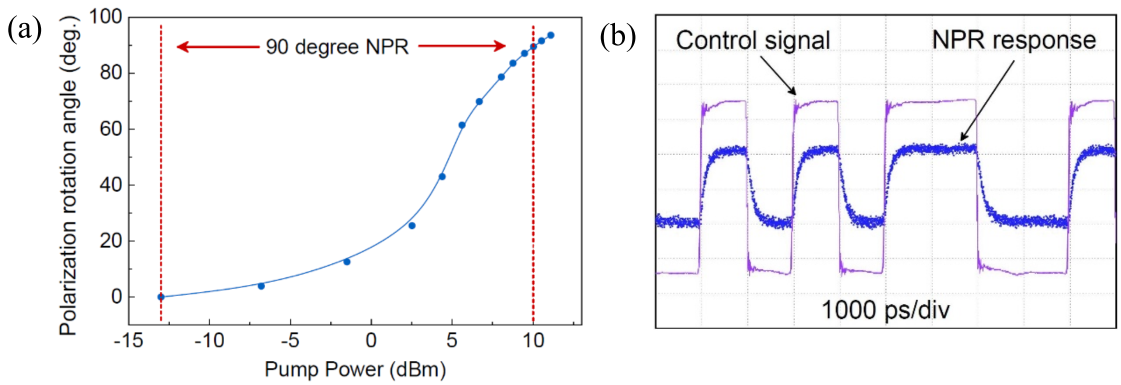

Figure 3.6. Nonlinear polarization rotation effect in a semiconductor optical amplifier. (a) Measured polarization rotation angles with respect to the optical pump powers. (b) Optically controlled tuning speed measurement. Solid: 1 Gb/s control signal of "10101100"; dotted: corresponding NPR output after SOA.

By adjusting the optical pump power, different polarization rotation angles are obtained at the circulator-SOA loop, resulting in an optical frequency comb with different comb spacings. Figure 5 shows the Gaussian broadband optical source spectrally sliced by the Lyot loop filter with different optical pump powers for polarization control. The optical spectra are measured by an optical spectrum analyzer with resolution of 0.8 pm. A piece of 9-meter PMF with a birefringence of 6.33×10^{-4} is used in the Lyot loop filter for generating the optical comb. During the experiment, the initial polarization rotation angle of the circulator-SOA loop is set to 90° such that no comb is observed when the pump signal is off. Then the pump power is gradually increased to obtain polarization rotation angles from 0° to 90°. As shown in Figure 3.7(a)-3.7(c), optical combs with a Gaussian profile and three different comb spacing are observed. The resultant comb spacings are no comb, 0.66 nm, and 0.33 nm, corresponding to a piece of PMF with an equivalent length of 0 m, 9 m, and 18 m, respectively. The optical pump power for different comb spacing is -13.0 dBm (pump off), +4.9 dBm, and +10.2 dBm, which corresponds to a polarization rotation angle of 90°, 45° and 0° at the circulator-SOA loop, respectively. The corresponding relationship is summarized in Table 3.1. When the pump power is set to 6.7 dBm, a polarization rotation angle of ~20° is achieved, and a higher-order optical comb with two different comb spacings interleaving with each other is observed, as shown in Figure 3.7(d). The co-existing of two optical combs makes it possible to generate two different passbands at the same time in the RF domain, which results in the dual-band state of the MWP filter. The dual-band state is a combination of the two single-band states when the polarization rotation angle is set to a value between 0° and 45°, such that the corresponded two single passbands (single-band 1 and single-band 2 in Table 3.1) can be generated

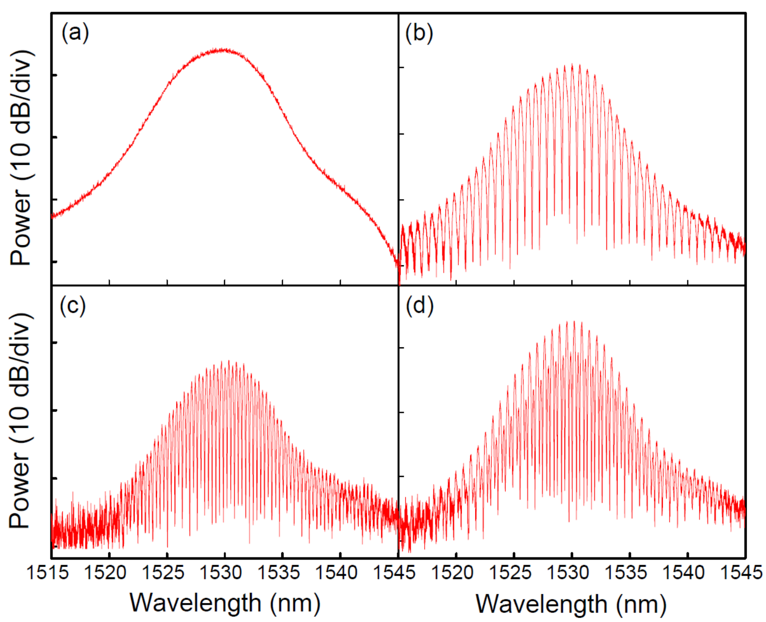

Figure 3.7. Measured optical spectra of the Lyot loop filter under different pump powers. (a) no comb at pump power of -13.0 dBm (pump off); (b) comb spacing of 0.66 nm, at pump power of +4.9 dBm; (c) comb spacing of 0.33 nm, at pump power of +10.2 dBm; (d) interleaved comb spacing of 0.33 and 0.66 nm, at pump power of +6.7 dBm.

at the same time [54]. The total bandwidth of the Gaussian optical combs is 30 nm and the extinction ratios are 20 dB for all the comb spacing combinations. It is worth noticing that cross gain modulation effect is also happening when the pump power is on, which can be seen from Figure 3.7. As the pump power increases, the overall power of the optical comb decreases. A 5-dB power change is observed when optical pump power of +10.2 dBm is used, as shown in Figure 3.7(c).

Table 3.1. Different Operation States of the Optically Controlled MWP Dual-Band Filter

Operation state	Polarization rotation angle	Comb spacing (nm)	MWP Filter passband (GHz)	Pump power (dBm)
All-block	90^{o}	Null	Null	-13.0
Single-band 1	45^{o}	0.66	1.1	+4.9
Single-band 2	0^{o}	0.33	2.2	+10.2
Dual-band	20^{o}	0.66 & 0.33	1.1 & 2.2	+6.7

The frequency response of the MWP filter generated from the corresponding optical combs are shown in Figure 3.8, measured by a network analyzer with an intermediate frequency bandwidth of 3 kHz. A piece of 10.2-km DCF with a dispersion of -149.36 ps/(nm·km) (at 1530 nm) is used as the dispersive medium, and the polarization rotation angle at the Lyot loop filter is controlled by optical pump power. In Figure 3.8(a), no passband is observed since the optical pump power is off and the initial polarization rotation angle of the circulator-SOA loop is 90°, and the RF filter is working in "all-block" state. While in Figure 3.8(b) and 3.8(c), the MWP filter is tuned to "single-band" state that only consists of one passband at either 1.1 GHz or 2.2 GHz. The MWP filter is resulted from the Lyot loop filter with comb spacing of 0.66 nm or 0.33 nm and an optical pump power of +4.9 dBm and +10.2 dBm, respectively. By setting the value of optical pump power to +6.7 dBm, both the passbands at 1.1 GHz and 2.2 GHz are observed at the same time and the MWP filter is working in "dual-band" state, as shown in Figure 3.8(d). The weaker power observed at the 1.1 GHz passband is due to the carrier-suppression effect during the phase-modulation to intensity- modulation conversion process in DCF [55]. The corresponding rotation angles, comb spacings and passband frequencies under different optical pump powers are listed in Table 3.1. The four different operation states of the MWP filter are fast switchable by adjusting the optical pump power launching into the SOA. Compared with the manual polarization controller based

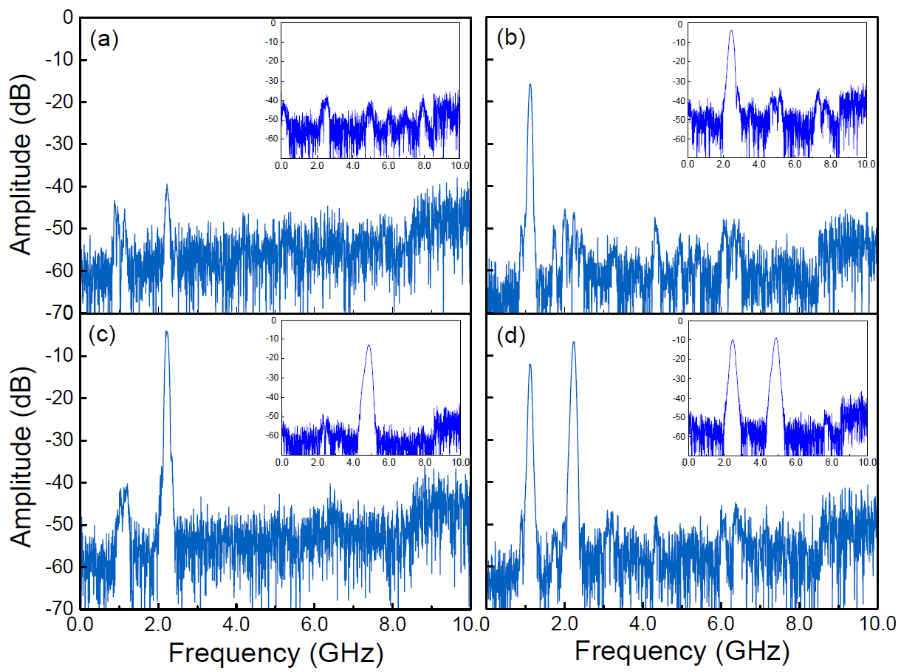

Figure 3.8. Measured RF amplitude response of the four operation states of the optically reconfigurable dual-band filter. (a) all-block state; (b) single-band state at 1.1 GHz; (c) single-band state at 2.2 GHz; (d) dual-band state with two passbands. Inserts: corresponding results with the use of shorter DCF (4.1 km), resulting in passbands with wider bandwidths and different frequencies.

tuning schemes [41][56], the switching time between different operation states is significantly improved to gigahertz speed. Furthermore, the use of the SOA could further amplify the optical frequency comb. As a result, both the modulated signal and the amplified spontaneous emission noise are amplified, resulting in an increase in both the RF power and the noise floor at the MWP filter. The 30-nm wide Gaussian optical comb provides a large number of taps for the MWP filter, resulting in good sidelobe suppression and clean filter profile. The total insertion loss of the MWP filter is ~8 dB. Both the passbands at 1.1 GHz and 2.2 GHz show uniform and clean filter profiles, with sidelobe suppression of 40 dB and 3-dB bandwidth of 90 MHz.

Center frequencies and bandwidths of the MWP filter passbands can be adjusted by using different lengths of PMF and DCF, as described in Eq. (3.9) and Eq. (3.10). The insets in Figure. 3.8(a)-3.(d) show the corresponding results when the DCF length is decreased to 4.1 km, while the length of PMF and other parameters of the system are kept same. As shown, two passbands with larger 3-dB bandwidths of 200 MHz are observed at 2.4 GHz and 4.8 GHz, which can be explained by Eq. (3.10). Figure 3.9 shows the measured results when two pieces of PMF of different lengths (9 m and 55 m) are used in turn, while the DCF length is kept at 10.2 km. As shown in Eq. (3.9), the passband center frequencies are adjustable by varying the lengths of PMF. When a piece of 9-m PMF is used, two passbands at 1.1 GHz and 2.2 GHz are achieved; while two passbands at 6.8 GHz and 13.6 GHz are resulted when the length of PMF is changed to 55 m. It can be seen that passbands at higher frequencies have wider bandwidth, this is caused by the difference in dispersion slopes of the dispersive medium (DCF) over different wavelengths [38]. A difference in noise floor power is observed at different PMF length, which is caused by the length difference (i.e. insertion loss difference) between the PMFs.

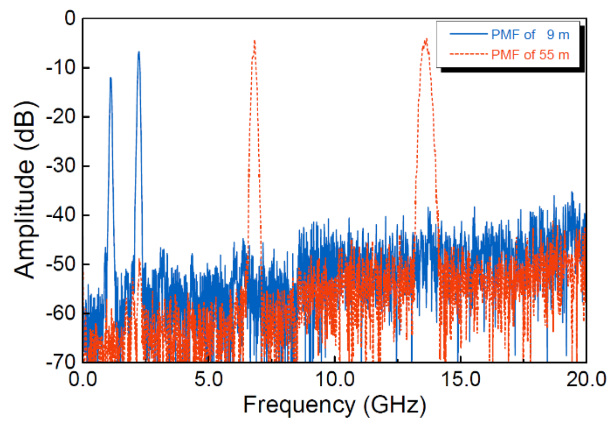

Figure 3.9. Measured RF amplitude response of the MWP dual-band filter with the use of different lengths of PMF. Solid, 9-meter PMF; dashed, 55-meter PMF.

Since NPR is an ultrafast optical effect, switching between different operation states can be performed at gigahertz speed. To investigate the switching speed of the proposed MWP dual-band filter, the power level of the pump light launching into the SOA is switched rapidly between -13.0 dBm and +4.9 dBm with the use of an electro-optic intensity modulator, such that the MWP filter is switching between all-block state and single-band state with a passband at 6.8 GHz. A 0.85-Gb/s "10001000" NRZ bit sequence is used as the control signal with a rise/fall time of ~130 ps, and a 6.8-GHz sinusoidal signal is launched into the MWP filter as the RF input signal. As shown in Figure 3.10, the input signal passes through the MWP filter and is well maintained during the single-pass state, and is blocked by the MWP filter during the all-block state. The transition time between the two states is within 200 ps, proving that high-speed switching of the MWP dual-band filter is achieved. Furthermore, it is worth noticing that the demonstration is based on a one stage Lyot loop filter with only one piece of PMF, such that center frequencies of the two resultant passbands with always be two times of the lower frequency one. By adding another piece of PMF with a different length to the Lyot loop filter, the maximum simultaneous number of passband can be dramatically increased to 12 with various passband combinations [56,57], which the passband number and frequency can also be rapidly reconfigured through nonlinear polarization rotation.

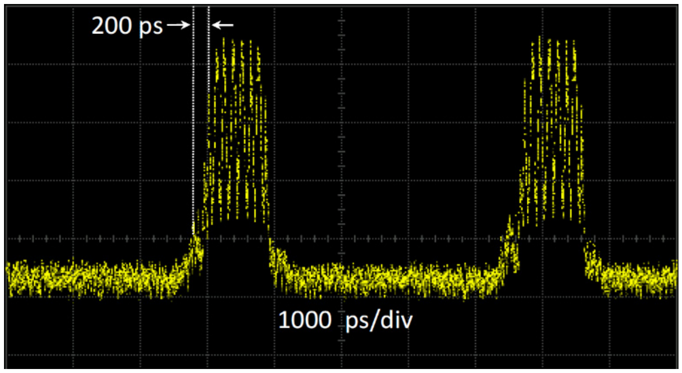

Figure 3.10. Tuning speed measurement of the optically controlled MWP dual-band filter, the filter is switching between all-block and single-block state with rise/fall time less than 200 ps.

3.5 Summary

In summary, a high-speed reconfigurable MWP dual-band filter is proposed and experimentally demonstrated. An optically controlled Lyot loop filter with switchable comb spacings is used to generate the optical comb with different frequency separations, resulting in four different operation states in the MWP filter. The four states are all-block state, dual-band state and single-band state with two different passband frequencies. The switching between different operation states is achieved by the use of ultrafast nonlinear polarization rotation in a semiconductor optical amplifier, and gigahertz speed tuning of the MWP filter is experimentally achieved. The MWP filter has a good selectivity that over 40 dB passband sidelobe suppression is obtained, with clean and sharp filter profile. A comparison of the tunability/reconfigurability as well as the tuning mechanisms among state-of-the-art RF multiband filters are summarized in Table II, including both RF electronics and photonics based approaches. As shown, the tuning speed is dramatically improved to tens of picoseconds level with the use of ultrafast NPR effect. Compared with state-of-the-art multiband RF filters, this design significantly improves the tuning speed of RF filter to gigahertz speed, which can potentially fulfill the critical needs in dynamic multiband systems and high-speed microwave signal processing applications. Furthermore, larger operation frequency range and wider bandwidth are achieved by the MWP filter, with both the passband center frequency and bandwidth being adjustable to fit various applications.

Table 3.2. Comparison of the Tuning Mechanism of State-of-the-art Multiband RF Filters

Reference	Technique	Number of passbands	Rejection level	Tunability/ Reconfigurability	Tuning mechanism
[31]	LTCC	3	20 dB	Not tunable	---
[32]	Stepped impedance resonator	6	25 dB	Not tunable	---
[30]	Microstrip + trimmer capacitor	4	40 dB	Continuously tunable/ Reconfigurable	Adjustable capacitor
[29]	Microstrip + varactor	2	35 dB	Continuously tunable	Adjustable varactor
[113]	RF-MEMS	2	30 dB	Discretely tunable	RF MEMS capacitor
[33]	Microstrip + DGS	3	30 dB	Reconfigurable	PIN diode
[55]	Broadband optical source	2	20 dB	Continuously tunable	Optical delay line
[40]	Optical frequency comb	3	35 dB	Discretely tunable	Optical switch
[41]	Optical frequency comb	3	35 dB	Reconfigurable	Manual polarization controller
[71]	Phase-shifted FBG	2	25 dB	Continuously tunable	Laser wavelength adjustment
[44]	Stimulated Brillouin scattering	6	20 dB	Continuously tunable/ Reconfigurable	Laser wavelength adjustment
[56]	Optical frequency comb	12	30 dB	Reconfigurable	Manual polarization controller
This work	Optical frequency comb	2	40 dB	Reconfigurable	Ultra-fast Nonlinear polarization rotation

*LTCC: low-temperature cofired ceramic, MEMS: micro-electro-mechanical system, DGS: defected ground structure, FBG: fiber Bragg grating.

CHAPTER 4

TUNABLE AND RECONFIGURABLE MWP MULTIBAND FILTER

4.1 RF Multiband Bandpass Filter

Due to the ever-increasing demand of multiband wireless and satellite systems, multi-service systems and multi-function devices, multiband communications are of critical need in various RF systems. Multiband communications have been extremely important for modern wireless communications and satellite communications in the commercial, defense, and civilian federal marketplace [58-60]. The use of cognitive wireless technology to solve the frequency resource shortage problem, as well as the capabilities and operational flexibility necessary to meet ever-changing requirements is necessary. Frequency multiplexing is extremely useful to improve system spectral efficiency and multi-function capability, where several frequency channels over a wide RF range are implemented simultaneously to provide multiple functions and services. Thus, to pre-select the desired band, and prevent interference in multiband communications, tunable multiband RF filters are critically needed.

Despite the increasing importance and critical needs, reconfigurable RF multiband filters are currently underdeveloped even both RF electronics and photonics technologies are being explored. This kind of RF bandpass filter is difficult to achieve using conventional RF electronic techniques because of the lack of reconfigurability; in addition, it is also difficult to simultaneously satisfy all the design parameters for all passbands [61-65] when a large number of simultaneous passbands is required, which would result in non-uniform and inconsistent merits of different passbands. For state-of-the-art electronics based RF multiband filters, the maximum number of simultaneous passbands recorded was six with fixed passband frequencies [32]; and very few tunable tri-band and quad-band filters have been realized with limited tunablity [29-31]. Although electronic approaches offer on-chip solutions, both the number of simultaneous passbands and passband tunability are limited [34]. A promising way to implement RF multiband filters with flexible passband reconfigurability and frequency tuning capability is urgently desired.

MWP RF filters have received increasing attention in recent years due to the significant improvements over conventional RF systems, such as low-loss, wide bandwidth, flexibility, tunability and reconfigurability [1-8]. Among these, MWP single bandpass filter is always an active topic and different approaches have been reported [35-39, 72-80]. Approaches include multi-tap delay line schemes [35-36, 72-74] and optical frequency comb schemes [37-41, 75-80]. However, most existing approaches either lack of the ability to support multiband operations, or the resultant passbands are periodic over a very wide frequency range, limiting its ability to isolate unwanted frequencies within a certain frequency range. In order to achieve multiple passbands with a MWP filter, the corresponding optical frequency comb must either simultaneously consist of multiple combs with different comb spacings [41] or it has to be sampled spectrally [79]. Unfortunately, due to the scalability, uniformity and selectivity of the above schemes, it is hard to achieve a MWP multiband filter with a large passband number, high selectivity, reconfigurable filter characteristics, and good passband uniformity. For example, a MWP multiband bandpass filter based on a high-birefringence loop mirror filter is proposed [41]. Three passbands with non-uniform bandwidths are achieved using three pieces of birefringence fibers, while a MWP multiband bandpass filter with sidelobe suppression of 10 dB is achieved with wavelength sampling technique [40].

In this chapter, we develop several schemes to achieve MWP multiband filters with large numbers of simultaneous passbands. The demonstrated MWP filter are based on FIR, that multiple comb spacings and FIR filter response are applied at the same time to generate multiple passbands. Both switchable and tunable MWP multiband filters are experimentally demonstrated, with up to 13 simultaneous passbands. Three different schemes are demonstrated to achieve the highly reconfigurable MWP multiband filters, which are based on Two-Stage Lyot Loop Filter structure, Lyot-MZI structure, and cascaded MZI structure.

As such, the following work is drawn from our paper published on Scientific Reports (vol. 5, p. 15882, Nov. 2015) by Jia Ge and Mable P. Fok, entitled “Passband switchable microwave photonic multiband filter”, and paper published on IEEE Photonics Conference (p. WA1, Oct. 2017) by Jia Ge and Mable P. Fok, entitled “Continuously tunable and reconfigurable microwave photonic multiband filter based on cascaded MZIs”, and paper published on Optical Fiber Communication Conference (p. W1G.2, Mar. 2016) by Jia Ge, A. E. James, A. K. Mathews, and Mable P. Fok, entitled “Simultaneous 12-passband microwave photonic multiband filter with reconfigurable passband frequency”.

4.2 Switchable Multiband Filter based on Two-Stage Lyot Loop Filter

The first demonstration is a reconfigurable MWP multiband filter with selectable and switchable passbands, which has a maximum of 12 simultaneous passbands evenly distributed from 0 to 10 GHz. The scheme is based on the generation of tunable optical comb lines using a two-stage Lyot loop filter, such that various filter tap spacings and spectral combinations are obtained for the configuration of the MWP filter. Through polarization state adjustment inside the Lyot loop filter, an optical frequency comb with 12 different comb spacings is achieved, which corresponds to a MWP filter with 12 selectable passbands. Center frequencies of the filter passbands are switchable, while the number of simultaneous passbands is tunable from 1 to 12. Furthermore, the MWP multiband filter can either work as an all-block, single-band or multiband filter with various passband combinations, which provide exceptional operation flexibility. All the passbands have over 30 dB sidelobe suppression and 3-dB bandwidth of 200 MHz, providing good filter selectivity.

4.2.1 Principle and Experimental Setup

Figure 4.1 shows the experimental setup of the proposed MWP multiband filter, where the two-stage Lyot loop filter is shown in the dashed box. A broadband amplified spontaneous emission (ASE) source is used as the light source and reshaped by an optical filter with a Gaussian profile. The reshaped broadband source is then launched into a two-stage Lyot loop filter via polarizer P1 for spectral slicing. Polarizer P2 is aligned with P1 like a classic Lyot filter [81]. At the output of P2, an optical comb source is generated and works as a multi-wavelength optical carrier for electrical-to-optical conversion, which is then modulated by the RF input signal through a phase modulator. Each of the comb lines generated by spectral slicing works as a single tap for the MWP filter, while the Gaussian optical filter is used to apodize the amplitude of the taps such that the MWP filter sidelobes can be greatly suppressed, resulting in a clean bandpass profile with high sidelobe suppression. The modulated signal is then launched into a piece of dispersion compensating fiber (DCF), which provides constant time delay between each filter taps. That is to say, each of the taps are weighted by the Gaussian filter and delayed by the DCF. The weighted and delayed signal is then fed into a photo-detector and converted back to a RF signal. In the experiment, a sweeping RF signal from a network analyzer is used as the RF input for measuring the frequency response of the proposed MWP multiband filter.

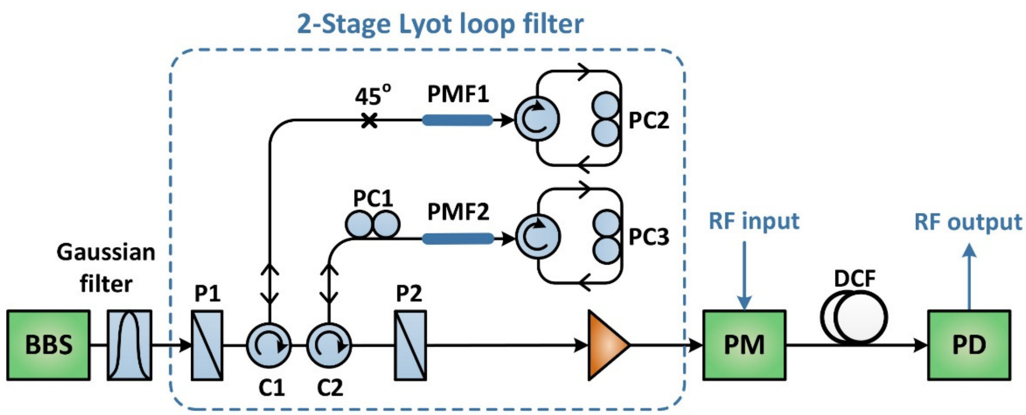

Figure 4.1. Experimental setup of the passband switchable MWP multiband filter. BBS: broadband source; P1-P2: polarizers; C1-C2: circulators; PC1-PC3: polarization controllers; PMF1-PMF2: polarization maintaining fibers; PM: phase modulator; DCF: dispersion compensating fiber; PD: photo detector.

The two-stage Lyot loop filter used in the MWP filter is shown in the dashed box in Figure 4.1. Each stage consists of a piece of PMF, two PC and two optical circulators. The operating principle of each stage is illustrated in Figure 4.2. Unlike the standard Lyot filter, light propagates through the PMF twice bi-directionally through a circulator-PC based loop in our Lyot loop filter, which significantly increases the number of comb spacing combinations. In the Lyot loop filter, a phase difference of $\Delta\varphi=2\pi BL/\lambda$ is obtained between the fast and slow axis when the light pass through the PMF at 45° ($\pi/4$) with respect to the fast axis, where B and L are the birefringence and length of the PMF, respectively, and λ is the wavelength of the light. By allowing the light to propagate twice in the PMF and adjusting the PC inside the loop to let the light have different polarization rotation angles ($\Delta\theta$) of 0, $\pi/4$ or $\pi/2$ at the circulator-PC based loop, a total phase difference ($\sum\Delta\varphi$) of $2\Delta\varphi$, $\Delta\varphi$ and 0 can be obtained at the output, respectively. With different polarization rotation angles $\Delta\theta$, each stage works as one piece of PMF with an adjustable equivalent length (L_e) of $2L$, L and 0, correspondingly. With a two-stage Lyot loop filter, 12 different equivalent lengths ($L_e = |mL_1 + nL_2|$, with m, n = 0, 1, or 2, shown in Table. 4.1) are obtained, where L_1 and L_2 are the physical lengths of PMF1 and PMF2, respectively. As a result, a comb filter with 12 selectable comb spacings is achieved, so that the comb spacing ($\Delta\omega$, in angular frequency) is determined by the equivalent length of PMF, as shown in Eq. (4.1).

$$\Delta\omega = \frac{2\pi C}{BL_e} \tag{4.1}$$

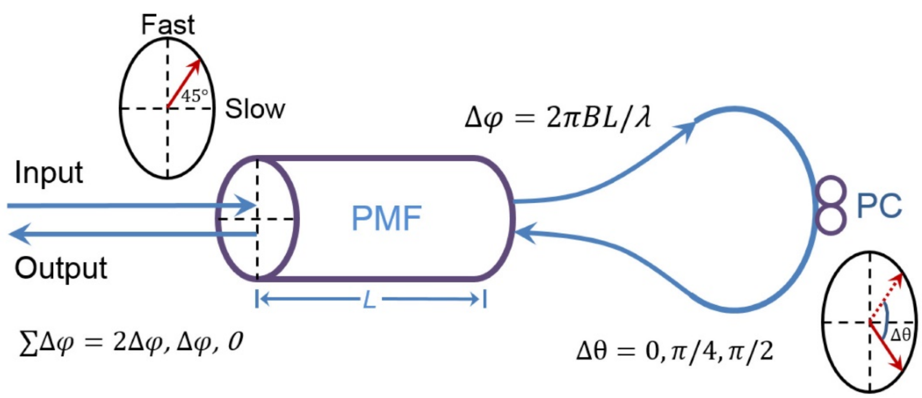

Figure 4.2. Operation principle of the comb spacing tunable Lyot loop filter using bidirectional propagation of light in a PMF. Input light propagates through a polarization maintaining fiber (PMF) twice bi-directionally via the circulator-PC loop (on the right) with a polarization rotation angle of 0, π/4 or π/2, resulting in a total phase difference of $2\Delta\varphi$, $\Delta\varphi$ or 0 at the output.

The comb spacing of the Lyot loop filter determines the carrier wavelength for each of the taps in the MWP filter, which in turn determines the temporal delay between taps after propagating in the DCF. By apodizing the tap amplitude with a Gaussian optical filter, a bandpass response in the RF domain with good sidelobe suppression and a clean passband profile can be achieved. The passband frequency (Ω_0) of the MWP filter is governed by Eq. (4.2), where β_2 and L_D are the group velocity dispersion and length of the DCF, which are fixed during the experiment. That is to say, the passband frequency is mainly governed by the optical comb spacing, which is tunable by adjusting the PC in the Lyot loop filter to change the $\Delta\theta$ in Figure 4.2. The 3-dB bandwidth of the passbands is determined by Eq. (4.3), where $\delta\omega$ represents the overall bandwidth of the Gaussian optical comb, detailed derivations can be found in [37,38]. As shown, the bandwidth of the MWP filter ($\delta\Omega_{3dB}$) is inversely proportional to the overall bandwidth of the optical comb and the length of the DCF. With the use of a longer piece of DCF, much narrower and further separated passbands can be obtained to meet specific requirements for different applications.

$$\Omega_0 = \frac{2\pi}{\beta_2 L_D \Delta\omega} = \frac{BL_e}{\beta_2 L_D C} \tag{4.2}$$

$$\delta\Omega_{3dB} = \frac{\sqrt{8\ln 2}}{\beta_2 L_D \delta\omega} \tag{4.3}$$

The Lyot loop filter can be tuned to have multiple combs with different comb spacings simultaneously by setting $\Delta\theta$ to a value between 0 and $\pi/4$, such that a higher order filter is resulted. As shown in Figure 4.3, two optical combs with a different comb spacing are observed by using a one-stage Lyot filter. This situation can be regarded as two optical combs with different spacings appearing at the same time and spectrally interleaved with one another, which makes it possible to generate a MWP filter with two passbands at the same time. Based on different comb spacing combinations, a MWP multiband filter with switchable frequency bands can be achieved: with a one-stage Lyot loop filter, an optical comb with 2 selectable spacings is obtained; when a second stage is added into the Lyot loop filter, up to 12 selectable spacings are achieved [21], corresponding to a MWP filter with 12 different possible passbands. Table 4.1 shows the 12 combinations of the two-stage Lyot filter, as well as the calculated relationship between the equivalent length of PMF (L_e) and the passband frequency of the MWP filter (Ω_0). L_1 and L_2 are the physical lengths of the PMF in the first and second stage, respectively. In the experiment, both L_1 and L_2 are set such that all the 12 equivalent lengths are different and the resultant passbands are evenly distributed within the frequency range of interest (0-10 GHz).

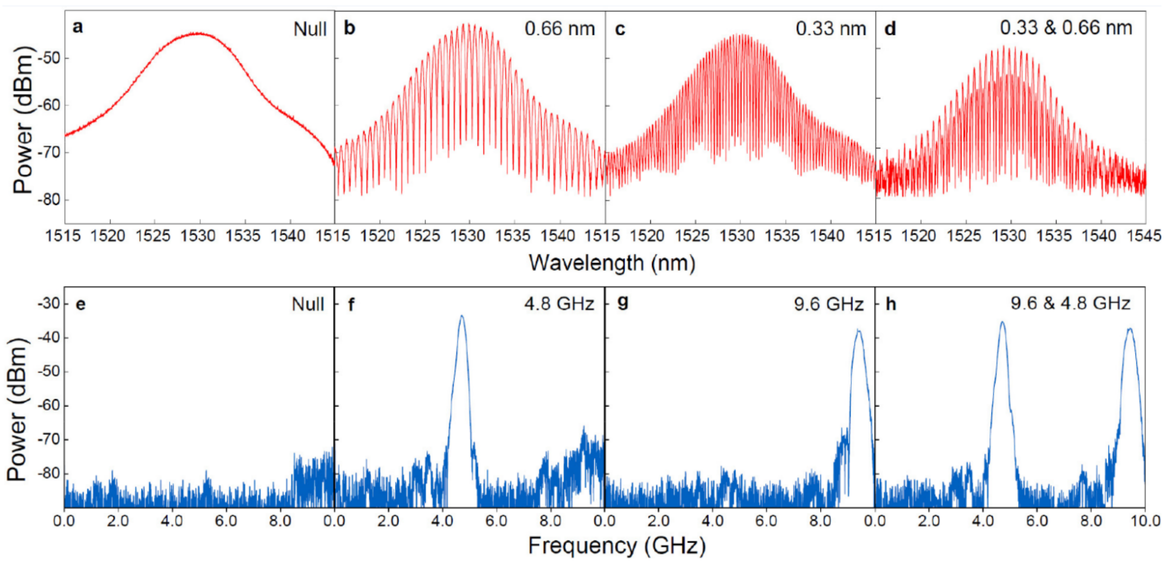

Figure 4.3. Measured optical comb spectra and frequency response of the one-stage Lyot loop filter based MWP multiband filter. (a)-(d) Gaussian optical frequency comb with different comb spacings: (a) no comb; (b) 0.66 nm; (c) 0.33 nm; (d) interleaved 0.33 nm & 0.66 nm. (e)-(h) Corresponding frequency response of the MWP multiband filter in 3 different operating states: (e) all-block state with zero passband; (f) single-band state with a passband at 4.8 GHz; (g) single-band state with a passband at 9.6 GHz; (h) multiband state with two passbands at 4.8 GHz and 9.6 GHz.

Table 4.1. Twelve combinations of the two-Stage Lyot loop filter based MWP multiband filter ($L_1 = 2$ m, $L_2 = 10$ m)

Number	Length Combination	Equivalent PMF length (L_e, m)	MWP Filter passband (Ω_0, GHz)
1	L_1	2	0.8
2	$2L_1$	4	1.6
3	$\lvert 2L_1-L_2 \rvert$	6	2.4
4	$\lvert L_1-L_2 \rvert$	8	3.2
5	L_2	10	4.0
6	L_1+L_2	12	4.8
7	$2L_1+L_2$	14	5.6
8	$\lvert 2L_1-2L_2 \rvert$	16	6.4
9	$\lvert L_1-2L_2 \rvert$	18	7.2
10	$2L_2$	20	8.0
11	L_1+2L_2	22	8.8
12	$2L_1+2L_2$	24	9.6

4.2.2 Results and Discussion

We first investigate the performance of our proposed MWP multiband filter with a one-stage Lyot loop filter. The spectrally sliced Gaussian broadband optical source with different comb spacings are shown in Figure. 4.3(a)-4.3(d). A piece of 12-m PMF with a birefringence of 6.6×10^{-4} is used in the one-stage Lyot loop filter. Through polarization state adjustment, 30-nm wide Gaussian optical combs with four different comb spacing combinations are observed (0, 0.66 nm, 0.33 nm and interleaved 0.66 nm & 0.33 nm), corresponding to a PMF equivalent length of 0, 12 m, 24 m, and interleaved 12 m & 24 m, respectively. The extinction ratios of the optical combs in Figure 3a-3d are over 20 dB for all combinations. RF spectra of the resultant MWP filter generated from the corresponding optical comb are shown in Figure 4.3(e)-4.3(h), measured by the RF network analyzer with an intermediate frequency bandwidth of 5 kHz. Figure 4.3(e), no passband is observed and the filter is working in the "all-block" state, corresponding to a polarization rotation angle $\Delta\theta$ of $\pi/2$. While in Figure 4.3(f) and 4.3(g), the filter is in a "single-band" state that only consists of one passband at either 4.8 GHz or 9.6 GHz ($\Delta\theta = \pi/4$ and 0, respectively). By properly adjusting the PC in the circulator-PC loop one can achieve two different comb spacings at the same time ($\Delta\theta$ is between 0 and $\pi/4$). Two clean passbands are observed and the filter is in "multiband" state, as shown in Figure 4.3(h). The four different configurations of the MWP filter are switchable by adjusting the PC to different rotation angles. The 30-nm wide Gaussian profile optical comb provides enough taps for the MWP filter, resulting in better sidelobe suppression and a clean filter profile. All the passbands show consistent performance, with a sidelobe suppression of 46 dB and a 3-dB bandwidth of 200 MHz.

With a two-stage Lyot filter, 12 different passband center frequencies can be obtained from the proposed MWP filter. Two pieces of PMFs with lengths of 2 m (L_1) and 10 m (L_2) are used in each state of the Lyot loop filter. The lengths of the PMFs are chosen to make the equivalent length (L_e) to have the same length difference between adjacent combinations, which results in an even frequency distribution of all the possible passbands, as shown in Table 4.1. First, the MWP filter is set to operate in the single-band state, i.e. only one passband appears at one time. Figure 4.4 shows the measured RF frequency spectra of all the 12 different single passband outputs of the MWP filter, i.e. from 12 different measurements. The single passband of the MWP filter is tuned to 12 different positions through polarization state adjustment in the two-stage Lyot loop filter. The 12 passbands are evenly distributed from 0 to 10 GHz with a same frequency spacing of 0.8 GHz, and the experimental result agrees well with the calculation in Table 4.1. The passband has a 3-dB bandwidth of 200 MHz and the sidelobe suppression is up to 40 dB, with a sharp and clean filter profile. It is worth noticing that the sidelobe suppression of the first passband at 0.8 GHz is about 30 dB, which is smaller than other passbands. This is due to the fact that the corresponding comb spacing of the first passband is relatively large, such that there is not enough comb lines (taps) for the MWP filter, which results in a relatively lower sidelobe suppression.

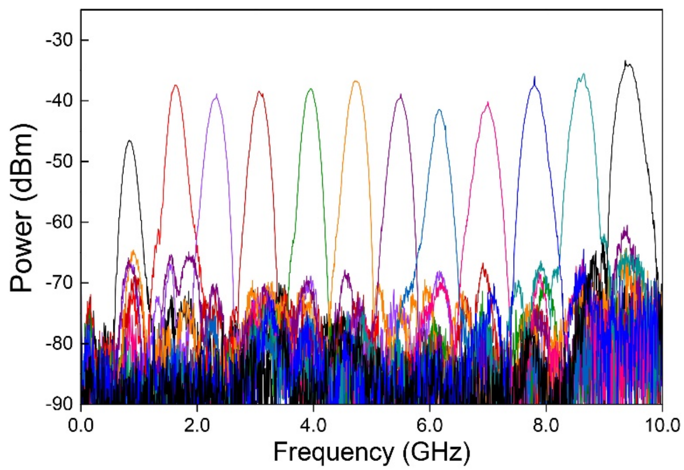

Figure 4.4. Measured frequency spectra of the MWP filter in single-band state. 12 single passbands are evenly distributed from 0.8 GHz to 9.6 GHz, with sidelobe suppression of 40 dB and 3-dB bandwidth of 200 MHz.

Frequency spectra of the proposed MWP multiband filter working in the multiband state are shown in Figure 4.5. By setting the two-stage Lyot loop filter to have more than one comb spacing combination interleaving spectrally, a MWP filter with multiple passbands is achieved. With the adjustment of $\Delta\theta$, various combinations of the number of passbands and passband frequencies are achieved. In Figure 5a, three passbands at 0.8 GHz, 3.2 GHz and 4.8 GHz are obtained simultaneously from the MWP multiband filter, while four passbands at 2.4 GHz, 4.8 GHz, 7.2 GHz and 9.6 GHz are observed in Figure 4.5(b). In Figure 4.5(c), 4.5(d) and 4.5(e), five, six and eleven passbands from 6.4 - 9.6 GHz, 1.6 - 5.6 GHz and 1.6 - 9.6 GHz are obtained, respectively. All the 12 passbands of the MWP multiband filter calculated in Table. 4.1 can be observed at the same time as shown in Figure 4.5(f), with an equal frequency spacing of 0.8 GHz between each passband. Sidelobe suppression is over 30 dB for all the passbands except the first passband at 0.8 GHz, as explained previously. Noticing that when adjacent passbands are chosen, the transition bandwidth between pass and stop bands are smaller. This can be improved by using a longer DCF or DCF with a higher dispersion, such that a narrower passband and wider transition bandwidth are resulted. Compared with current state-of-the-art multiband RF filters, the proposed MWP multiband filter has uniform passband response, flexible reconfiguration capability and a much larger number of simultaneous passbands.

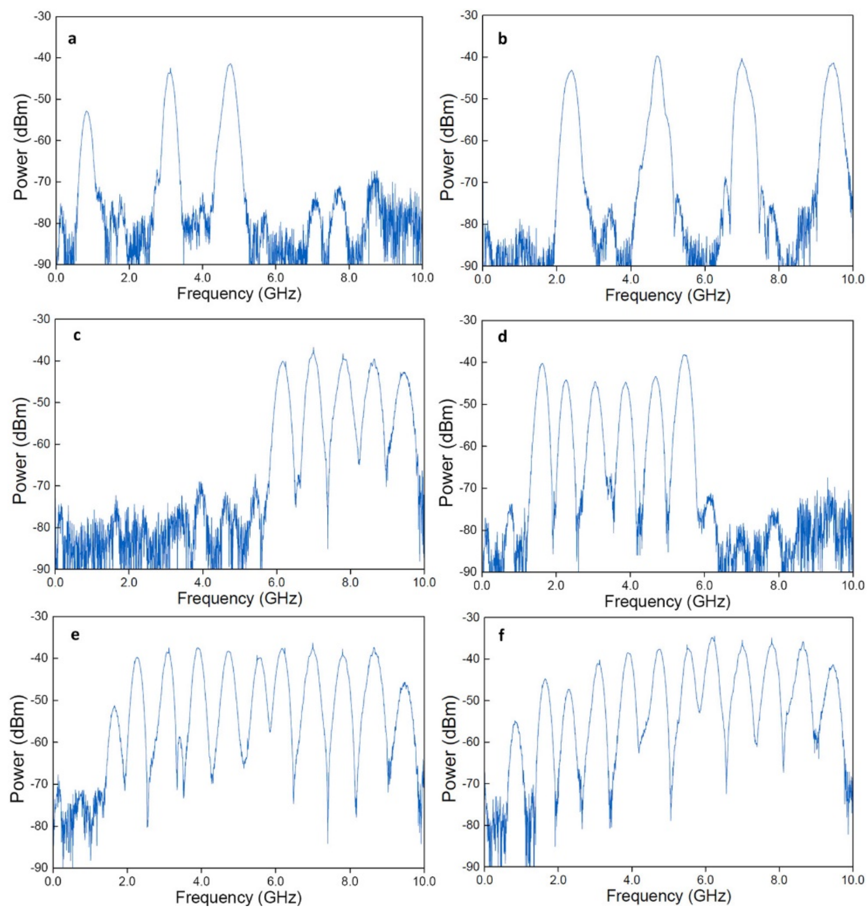

Figure 4.5. Measured frequency spectra of the MWP filter in multiband state with different combinations of passbands.

4.2.3 Implementation through one-stage Lyot filter with two pieces of PMF

The previous results are based on the scheme of two-stage cascade Lyot loop filter, the system setup is relative complex that two polarizer with four circulator are used. In real-world application, the setup can be simplified into a one-stage structure with two cascade PMF, as introduced in this section. Furthermore, different lengths of the PMF and DCF are used and the 3-dB bandwidth of the generated passbands are reduced for better filter selectivity.

Figure 4.6 shows the experimental setup of the simplified structure. The Lyot loop filter now consists of two pieces of PMF, and a PC1 is added between them. With two pieces of PMFs in series, effective length (L_e) of the PMF depends on the polarization rotation introduced by PC1. If PMF1 and PMF2 are aligned, then the length add up; if PMF1 and PMF2 are orthogonal, the length subtracts; if PMF1 is aligned at 45° with PMF2, then PMF2 is "invisible", resulting in different phase differences. In the Lyot loop filter, input light propagates through the two PMFs twice bi-directionally through a circulator-PC based loop at the far end. Thus, with two pieces of PMFs, up to 12 different equivalent lengths can be obtained ($L_e = |mL_1 + nL_2|$, with m, n = 0, 1, or 2, shown in Table. 4.1), where L_1 and L_2 are the physical lengths of PMF1 and PMF2. By adjusting the polarization rotation angles of the light through PC1 and PC2, different effective lengths is resulted, thus, the two PMFs essentially perform like a single piece of PMF with adjustable equivalent lengths. Table 4.1 shows the 12 possible comb spacings ($\Delta\omega$) that can be obtained from the use of two pieces of PMFs, as well as the corresponding relationship between the equivalent length of PMF (L_e) and the passband frequencies of the MWP filter (Ω_0). In the experiment, length of the two PMFs, L_1 (11 m) and L_2 (55 m) are chosen such that all the 12 equivalent lengths are different and the resultant passbands are evenly distributed throughout the frequency range of interest (0-18 GHz).

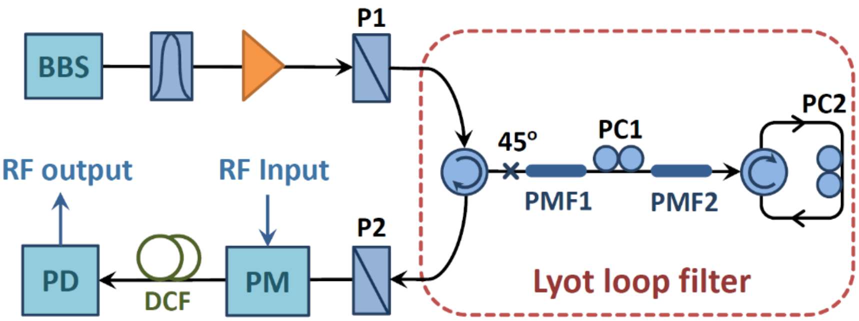

Figure 4.6. Experimental setup of the reconfigurable MWP multiband filter based on Lyot loop filter. BBS: broadband optical source; P1-P2: polarizers; PC1-PC2: polarization controllers; PMF1-PMF2: polarization maintaining fibers; PM: optical phase modulator; DCF: dispersion compensating fiber; PD: photo-detector.

Table 4.2. Twelve combinations of the two-PMF Lyot loop filter based MWP multiband filter (L_1=11 m, L_2=55 m)

Number	Length Combination	Equivalent PMF length (L_e, m)	Comb spacing ($\Delta\omega$, pm)	MWP Filter passband (Ω_0, GHz)
1	L_1	11	336.19	1.3
2	$2L_1$	22	168.09	2.6
3	$\lvert 2L_1-L_2 \rvert$	33	112.06	4.0
4	$\lvert L_1-L_2 \rvert$	44	84.04	5.4
5	L_2	55	67.24	6.7
6	L_1+L_2	66	56.03	8.1
7	$2L_1+L_2$	77	48.02	9.5
8	$\lvert 2L_1-2L_2 \rvert$	88	42.02	10.9
9	$\lvert L_1-2L_2 \rvert$	99	37.35	12.2
10	$2L_2$	110	33.62	13.6
11	L_1+2L_2	121	30.56	14.9
12	$2L_1+2L_2$	132	28.01	16.2

Figure 4.7 shows an optical comb with three interleaved comb spacings where the comb spacings are 28 pm, 67 pm and 168 pm. This situation can be regarded as three optical combs with different comb spacings appearing at the same time, making it possible to generate a MWP filter with three passbands simultaneously.

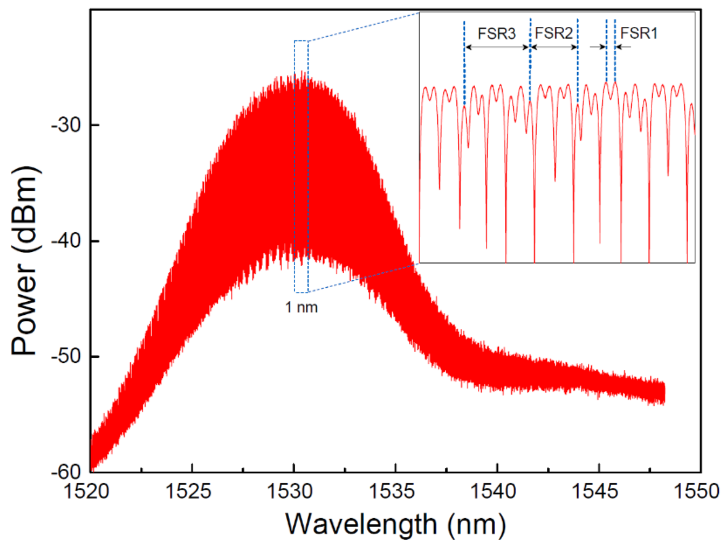

Figure 4.7. Measured optical spectrum of the second-order Lyot loop filter with 3 different comb spacings interleaving with each other. FSR_1= 28 pm, FSR_2= 67 pm and FSR_3=168 pm.

Frequency spectra of different passbands combinations from the simplified structure are shown in Figure 4.8. By adjusting the polarization rotation angle inside the Lyot loop filter, different comb spacing combinations can be obtained, resulting in various combinations of the number of passbands and passband frequencies in the multiband RF filter. In Figure 4.8(a), one single passband at 5.4 GHz is observed with the MWP RF filter working in a single-band state, while in Figure 4.8(b) two passbands at 8.1 GHz and 16.2 GHz are recorded with the MWP RF filter working as a dual-band filter. Figure 4.8(c) to 4.8(f) show the measured results of multiple passbands, the passband numbers are adjusted so that the MWP RF filter simultaneously can have 3, 5, 7, and 12 passbands, respectively. All 12 passband frequencies calculated in Table 4.2 are observed at the same time in Figure 4.8(f), which are evenly distributed between 1.3 GHz to 16.2 GHz. The 12 passbands are equally separated with a frequency spacing of 1.3 GHz. Furthermore, all the passbands can be switched off such that the MWP filter can work as an all-block filter. In this demonstration, the length of the DCF is increased to 10.4 km, which results in narrower 3-dB bandwidth of the generated passbands. Sidelobe suppression is over 35 dB for all the passbands, and all the passbands have very clean and sharp passband profiles, providing good filter selectivity.

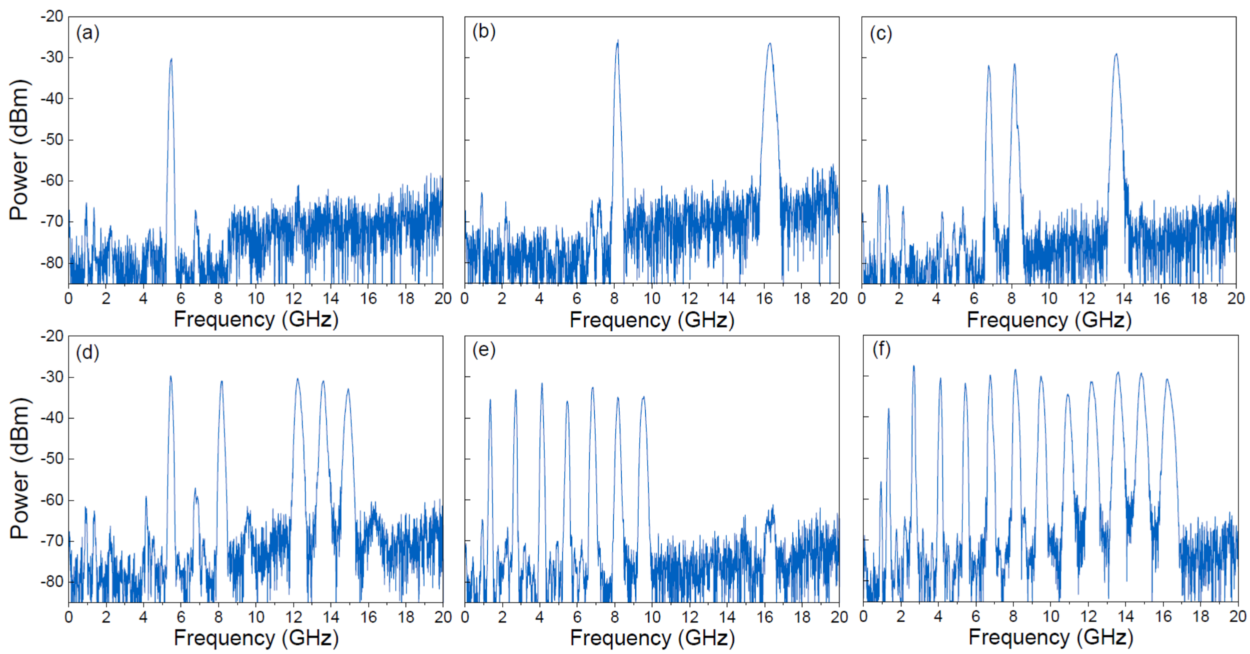

Figure 4.8. Measured frequency spectra of the reconfigurable MWP multiband filter with different passband combinations. (a) One single passband at 5.4 GHz. (b) Two passbands at 8.1 GHz and 16.2 GHz. (c) Three passbands at 6.7 GHz, 8.1 GHz and 13.6 GHz. (d) Five passbands at 5.4 GHz, 8.1 GHz, 12.2 GHz, 13.6 GHz, and 14.9 GHz. (e) Seven passbands from 1.3 GHz to 9.5 GHz. (f) Twelve passbands from 1.3 GHz to 16.2 GHz (All twelve passbands shown in Table 4.2).

4.2.4 Summary

In summary, a MWP multiband filter with reconfigurable passband numbers and center frequencies is experimentally demonstrated. Up to 12 different passbands can be selected simultaneously and are evenly distributed from 0 to 10 GHz. The adjustment of passband numbers and center frequencies are achieved through polarization state adjustment in the two-stage Lyot loop filter. Sidelobe suppression of all the passbands is over 30 dB and each passband has a 3-dB bandwidth of 200 MHz with a sharp and clean bandpass profile, providing good filter selectivity. Moreover, the proposed MWP multiband filter can work either as an all-block, single-band, or multiband RF filter with adjustable multi-passbands combinations. A simplified structure is also introduced to implement the 12 simultaneous passbands, but with a much narrow 3-dB bandwidth and better filter selectivity. This design significantly increases the number of passbands that can be achieved with a MWP multiband filter as well as providing exceptional operation flexibility.

4.3 Tunable and Switchable Multiband Filter based on Lyot-MZI scheme

In the previous section, a big step is taken forward through the use of a two-stage Lyot loop filter scheme, that a switchable MWP multiband filter with up to 12 simultaneous passbands is achieved. However, the passbands can only be configured to 12 specific pre-designed frequency channels, tuning of the center frequencies of the passbands require the adjustment of the length of the PMF, which is not practical in real world applications. To fulfill the functionality and flexibility needed in dynamic multiband systems, continuously tuning of the multiple passbands to cover a wide frequency range is highly desired and will significantly advance filter capability to the next level.

In this section, we present a MWP multiband filter with continuously tunable and reconfigurable passbands. The passband frequencies are continuously tunable and can cover a large frequency range without any dead-points, while the number of simultaneous passbands is adjustable from zero to seven. The proposed scheme is based on the utilization of a tunable Mach-Zehnder interferometer (MZI) and a reconfigurable Lyot loop filter to generate high-order optical comb with variable comb spacing. As a result, the MWP multiband filter can operate in several states through the same system setup --- single-band state, all-block state, dual-band and multiband states --- all with tunable and reconfigurable passbands.

4.3.1 Principle and Experimental Setup

The demonstrated MWP filter is also based FIR introduced in Chapter 3. The tunable MZI brings the continuous tunability to the RF filter design and the Lyot loop filter provides the reconfigurability of the number of simultaneous passbands. Figure 4.9 shows the schematic diagram of the proposed MWP multiband filter based on finite impulse response filter scheme, that a finite set of delayed and weighted signal taps are combined to implement the desired filter response. A broadband source is used as the light source and spectrally reshaped by a 30-nm wide optical Gaussian filter. The reshaped broadband source is then spectrally sliced by a tunable MZI and a Lyot loop filter to generate optical frequency comb with variable comb spacings. In this way, the tunable MZI provides continuously tunability of the comb spacings, while the Lyot loop filter enables dynamic selection of passband channels. Each of the comb lines works as a single tap, which is temporally delayed by the DCF and weighted by the Gaussian optical filter to construct the desired MWP filter response. The weighted and delayed signal is then fed into a photo-detector and converted back to a RF signal at the output. The comb spacings $\Delta\omega$ of the MZI and Lyot loop filter determine the carrier wavelength for each of the taps in the MWP multiband filter. For a system that has a fixed dispersion, passband frequency can only be adjusted by varying the frequency spacing of the filter taps ($\Delta\omega$), as described by Eq. (4.2) in the previous section.

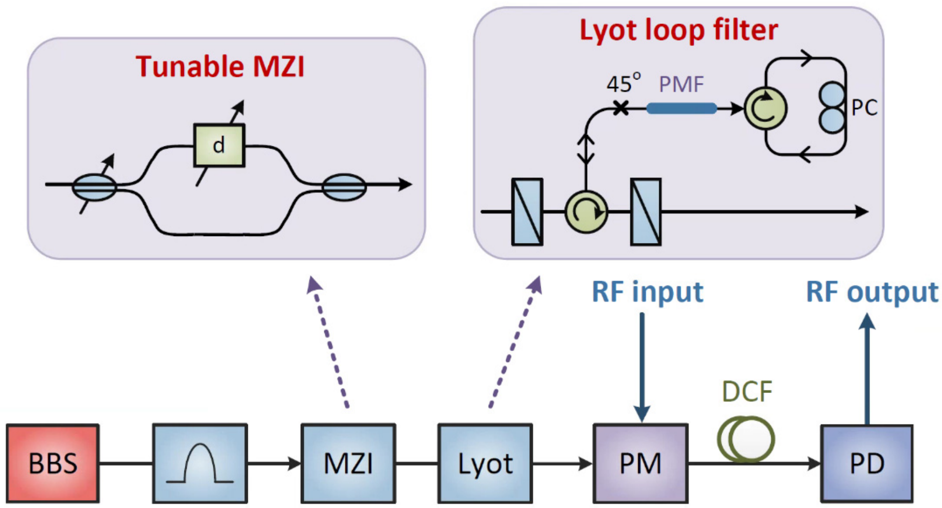

Figure 4.9. Schematic diagram of the tunable and reconfigurable MWP multiband RF filter. BBS: broadband light source; MZI: Mach-Zehnder interferometer; d: tunable temporal delay line; PC: polarization controller; PM: phase modulator; DCF: dispersion compensating fiber; PMF: polarization maintaining fiber; PD: photo-detector.

We first investigate the performance of the tunable MZI and its corresponding frequency response in the MWP filter by disabling the Lyot loop filter. As illustrated in the inset of Figure 4.9, the MZI is a modified two-branch interferometer, which consists of a tunable coupler at the input to adjust the power ratio of the two branches, and a tunable delay line to vary the path length difference between the two branches. A standard 50:50 coupler is used to combine the two branches for interference. Based on the path difference d between the two branches, the two beams arrive at the coupler with a phase difference such that different extent of constructive interference or destructive interference is resulted at each wavelength λ. The transmission function and the comb spacing of the resultant optical comb filter is determined by Eq. (4.4) and Eq. (4.5),

$$\varphi(\lambda) = \frac{2\pi n_e d}{\lambda} \tag{4.4}$$

$$\Delta\omega = \frac{2\pi c}{n_e d} \tag{4.5}$$

where n_e is the refractive index of the fiber used in the tunable MZI. Figure 4.10(a) shows the measured optical spectrum of the broadband source that is reshaped by a Gaussian optical filter and spectrally sliced by the MZI. A close-up look of a 1 nm portion of the optical comb is shown in Figure 4.10(b), showing a comb spacing of 65 pm. The corresponding RF response is shown in

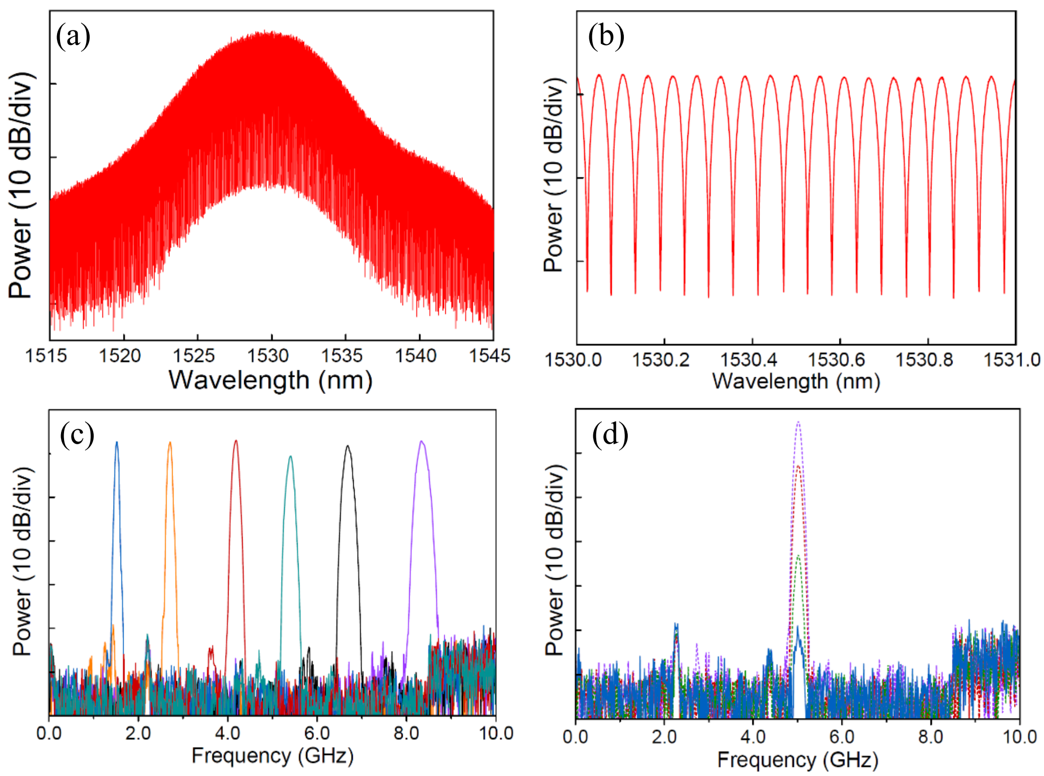

Figure 4.10. Mach-Zehnder interferometer based MWP single bandpass filter with continuously tunability and reconfigurability. (a) Measured optical spectrum of the Gaussian profile optical frequency comb generated from the MZI; (b) Close-up of the optical comb in 1 nm range with a frequency spacing of 65 pm; (c) Measured frequency response of the RF single bandpass filter tuned to different frequencies; (d) The passband can be adjusted between ON/OFF states.

Figure 4.10(c), where a single bandpass RF filter is observed and the center frequency is tunable over a wide frequency range by adjusting the comb spacing of the MZI through the tuning of the delay line. A tunable optical coupler with adjustable coupling ratios is used to vary the power ratio between the two MZI branches, such that the amplitude of the resultant passband is dynamically tunable over a 58 dB range, which essentially can go down to the noise floor --- switching off the channel, as shown in Figure 4.10(d).

While the tunable MZI generates a single passband filter and provides continuous tunability, system reconfigurability is provided by the Lyot loop filter. The operating principle of the Lyot Loop filter and its corresponding MWP filter are detailed introduced in the previous section, that two switchable passbands can be generated with a one stage Lyot loop filter. The proposed RF multiband filter utilizes the MZI-Lyot architecture to enable continuous tunability, multiband capability, and high reconfigurability of the passbands. The MZI is a tunable first order comb filter, while the Lyot loop filter is a reconfigurable second-order comb filter, thus, by cascading the MZI and Lyot loop filter together, a higher order comb filter with multiple comb spacings and reconfigurability can be achieved. As a result, the resultant multiple passbands will be highly flexible and dynamic.

4.3.2 Results and Discussion

Figure 4.11 shows the measured tuning results of the MWP multiband filter, seven passbands are generated at the same time and marked as #1 to #7. Passbands #1 and #2 are generated directly from the comb lines of Lyot loop filter, as shown in the previous section. Passband #5 is generated directly from the tunable MZI, while passbands #3, #4, #6 and #7 are generated by the addition and subtraction of the cascaded MZI and Lyot loop filter, as described by Table 4.3. As shown, passband #4 and #6 are generated from the interacting between the first passband from Lyot loop filter and MZI (Lyot1: #1 and MZI: #5), such that the frequency spacing between #4 (#6) and #5 is 1.35 GHz, which is explained as MZI – Lyot 1 and MZI + Lyot 1, as shown in Table 4.3. Correspondingly, passband #3 and #7 are the cascading results of the second passband of Lyot loop filter and MZI (Lyot2: #2 and MZI: #5), which has a frequency spacing of 2.70 GHz away from passband #5 and is explained as MZI − Lyot 2 and MZI + Lyot 2. The relationship between all seven passbands and their corresponding comb spacings generated from the cascaded MZI and Lyot loop filter are summarized in Table 4.3, where the seven passbands are set to be evenly distributed within a 10 GHz range with the same frequency spacing of 1.35 GHz, as indicated in Figure 4.11(a). Since passband #5 is generated from a continuously tunable MZI, any passbands related to #5 are also continuously tunable, which are passbands #3, #4, #5, #6 and #7. Figure 4.11(c) to 4.11(e) show the measured tuning performance, the right five passbands (#3 to #7) generated from the MZI are continuously tuned over 20 GHz. The MSSR for all the passband are over 35 dB and the average 3-dB bandwidth is about 100 MHz, resulting a passband Q-factor of 200 at 20 GHz. The frequency spacing between each passband among the five tunable passbands is kept the same (1.35 GHz), which is determined by the length of the PMF inside the Lyot loop filter. Figure 4.11(b) shows the measured relationship between the passband frequency and the time delay between the two branches of the MZI. The maximum frequency tuning range is up to 35 GHz, and is determined by the adjustable range of the delay line.

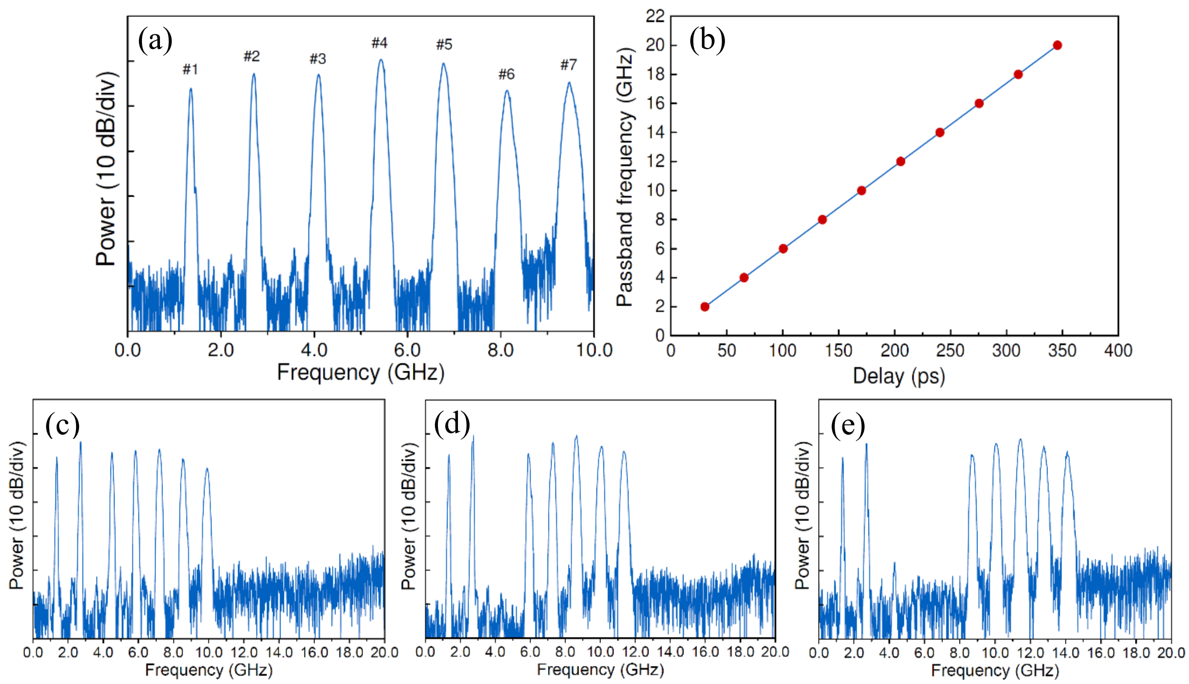

Figure 4.11. Demonstration of the continuous tunability of the RF multiband filter. Measure frequency response of the multiband filter. (a) Seven single passbands are evenly distributed from 1.35 GHz to 9.45 GHz, with the same frequency separation of 1.35 GHz between each adjacent passband; (b) Passband frequency tuning in response to the time delay between the two branches of the MZI; (c)-(e) The right five passbands are continuously tuned within a frequency range of 20 GHz.

Table 4.3. Seven passbands of the MZI-Lyot filter based MWP multiband filter

Number	Optical comb combination	Tap frequency spacing ($\Delta\omega$, pm)	Passband frequency (Ω_0, GHz)
#1	Lyot 1	304.2	1.35
#2	Lyot 2	152.1	2.70
#3	MZI – Lyot 2	101.4	4.05
#4	MZI – Lyot 1	76.0	5.40
#5	MZI	60.9	6.75
#6	MZI + Lyot 1	50.8	8.10
#7	MZI + Lyot 2	43.5	9.45

Passband reconfigurability is achieved by adjusting the polarization rotation angle $\Delta\theta$ inside the Lyot loop filter. Since each of the passband generated from the Lyot loop filter can be independently switched ON or OFF, any passbands generated from Lyot 1 and Lyot 2 are also reconfigurable. From Table 4.3, one can see that all the passbands except #5 are related to the Lyot loop filter and, therefore, are all ON/OFF switchable. While passband #5 is also switchable itself through the control of the tunable optical coupler. Furthermore, since the right five passbands (#3 to #7) are continuously tunable, these passbands can be tuned to the frequencies such that they are overlapping with passbands #1 or #2 --- two passbands at the same frequency, acting like one single passband. Figure 4.12 shows the RF multiband filter with different numbers of simultaneous passbands. The initial center frequencies of the passbands are set to be evenly distributed within 0 to 10 GHz, and the numbers of simultaneous passband are adjustable from six to three. Figure 4.12(a) to 5d are achieved by tuning the right five passbands (#3 to #5) to the same frequencies as the Lyot 1 and Lyot 2 (#1 & #2), such that two or three passbands are overlapping at the same frequency, consequently varying the simultaneous numbers of passband. In particular, in Figure 4.12(a) passbands #2 & #3 are at the same frequency, while in Figure 4.12(b) passbands #1 & #3 and passbands #2 & #4 are both overlapping. The passband overlapping in RF domain is resulted because the optical comb spacings generated from the cascaded MZI-Lyot filter and the Lyot loop filter itself are the same. Furthermore, the simultaneous numbers of passbands is adjustable by switching off Lyot 1 or Lyot 2, such that a quad-band filter is resulted, with one passband being fixed and the other three are tunable. By doing this the frequency spacings of the continuously tunable passbands is adjusted between 1.35 GHz and 2.70 GHz, as shown in Figure 4.12(e) and 4.9(f), respectively. Since both the MZI and Lyot loop filter can be switched off separately, the number of simultaneous passbands can be adjusted to any value between zero and seven. The passbands selection is based on polarization state adjustment, high-speed and programmable tuning of the passbands can be potentially achieved up to gigahertz speed with the use of an electrically tunable polarization controller or through optical nonlinear polarization rotation effect [45-48]. All the passbands show consistent performance with uniform and sharp passband profiles, and the passband qualities are well maintained during both the tuning and reconfiguring processes.

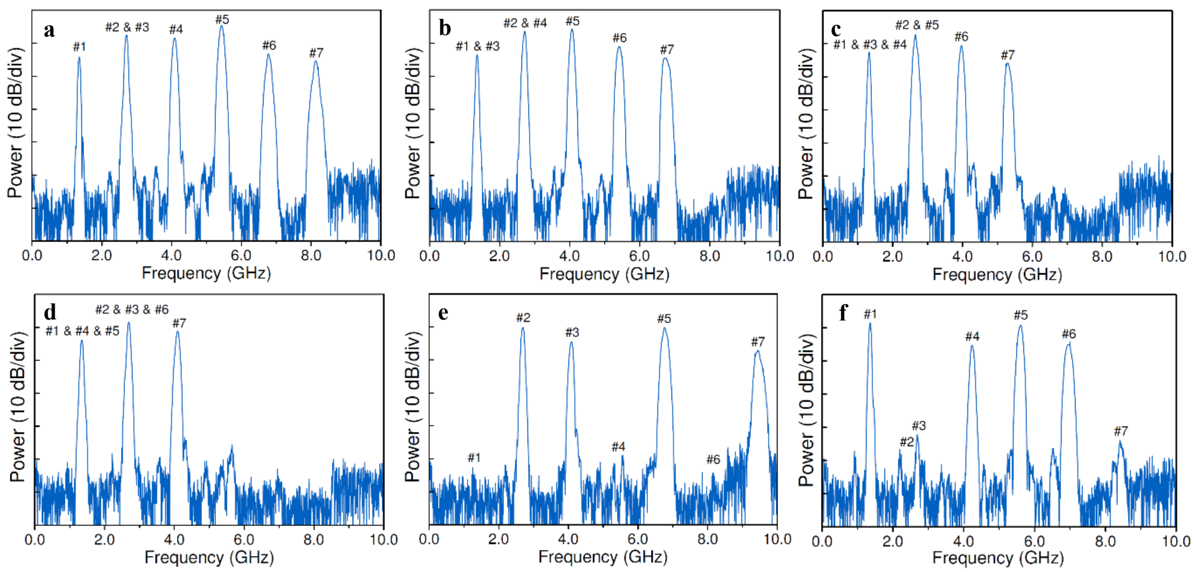

Figure 4.12. Demonstration of the passband reconfigurability of the multiband RF filter. The simultaneous passband number is adjusted from three to seven, with different frequency combinations. (a) Six passbands at 1.35 GHz, 2.70 GHz, 4.05 GHz, 5.40 GHz, 6.75 GHz and 8.10 GHz. (b) Five passbands at 1.35 GHz, 2.70 GHz, 4.05 GHz, 5.40 GHz and 6.75 GHz. (c) Four passbands at 1.35 GHz, 2.70 GHz, 4.05 GHz and 5.40 GHz. (d) Three passbands at 1.35 GHz, 2.70 GHz and 4.05 GHz. (e) Four passbands when Lyot 1 (@1.35 GHz) is switched off. (f) Four passbands when Lyot 2 (@2.70 GHz) is switched off.

Another factor that determines passband frequencies, bandwidths and frequency spacings of the proposed multiband filter is the amount of dispersion, as shown in Eq. (4.2) and Eq. (4.3).

Figure 4.13 shows the above tuning performance of the multiband filter while the length of the DCF is changed, where the orange filter profiles are captured when a piece of 10.2-km DCF is used and the blue ones are based on a piece of 6.1-km DCF. As shown in Figure 4.13(a), with the same MZI and Lyot loop filter, the seven evenly distributed passbands are spanned to a 14 GHz range instead, and the frequency spacing between two adjacent passbands is increased to 1.9 GHz. The average 3-dB bandwidth of the passbands is adjusted from 100 MHz (orange) to 180 MHz (blue). With the same DCF length as in Figure 4.13(a), Figure 4.13(b) shows the corresponding result when the right five passbands are continuously tuned through temporal adjustment in the MZI. The adjustment of the dispersion and length of PMF of the system is to match the initial design requirements of various applications, and the proposed filter tunability and reconfigurability are not relying on any physical change of the components. Furthermore, the maximum simultaneous passband number can be further increased by using a two-stage Lyot loop filter [56], or cascading another optical comb filter to have more comb spacing combinations.

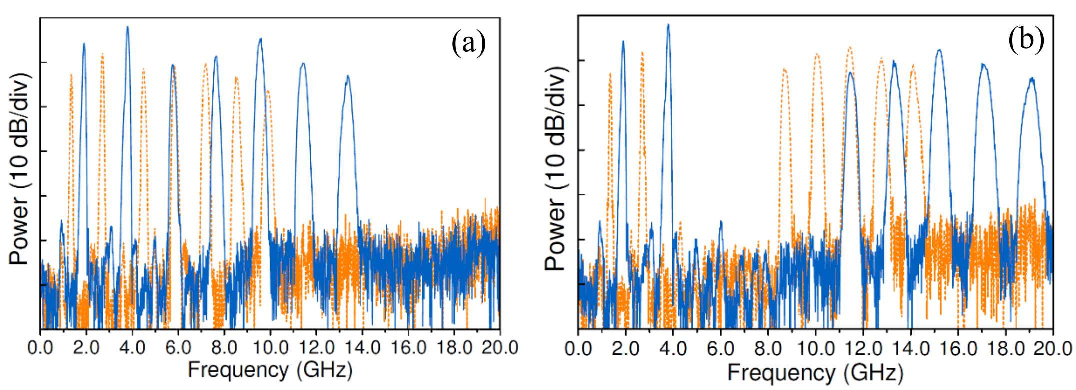

Figure 4.13. Passband bandwidth adjustment of the multiband RF filter. The bandwidths of the passbands are broadened with the use of shorter dispersion compensating fiber. Orange: with the use of a piece of 10.2-km DCF; Blue: with the use of a piece of 6.1-km DCF.

4.3.3 Summary

In summary, a continuously tunable and highly reconfigurable MWP multiband filter is proposed and experimentally demonstrated. The number of simultaneous passbands is adjustable between zero and seven, functioning as an all-block, single-band, dual-band, or multiband filter, while the passband frequencies are continuously tunable over a 35 GHz range. The scheme utilizes a cascaded MZI and Lyot loop filter architecture, such that various optical comb spacing combinations are obtained for the implementation of the MWP multiband filter. The MSSR of all the passbands are over 35 dB with sharp and uniform passband profiles, providing good filter selectivity. The MWP multiband filter shows stable and consistent performance during the tuning and reconfiguring processes. Furthermore, the proposed work demonstrated a general methodology to implement MWP multiband filters through cascading multiple optical comb filters with various functionalities. Compared to the state-of-the-art RF multiband filters [30], this design significantly increases the simultaneous number of passband as well as providing exceptional operation flexibility.

4.4 Fully Tunable and Reconfigurable Multiband Filter based on Cascaded MZI Scheme

In the previous section, the demonstrated MWP filter has both fixed and tunable passbands, which is suitable for a multiband system with both fixed and dynamic channels. In general, Lyot loop filter structure provides better stability in terms of the center frequency of the generated passbands, since it is only determined by the length of the PMF, which is very stable. However, in other scenarios where all the channels are changing over time, a multiband filter with fully tunable passbands is required.

In this section, we present a fully tunable and reconfigurable MWP multiband filter with up to 13 simultaneous passbands. The number of passbands is adjusted from 1 to 13, while the passband frequencies of all the passbands are continuously tunable from 0 to 20 GHz with no blind spot. The proposed multiband filter is based on the generation of high order optical frequency combs from three cascaded MZIs. The cascaded MZI structure is compact, and has been widely used in various integrated optical devices, making it an excellent candidate for potential integration. To the best of our knowledge, this is the first demonstration of a RF multiband filter to achieve a large number of simultaneous passbands with such continuously tunability and reconfigurability. Furthermore, all the passbands have 35 dB sidelobe suppression, providing good filter selectivity.

4.4.1 Principle and Experimental Setup

The proposed scheme is based on the utilization of three cascaded tunable MZIs to generate high-order optical comb with variable comb spacings for implementing a MWP multiband filter, experimental setup is shown in Figure 4.14. A superluminescent diode (SLD) is used as the optical source to generate broadband light, and is then spectrally sliced by three cascaded MZIs. An optical frequency comb consists of a large number of comb lines is obtained, which works as a multi-wavelength optical carrier. The RF input signal is then modulated onto the comb lines through an EOM, where each line in the comb contains a copy of the RF input signal. The modulated signal is then launched into a piece of wavelength dependent DCF such that each of the copies of the RF signal is properly delayed in time. A 4-nm optical filter with Gaussian profile is used after the SLD to weight each of the comb lines, essentially weighting the amplitudes of the RF signal copies. The weighted and delayed copies are then added up and converted back to an RF signal through a photo-detector. A finite impulse response RF filter with a bandpass profile can be obtained.

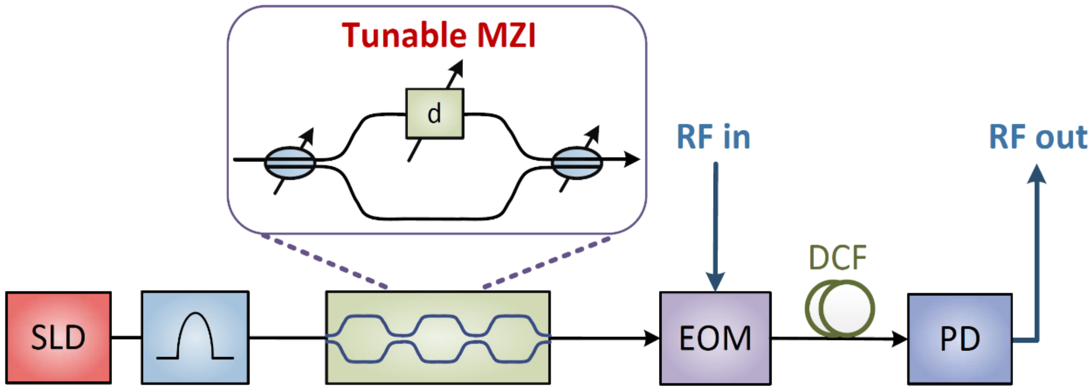

Figure 4.14. Experimental setup of the MWP multiband filter based on cascaded MZIs. SLD: Superluminescent diode; MZI: Mach-Zehnder interferometer; EOM: Electro-optic modulator; DCF: dispersion compensating fiber; PD: photo-detector. (b) Measured optical spectrum of the cascaded MZIs.

Since center frequency of the passband is determined by Eq. (4.2), in order to generate multiple tunable passbands at the same time, an optical frequency comb with multiple tunable comb spacings is required. This is achieved by cascading three MZIs in series and simultanously generating multiple length differences. The path length difference of the first MZI is d_1, such that the generated comb spacing is $\Delta\omega = 2\pi c/nd_1$. By cascading a second MZI with a branch length difference of d_2 and adjusting the coupling ratios of the tunable couplers, four length difference combinations can be achieved at the same time, which are d_1, d_2, $d_1 + d_2$, and $d_1 - d_2$. As a result, four different comb spacings are obtained which corresponds to four RF passbands at different center frequencies. When three MZIs are cascaded, up to 13 different combinations can be obtained and resulting in 13 different passbands, as summarized in Table 4.4. Figure 4.15 shows an example of the optical comb generated by the three cascaded MZIs. A tunable optical coupler with adjustable coupling ratio is used to vary the power ratio between the two MZI branches to achieve different extents of interference, such that amplitude of the resultant passband can be adjusted. Furthermore, each of the MZIs can be independently switched on/off, such that the simutanoues passband number can be flexibly adjusted to obtain various combinations. Since the length differences (d_1, d_2 and d_3) can be continously adjusted by the tunable delay lines inside each MZI, all the resulted passbands are continously tunable in frequency. The passbands can be tuned to match with different frequency channels, therefore, a highly reconfigurable and continuously tunable MWP multiband filter is achieved.

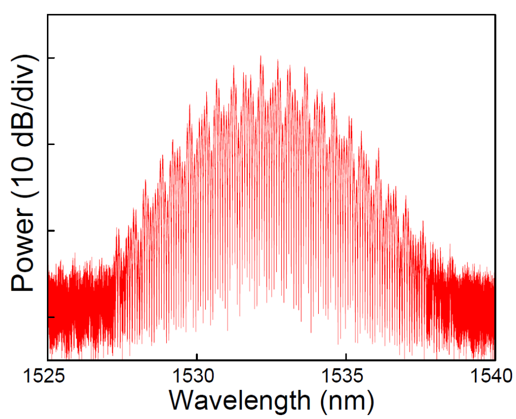

Figure 4.15. Measured optical spectrum of the cascaded MZIs, which is a high-order optical frequency comb consists of multiple comb spacings.

Table 4.4. Passband combinations of the proposed MWP multiband filter when three MZIs are cascaded in series

Number	One MZI	Two MZIs	Three MZIs
1			$d_1 - d_2 - d_3$
2		$d_1 - d_2$	$d_1 - d_2$
3			$d_1 - d_2 + d_3$
4			$d_1 - d_3$
5	d_1	d_1	d_1
6			$d_1 + d_3$
7			$d_1 + d_2 - d_3$
8		$d_1 + d_2$	$d_1 + d_2$
9			$d_1 + d_2 + d_3$
10			$d_2 - d_3$
11		d_2	d_2
12			$d_2 + d_3$
13			d_3

4.4.2 Results and Discussion

In the experiment, a frequency-sweeping signal from an electrical network analyzer is used as the RF input for measuring the frequency response of the proposed MWP multiband filter. The measured results of different passband combinations are shown in Figure 4.16. By adjusting the tunable couplers inside the three MZIs (i.e. enabling/bypassing some of them), the MWP filter is reconfigured to have various simultaneous passbands. A single bandpass filter at 5.4 GHz is shown in Figure 4.16(a), which is achieved by setting the tunable couplers inside MZI2 and MZI3 to be 100:0 such that these two interferometers are bypassed. As a result, only one comb spacing is generated from MZI1 and a single bandpass filter is obtained. When only MZI3 is bypassed, four passbands are observed as shown in Figure 4.16(c). The four-passband filter can turn into a three-passband filter by adjusting the tunable delay line in MZI2, such that two of the passbands are tuned to the same frequency and are overlapping with each other, as shown in Figure 4.16(b).

When all the three MZIs are employed, all of the thirteen passbands shown in Table 1 are obtained. The passbands can be set to be evenly distributed from 0 to 8 GHz with same frequency spacings of 0.6 GHz, as indicated in Figure 4.16(f). On the other hand, the passbands can be adjusted to overlap with each other, such that various passbands combinations are achieved. Figure 4.16(d)-4.16(e) show the results when the MWP filter is configured to have five and eight passbands, providing flexible operation reconfigurability. The thirteen passbands can also be tuned to spread across a 20 GHz range. Figure 4.17(a) shows an example of an eleven-passband configuration across a 20 GHz bandwidth. Since the center frequencies of the passbands are determined by the length differences between the two branches of the MZIs, all the demonstrated passbands' frequency can be continuously tuned by adjusting the tunable delay lines insides each of the MZIs. As shown in Figure 4.17(b), all the thirteen passbands are tuned to different frequency positions that are not on fixed preset channels. The frequency tuning range is governed by the adjustable range of the delay lines. In our setup, a 17.5 ps time delay can result in a 1 GHz frequency tuning (shown in Figure 4.17(c)), and up to 35 GHz frequency tuning is achieved with the use of a 600 ps tunable delay line. Furthermore, all the passbands show good filter selectivity, with sharp bandpass profiles and over 35 dB sidelobe suppression.

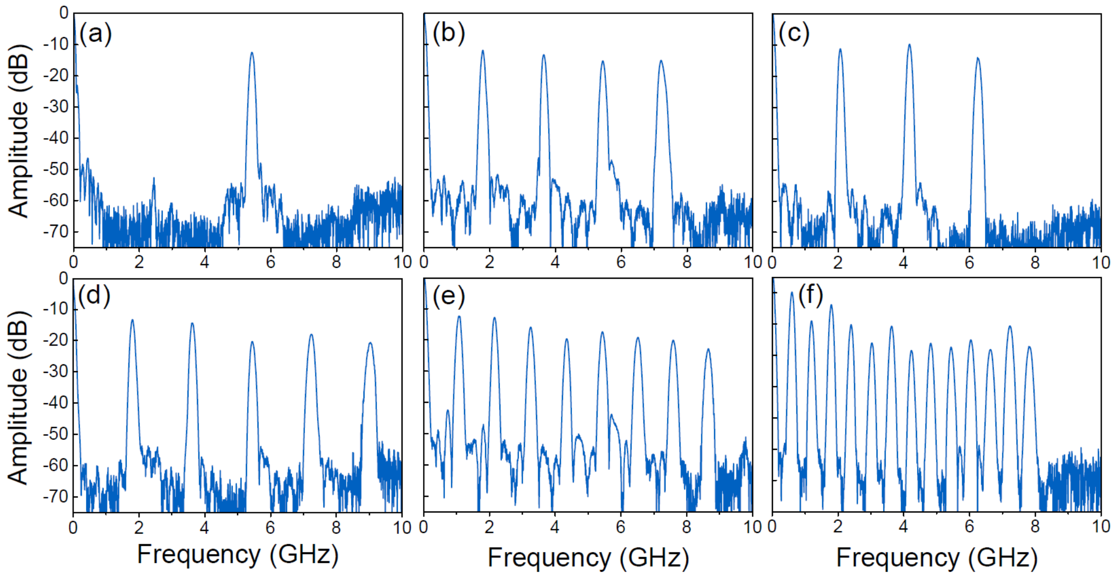

Figure 4.16. Measured RF amplitude response of the MWP multiband filter with different passband combinations. (a) One single passband at 5.4 GHz. (b) Four passbands from 1.8 to 7.2 GHz. (c) Three passbands at 2.0 GHz, 4.1 GHz and 6.2 GHz. (d) Five passbands from 1.8 to 9.0 GHz. (e) Eight passbands from 1.0 to 8.7 GHz. (f) Thirteen passbands from 0.6 to 8.0 GHz.

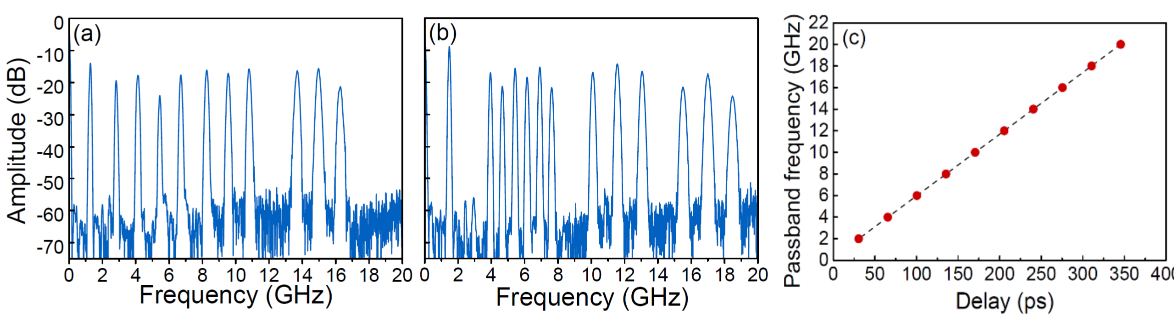

Figure 4.17. Demonstration of continuous tunability of the MWP multiband filter. (a) Eleven passbands from 1.2 to 16.3 GHz. (b) All the thirteen passbands are tuned to unevenly spread across a 20 GHz range. (c) Passband frequency tuning in response to the time delay.

4.4.3 Summary

In summary, a fully tunable MWP multiband RF filter with up to 13 simultaneous passbands is demonstrated based on three cascaded MZIs. The number of simultaneous passbands is adjustable from 1 to 13, and the passband frequencies are continuously tunable over 20 GHz, providing the flexibility to dynamically to select different frequency channels. To date, the proposed MWP multiband RF filter has the largest number of simultaneous passband – a total of 13, with an exceptional tunability and reconfigurability, as well as uniform and good filter selectivity. Furthermore, since MZI is a well developed structure in photonic integrated circuit [85,86], the proposed scheme has great potential to be integrated with multiple cascaded on-chip MZIs. A photonics based programmable RF processor can be potentially achieved with an integrated 2D waveguide structure as introduced in [87], which could dramatically improve and RF signal processing functionality and meanwhile reduce the size of the system.

4.5 Summary

In this chapter, we demonstrated MWP multiband filters based on three different approaches – Lyot loop filter structure, Lyot-MZI structure and cascade MZIs structure. The simultaneous passband number is significantly increased to up to 13, which is achieved through high-order optical frequency combs with multiple comb spacings. Switchable, reconfigurable and fully tunable passbands are experimentally demonstrated, providing extraordinary operating flexibility for dynamic RF systems. All the demonstrated MWP multiband filters show stable and consistent performance during the tuning and reconfiguring processes, with up to 40 dB MSSR and sharp filter profiles. Compared to the state-of-the-art RF multiband filters [30], this design significantly increases the simultaneous number of passband as well as providing exceptional operation flexibility. The proposed multiband RF filter could dramatically enhance multiplexing capabilities, functionality, and performance of multiband RF systems, where the channel frequencies could dynamically adapt to diverse environments with various desired functions and spectral availability. Furthermore, the use of different combinations of tunable MZI and reconfigurable Lyot loop filter demonstrates a general methodology for MWP multiband filter implementation, which has instructive values for existing MWP filter techniques.

CHAPTER 5

BROADBAND AND RECONFIGURABLE RF SPECTRAL SHAPER AND EQUALIZER

5.1 RF Spectral Shaper and Equalizer

RF signal processing is ubiquitous in a number of field where arbitrary shaping of the RF spectrum is extremely desired to achieve various signal processing functions. A reconfigurable RF spectral shaper with the capability to flexibly manipulate a wide range of RF components is extremely power as a universal RF processor. Arbitrary shaped pulses and waveforms are widely used in various applications, including wireless and optical communications, radar and satellite systems, and biological imaging and spectroscopy [88,89]. Furthermore, due to the nature of electronics, RF devices and systems always have frequency dependent performance, that the gain or loss of the components varies a lot at different frequency bands. For example, the most commonly used components – RF cables and amplifiers – have uneven loss/gain curves over frequencies, and varies dramatically between different brands and manufactures [94-96]. When designing a system consists of a series of components, the optimization of system design can only achieve a relative narrow operation bandwidth, the uneven performance and limited bandwidth greatly hinder their applications from wideband systems. Similar situation happens in multiband communication networks, where multiple radio channels at different frequencies are transmitted at the same time and the carrier frequencies may change dynamically over time [58-60]. The uneven losses during the transmissions would result in tremendous received power differences, and thus greatly deteriorate the received signal quality. In these cases, a broadband and reconfigurable RF spectral shaper or equalizer is required to compensate and balance the frequency dependent gain/loss for better system performance. The need is clear and urgent, however, there is still no promising solution so far.

Current existing RF spectral shaper and equalizers are all electronics based, usually achieved through the use of a wideband tunable attenuator plus a fixed bandpass/bandstop filter [96]. By adjusting the attenuation coefficient, frequency response curves with different slopes are achieved over a relative narrow bandwidth. However, the available functions are very limited that only linear and first-order parabolic signal processing functions can be obtained. Furthermore, since the electronic devices are in general lack of reconfigurability, the processing functions are either fixed or can only be slightly adjusted. These existing approaches are limited for compensating linear gain/loss in RF cables and certain systems, while a more comprehensive RF spectral shaper with arbitrary processing functions and multiple control points over a wider frequency range are desired for versatile applications. Although the capability to flexibly manipulate a wide range of RF spectral components is extremely desired, spectral shaping using RF electronics is very challenging due to its tight design criteria to satisfy a wide range of frequency range as well as its limited tuning and reconfiguring abilities. Therefore, RF electronics can only provide very limited shaping functions and can hardly be tuned, such as limited gain slope control, bandpass filtering, and pulse superimposing [114]. The key component for achieving such functionality is a reconfigurable multiband filter, which consists of multiple tunable and reconfigurable passbands – working as the multiple control points. However, this kind of filter is extremely challenging to achieve through conventional RF electronic technique due to the lack of reconfigurability; in addition, it is also very difficult to simultaneously satisfy the design parameters for multiple passbands over a wide frequency range [61-65]. A RF multiband filter with flexible passband reconfigurability and wide frequency tuning range is the key for implementing the desired RF spectral shaper.

Microwave photonics technique has attracted considerable attentions to achieve unique functions and enhancements on RF systems, thanks to its unique properties like wide bandwidth and flexible tunability, photonics matches the flexibility requirement urgently needed in current and future RF systems. Among these, tunable MWP filter is always an active topic and various schemes have been successfully demonstrated, as introduced in the previous chapters. However, there is still no successful demonstration of photonics based RF spectral shaper due to the challenge to simultaneous generate multiple tunable and reconfigurable passbands. MWP arbitrary pulse shaping and waveform generation techniques have been demonstrated by line-by-line spectral shaping of optical frequency comb through spatial light modulator [90], on-chip spectral shaper [91] or 2D ring resonator arrays [92], and frequency-to-time mapping in a dispersive medium [93]. Through these approaches, arbitrary pulse and waveform generation is usually achieved by spectrally shaping the optical frequency combs and then mapping them into time domain, which is a signal generation approach instead of processing an existing RF signal, and the demonstrated functions are not suitable for equalization purpose. Direct RF spectrum shaping would be the most efficient and straight forward way to achieve the pulse shaping, however, this requires the capability to process the broadband RF components, which is still quite challenging. Although microwave photonic signal processing technique has shown its enormous potential, the unique advantages from photonics have not been fully explored and developed. Overall, both the electronics and photonics based existing approaches cannot fulfill the functionality of a highly reconfigurable RF equalizer, where flexible gain/loss equalization over a wide range of frequency is desired.

With the powerful MWP filters demonstrated in the previous chapters, we are able to separately control the frequency components over a wide frequency range through the multiple tunable passbands, which enables us the capability for spectral shaping and equalization purpose. In this chapter, for the first time we present a photonics based RF spectral shaper with highly reconfigurable functionalities. Wideband and flexible spectrum shaping and equalization functions are achieved through the use of a highly tunable and reconfigurable MWP multiband filter. The RF spectral shaper is first tested as an equalizer for broadband equalization purpose, then the functionality and performance of is tested through arbitrary pulse shaping. The demonstrated RF spectral shaper shows extraordinary operation flexibility that it can be switched between different signal processing functions.

5.2 Photonic Implementation based on a MWP Multiband Filter

As mentioned in the previous section, the key to implement a highly reconfigurable RF spectral shaper is to generating multiple flexible passbands with wide frequency tuning range. The proposed photonics based approach is achieved through a tunable MWP multiband filter and its addition/subtraction interaction with an all-pass response. The system setup is shown in Figure 5.1, a multi-wavelength optical comb works as the optical carrier, which is generated from a broadband light source (BBS) and cascaded Mach-Zender interferometers (MZI). Each MZI consists of a tunable coupler and a tunable delay line, such that the amplitude and the wavelength spacing of the multi-wavelength optical comb can be adjusted. A waveshaper is used to reshape the overall spectral profile of the 4-nm multi-wavelength optical comb for fine-tuning of the equalization curves. The RF input signal is then modulated onto this multi-wavelength carrier through an EOM. The modulated signal is then split into two branches -- a bandpass response branch and an all-pass response branch. As shown in Figure 5.1, the upper branch consists a piece of DCF which provides linear time delays among different carriers (taps), then RF bandpass filter response is formed in the photo-detector based on the finite impulse response. While in the bottom branch, a piece of single-mode fiber (SMF) is used to match the lengths of the two branches, and simply forms an all-pass response since the dispersion of the SMF is unneglectable compared with the DCF. Then the all-pass branch and the bandpass response are combined in a balanced photo detector (BPD), where an optical tunable attenuator and delay line are used to precisely adjust the amplitude and phase of the two branches before the balanced detection. The combination of the FIR filtering response and the all pass response are used to shape the RF spectrum of the input signals, since the setup is highly reconfigurable, arbitrary shaping of the RF spectrum is achieved at the output.

Arbitrary spectral shaping in RF domain requires the capability of manipulating the RF frequency components over a wide frequency range. The number of the control points determines the reconfigurability of the RF spectral shaper, multiple adjustable control points are desired to flexibly control the amplitudes at different frequency bands, which is the primal limitation of

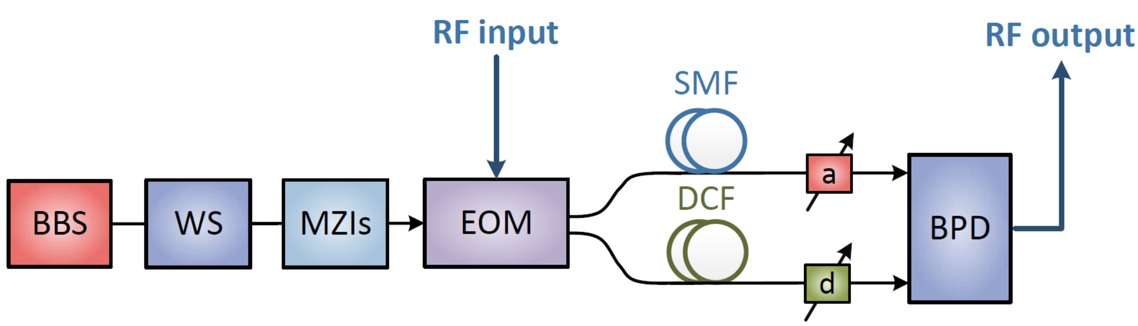

Figure 5.1. Schematic diagram of the photonics based reconfigurable RF spectral shaper. BBS: broadband source; WS: wave shaper; MZI: Mach-Zehnder interferometer; EOM: electro-optic modulator; SMF: single mode fiber; DCF: dispersion compensating fiber; BPD: balanced photo-detector.

electronics based solutions. In order to have multiple control points, a MWP multiband filter is implemented in the proposed scheme that 4 tunable and reconfigurable passbands are generated through the use of two cascaded tunable MZIs and work as the control points. For a microwave photonic FIR filter, the center frequency of the passband (Ω_0) the can be described as Eq. (5.1),

$$\Omega_0 = \frac{2\pi}{\beta_2 L_D \Delta\omega} \tag{5.1}$$

$$\delta\Omega_{3dB} = \frac{\sqrt{8ln2}}{\beta_2 L_D \delta\omega} \tag{5.2}$$

where β_2 and L_D are the group velocity dispersion and length of the DCF, and $\Delta\omega$ is the frequency spacing between each filter taps (or optical carriers). Since the total dispersion is fixed in the system, the center frequency of the passband is solely determined by the spacing of the optical carriers, which can be controlled by adjusting the delay line inside the MZI. This multiband capability can be achieved by using high-order optical filter for comb generation, as introduced in the previous chapter. With the use of two cascade MZIs, an optical comb consists 4 different comb spacings can be generated at the same time, resulting in 4 passbands as the tunable control points. Furthermore, beside the center frequency, both the bandwidth and the profile of the control points can also be adjusted. The 3-dB bandwidth of the passbands ($\delta\Omega_{3dB}$) is determined by Eq. (5.2) when the dispersion slope of the DCF is neglected, where $\delta\omega$ represents the overall bandwidth of the optical comb. As shown, the 3-dB bandwidth of the MWP filter is inversely proportional to the overall bandwidth of the optical comb, which can also be adjusted through the wave shaper. The profile of the MWP filter passband is governed by the overall amplitude profile of the filter taps, an inverse Fourier transform can be performed to precisely tailor the amplitude and phase of each filter tap in wave shaper for generating desired passband profiles [97]. Gaussian, flat-top and chirped passband profiles have been demonstrated previously and can be used for different functionalities of the multiple control points [46]. As a result, multiple highly reconfigurable control points of the RF spectral shaper are achieved, with adjustable positions, bandwidths, profiles, as well as the overall counts. Instead of shaping the RF signals in optical domain, which is limited by the resolution of shaper (~10 GHz), the shaping function is directly realized by the highly reconfigurable frequency response in the RF domain.

5.3 Equalization Functions

In this section, the proposed RF spectral shaper is first tested as a RF equalizer to compensate the inconsistent frequency dependent gain/loss for a broadband RF system. The demonstrated functions include positive/negative linear slopes, parabolic and inverted parabolic responses, and high-order and multiple-peak equalizations.

5.2.1 Linear equalization curves

Various equalization functions can be achieved from different combinations of the multiple control points, including positive/negative linear compensations, parabolic and inverted parabolic equalizations, and high-order and multiple-peak equalizations. We first investigate the implementation of linear equalization curves, which are commonly applied for compensating linear losses in systems where large scale of waveguide or RF cables are used. When a Sinc-square spectral profile is applied to the optical comb, a triangular profile of the passband can be achieved such that the edge of the passband can be used as linear compensation curves. As shown in Figure 5.2(a), the 8-nm optical comb is reshaped to a Sinc-square profile through the wave shaper, and the corresponding profile of the generated passband is shown in Figure 5.2(b). As plotted in both linear (red) and log (blue) scale, a triangular passband with linear sloped passband edge is obtained, which is ideal for linear compensation application. In our demonstration, a single triangular bandpass filter is implemented by enabling one MZI in the system, and the all-pass branch is switched off by applying a large attenuation. This triangular bandpass filter is first located at zero frequency such that the right half of the passband can work as negative compensation curve. The bandwidth of the passband follows Eq. (5.2), and can be controlled by adjusting the bandwidth of the optical comb ($\delta\omega$) through the Wave shaper. As shown in Figure 5.3(a), linear compensating curves with different negative slopes are obtained when different bandwidth of the optical comb ($\delta\omega$) is applied. Similarly, positive compensation curves can be achieved by tuning the center frequency of the passband to a higher frequency, such that the left half of the passband can work as positive compensation curve, as shown in Figure 5.3(b). Both the positive and negative compensation curves are adjusted to cover different frequency ranges and up to 50 dB compensation depth are obtained.

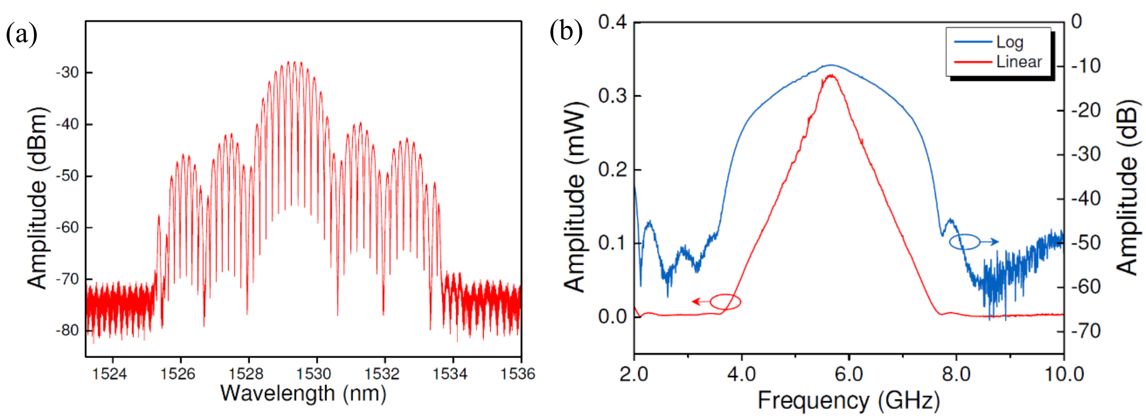

Figure 5.2. Triangular passband and its corresponding optical comb spectrum with a Sinc-square profile.

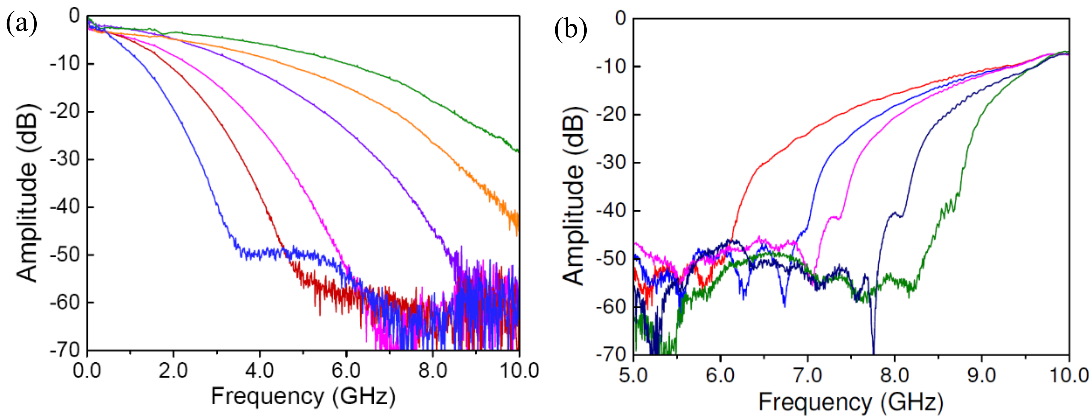

Figure 5.3. Linear negative and positive slope compensation curves.

5.2.2 Parabolic shaped equalization curves

Half-sine parabolic shaped equalizer are primarily used to compensate the gain variations in wideband devices or systems where the maximum amplification/attenuation occurring at the mid-band, such as travelling-wave-tube and solid-state amplifiers. Parabolic shaped compensation curves can be generated through single bandpass filters with Gaussian profile. In this scenario, the all-pass branch is also switched off and a phase modulator is used for EO conversion so that the baseband response is removed. As shown in Figure 5.4(a), different parabolic compensation curves covering various frequency ranges are achieved through the adjustment of the overall bandwidth of the optical comb ($\delta\omega$). The equalization curves are centered at 5.0 GHz, and can be tuned to different center frequencies by adjusting the optical tunable delay line in the tunable MZI. Meanwhile, inverted-half-sine parabolic can be achieved through the combination of two Gaussian passbands (two control points). By adjusting the center frequency and bandwidth of the two passbands, different depths and slopes of the compensation curves can be obtained. As shown in Figure 5.4(b), inverted parabolic compensation curves are generated with the use of a baseband filter and a bandpass filter through an intensity modulator and a MZI. The compensation depth is adjusted from 10 dB to 50 dB when different bandwidths of the passbands are applied.

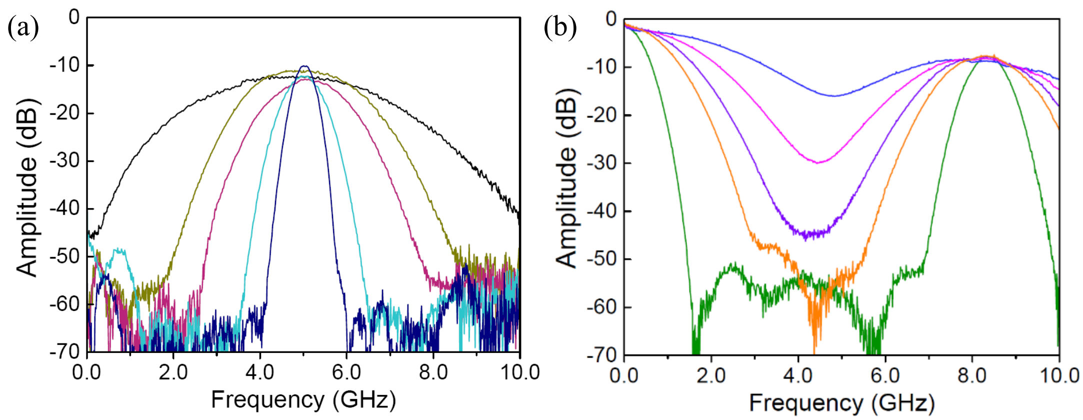

Figure 5.4. Demonstration of parabolic and inverted-parabolic equalization functions. (a) Parabolic compensation curves with various compensation slopes. (b) Inverted-parabolic compensation curves with various compensation slopes and depths.

5.2.3 Tunable attenuation floor

Besides the flexible reconfigurability from the MWP filters, the all-pass branch can work as a tunable attenuation floor over the entire operation range. The frequency response of the all-pass branch is shown by the black curve in Figure 5.5(a), when the bandpass response branch is switched off. A flat response over 10 GHz range is observed, and the amplitude difference is within 1 dB. This tunable attenuation floor provides additional flexibility on adjusting the compensating depth to all the equalization functions. The rest curves in Figure 5.5(a) show the equalization performance when a baseband filter and a single bandpass filter is combined with the tunable attenuation floor. The attenuation of the out-of-band response is adjusted up to -60 dB through the optical tunable attenuator in the all-pass branch, without affecting the profile of the passband. Furthermore, when the bandpass channel and all-pass channel are both enabled, and the response are combined in the balanced photo-detector with similar received power, corresponding addition or subtraction function between these two channels can be achieved. The addition or subtraction will result in bandpass response or bandstop response, depending on the relative phase between these two channels, which can be controlled by a tunable delay line in one of the channel. The bandpass response is converted into bandstop response and a notch filter response is obtained as shown by the pink curve in Figure 5.5(a), providing notch filtering function when a certain portion of the frequency band is undesired.

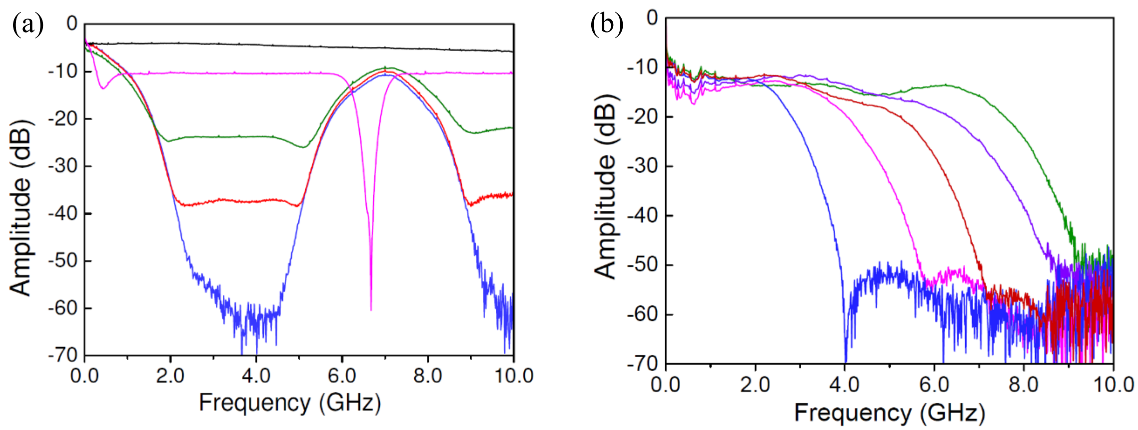

Figure 5.5. (a) Bandpass response with tunable attenuation floors. (b) Low-pass response with tunable bandwidth.

5.2.4 Arbitrary equalization curve with multiple control points

The above functions are achieved through the use of a single MZI, which compose the basic functions of the RF equalizer for limited operation bands. While in wideband and multiband systems, usually more complex equalization curves with different compensation depths are needed for various frequency bands. In this case, an arbitrary compensation curve is desired to balance the powers between different bands. Based on various combinations of the basic functions, high-order and complex equalization curves can be obtained when multiple control points are generated through cascaded MZIs. Low-pass filter response is first implemented by using a baseband filter and a bandpass filter, by adjusting the bandwidth and center frequency of each of the passband, the overall 3-dB bandwidth of the low-pass filter is adjusted from 2.5 GHz to 7.0 GHz, as shown in Figure 5.5(b). Then four passbands are generated based on two cascaded MZIs, and work as four individual control points for balancing different channels, as shown in Figure 5.6(a). The center frequencies of the four passbands are set equally distributed over 10 GHz, and both the position and amplitude of all the four passbands are tunable. By adjusting the profile, bandwidth, position of each passband and the power and phase of the all-pass branch, various compensation curves with arbitrary profiles can be achieved. The equalization curves shown in Figure 5.6(a) are designed for multiband communications, that five frequency bands (baseband, 2.2 GHz, 4.4 GHz, 6.6 GHz and 8.8 GHz) are transmitted at the same time, and frequency components at other undesired bands are suppressed. Figure 5.6(b) shows two special functions from the RF equalizer, the purple curve is a multiband notch filter to remove multiple undesired bands, and the red curve is a saw-tooth-like function for spectrum shaping in signal processing applications.

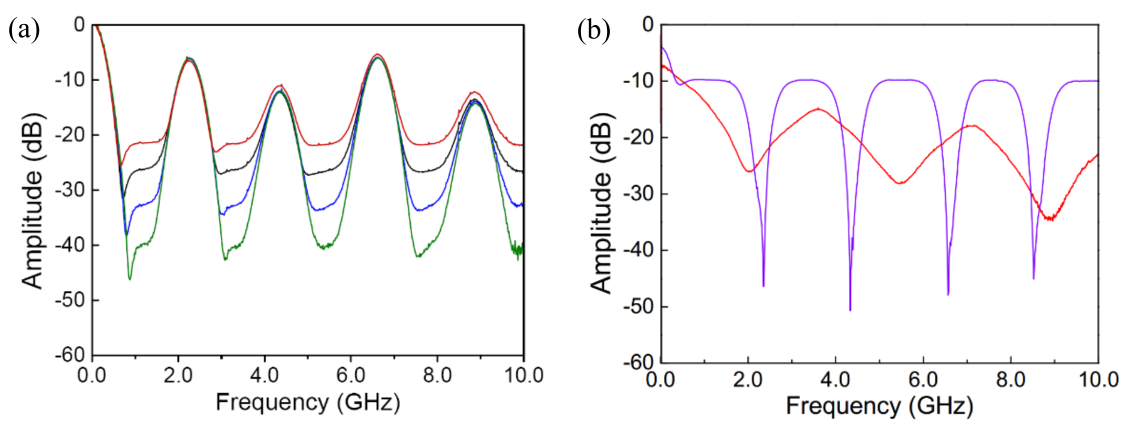

Figure 5.6. High-order equalization curves with multiple control points.

5.4 Arbitrary Spectral Shaping

To demonstrate the arbitrary RF pulse shaping performance and capability of the proposed RF spectral shaper, a 125 Mbit/s square-like pulse train is used as the input RF signal and is launched into the RF spectral shaper for reshaping. The original waveform and RF spectrum are shown in Figure 5.7(a) and 5.7(d). To shape the square-like pulse into a Gaussian pulse, the RF spectral shaper is configured into a low-pass filter with a Gaussian profile and cut off frequency at 1 GHz, i.e. inverse Fourier transform of Gaussian. This can be achieved by setting the waveshaper into an overall Gaussian profile, and only active one stage of the MZI. The resultant RF pulse is now reshaped into a Gaussian pulse, as shown in Figure 5.7(b), with its corresponding Gaussian RF spectrum shown in Figure 5.7(e). Next, we reconfigured the RF spectral shaper to reshape the square-like pulse into a triangular pulse, by setting the RF spectral profile into a Saw-tooth-like function. The waveshaper is then set to an overall Sinc-square profile while the cascaded MZI is set to have 4 interleaving comb spacings. Figure 5.7(c) shows the resultant shaped triangular pulse, while the corresponding RF spectrum is shown in Figure 5.7(f). 4 spectral control points are used at the same time to shape the RF spectrum into a Sinc-square profile. The reshaped pulse trains has exactly the same repetition rate as the input pulse train. The insertion loss of the RF spectral shaper is about 4 to 10 dB depending on the frequency, which can be compensated by optical amplification. As a result, the noise floor of the reshaped waveforms is 5 dB higher than the original RF input, as observed in Figure 5.7 (e) and 5.7(f). Besides shaping the profile of the input RF pulse, both the 3-dB bandwidth and the slope of the reshaped Gaussian and triangular pulses can be adjusted by precisely tailoring the corresponding frequency components through the RF spectral shaper, the reshaped results are shown in Figure 5.8.

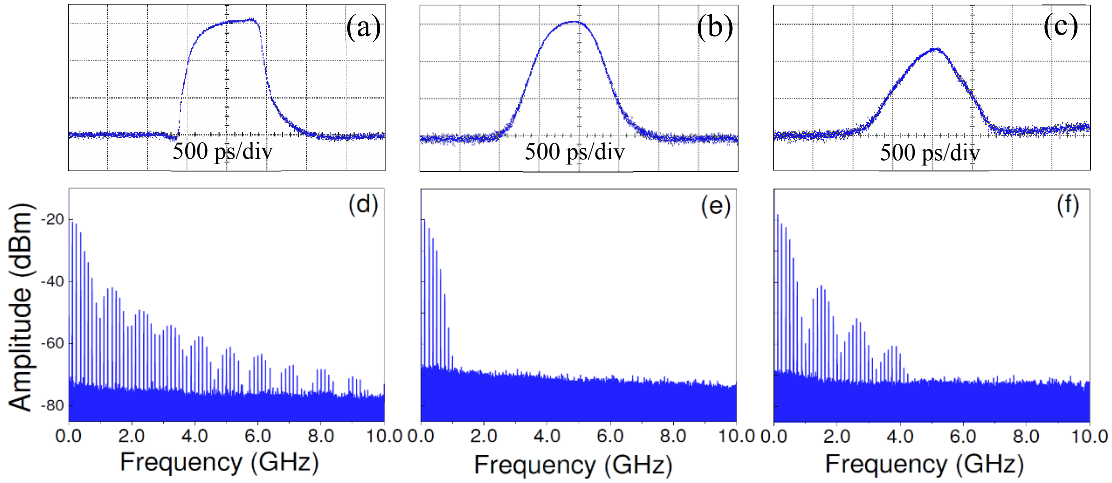

Figure 5.7. Demonstration of the arbitrary pulse shaping using the RF spectral shaper. (a) Original square-like pulse in time domain. (b) Reshaped to a Gaussian pulse through the low-pass equalization function. (c) Reshaped to a triangular pulse pulse trough the saw-tooth equalization function. (d)-(f) Corresponding RF spectra of the pulses.

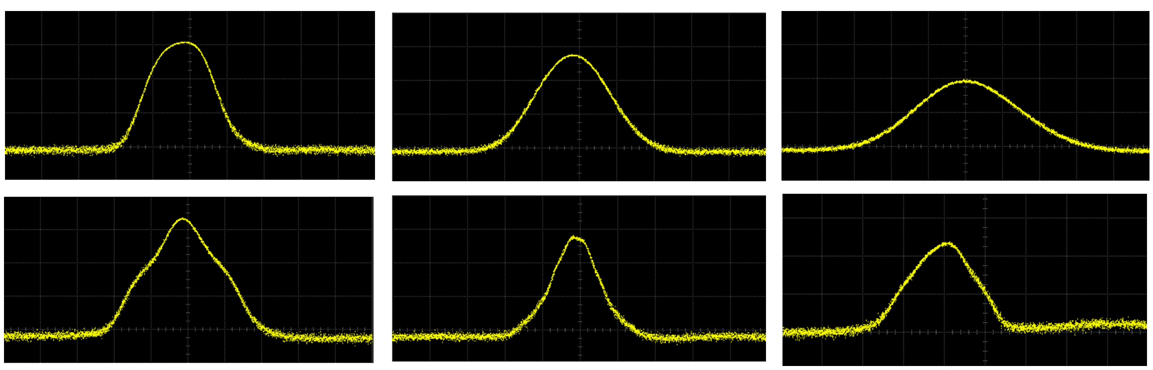

Figure 5.8. The 3-dB bandwidth and profile of the reshaped pulses are adjusted by the RF spectral shaper, scale: 500 ps/div.

As can be seen, the multiple control points and flexible reconfigurability are the keys of the RF spectral shaper, which are achieved through cascaded MZIs. With the use of two serial cascaded MZIs as demonstrated in this paper, 4 different control points are obtained to cover 10 GHz operation range. Increasing the number of cascaded MZIs will significantly increase the number of simultaneous control points, which will in turn result in better flexibility and wider operation range. For example, 3 serial cascaded MZIs will result in 13 different control points [98], and 49 control points can be obtained when 4 MZIs are used. Meanwhile, it is very promising to integrate the RF equalizer into a chip with a larger number of cascaded MZIs in a 2-dimentional mesh structure, such that a programmable photonic signal processor for wideband spectrum shaping can be achieved. The possibility and potential plans for the system integration will be discussed in the next chapter.

5.5 Summary

In summary, we experimentally demonstrated a highly reconfigurable microwave photonic RF spectral shaper for wideband gain/loss equalization and RF spectrum shaping. The proposed scheme is based on the use of a MWP multiband filter, which consists of multiple tunable and reconfigurable passbands. Four highly tunable control points are experimentally achieved with adjustable center frequencies, bandwidths and compensating profiles, resulting in flexibly adjustable compensating curves and various equalization functions. Both equalization and spectrum shaping functions are experimentally demonstrated, with good reconfigurability and noise performance. To the best of our knowledge, this is the first demonstration of a photonics based solution for wideband gain/loss equalization and spectrum shaping, which significantly improves the functionality and operation flexibility of existing electronic counterparts. The wideband operation range and extraordinary reconfigurability make the proposed RF spectral shaper suitable for a variety of applications, including RF/microwave signal processing, spectrum shaping and multiband communications.

CHAPTER 6

FUTURE WORK AND CONCLUSIONS

6.1 Future Work – System Integration

Thanks to the unique properties from photonics, the performance and functionality of conventional RF systems have been significantly enhanced through microwave photonic techniques. However, the cost of the improvements is also non-negligible – the extra optical components, EO and OE conversions significantly increase the complexity, size, power consumption and cost of the systems, which hinder microwave photonic system from practical applications. Although the demonstrated capabilities and functionalities from microwave photonics are of great interest, a solution to reduce these extra cost is urgent desired.

Integrated photonics becomes increasingly popular in both tele-communication industry and optical interconnections since the tremendous data explosion in recent years. The ever-increasing demand of high-speed internet and wide bandwidth require a large number of optical devices, which extremely stimulates the development of photonic integrated circuit. By now, products based on integrated photonics are already commercially available, mainly used in tele-communications and large-scale data centers. Integration could significantly reduce the complexity, power consumption and size of system, at the meanwhile, since many of the integration techniques are compatible with the well-developed micro-electronics industry, the cost for large-scale photonic integrated circuit fabrication is actually practical. These make integrated photonics a promising solution for existing microwave photonics system. During the last few month of our study, we started the integration of our developed systems. In this section, we will discuss the possibility and challenges of integrating the demonstrated systems of our study.

6.1.1 Platforms

Among different photonic integration platforms, III–V materials (InP, GaAs, etc.) and silicon are the two most promising and commonly used material platforms, with their own advantages and limits. Most of the passive optical components are available on both platforms with good performance, active devices are the real challenges. III–V platform has unique advantages on integrating active devices, including chip based light sources (both laser and SLD), modulators, semiconductor optical amplifiers and photo-detectors, which allows the fully integration of various active and passive functions on the same chip [99]. However, the design difficulty and material/fabrication cost of III–V based platform are relative high, since it is not commonly used in other electronic industries. On the contrary, silicon based technique is much widely used in current electronic industries, billions of dollars have been spent to develop silicon based fabrication tools, processes and facilities, and the techniques are already very mature. We can use the same platform designed for electronic chips to fabricate integrated photonic circuits (e.g. CMOS compatible silicon photonic circuit) with just some minor modifications, this is a huge advantage of silicon photonics. Over the last decade, it has been proved that silicon is actually a fantastic material system for building photonic devices, most of the optical passive components have been successfully demonstrated based on silicon based waveguides (or silicon-on-insulator, SOI). On the active components side, light modulation and detection techniques also have rapid progresses that both silicon-based EO modulators and photo detectors or receivers are reported [107][108]. The most remained challenging aspect is to integrate a reliable and efficient light source onto the chips – a silicon wafer based laser source. The challenge comes from the nature of material – silicon is not an efficient light-emitting material to build lasers. By far, the two most promising solutions would be: (1) to integrate gain materials, such as III–V materials (InP, GaAs) or Ge directly onto silicon wafers to build hybrid lasers [109], or (2) to use quantum dots as the active material to build on-chip lasers [101]. Based on our partial integration plan, for the first step we plan to use silicon photonics technique to implement the integration of all the passive components in our system.

6.1.2 Hybrid Integration or Fully Integration

There is no doubt that fully system integration will bring huge benefit to our bench-top systems on the system size, power consumption and cost, which makes the developed functions more practical for real world applications. An ideal fully integrated photonic system will require the integration of all the active and passive devices onto one single chip. For our systems, active optical devices usually include the light source, EO-modulator and photo-detector, which are standard commercial available devices and have been proved possible to be integrated separately [100-102]. Passive components are relative easier to be integrated compared with active devices, due to the simple structures and functions. Researchers have been intensively developing all-in-one integration techniques for years and had many ground-breaking progresses recently. An exciting step was just taken forward this past year that the first monolithic integrated microwave photonic filter have been successfully demonstrate with the use of InP technique [99]. The entire system was integrated onto one single chip, including all the active and passive devices, making fully integrated microwave photonic system very promising in the coming future. However, by far the performance of integrated devices are not as good as discrete devices. For example, the insertion loss of a 3.5 mm integrated phase modulator is about 15 dB, with a modulation extinction ratio of only10 dB [105], while a non-integrated phase modulator only has a loss of 4 dB, with a modulation extinction ratio of up to 40 dB [106]. The large insertion loss and low modulation efficiency would require extra amplifiers and significantly degrade the signal quality [103,104]. Although fully system integration shows exceptional advantages and has been proved promising, integrating all kinds of devices onto one single chip is still very challenging.

In order to take advantages from the good performance of those commercial available non-integrated devices, and reduce the system size at the same time, partial integration could be a transitional choice. The discrete passive optical components in our current system are very bulky, and cost most of the spacing – integrating them will significantly reduce the overall size of the system. The major passive components in our system are tunable Mach–Zehnder interferometers (MZI), which have been well studied and successfully demonstrated on silicon waveguide with competitive performance [85][86]. So our first feasible step of the system integration is to build a hybrid system – put all the passive optical components onto one chip, and incorporate with other discrete active devices (SLD, EOM and PD). Since the sizes of other discrete devices are acceptable, by doing this the overall size of the system can be greatly reduced with relative low design and fabrication difficulty, and still maintain a competitive overall system performance. Furthermore, the integrated passive components are not as sensitive as integrated active devices when temperature changes, and do not need extra temperature stabling circuit.

6.1.3 Integration of the key components

Since most of the commonly used optical devices have already been demonstrated integratable, in this section we will discuss about the possible integration of the special designed components that are required in our systems. The key element of our system is tunable MZIs, basic MZI structure has been studied thoroughly and has been successfully integrated into photonic chips through various techniques [99,85,86,112]. The tunable MZI mainly consist of a tunable optical coupler and a tunable optical delay line, which are required in our design for the tunability and reconfigurability of the proposed functions. Furthermore, a dispersive medium with large dispersion is required in the current system, which is needed to be replaced by a dispersive component in smaller size.

(a) Tunable delays line: In order to have the capability to tune the passbands over a wide frequency range (tens of gigahertz), a tunable delay line with large tuning range is required (> 100 ps). However, by far the reported integrated tunable delay lines can only provide a continuously tuning range of ~10 ps, and there is no promising approach that leads to a successfully implementation of an on-chip optical delay line with a continuous tuning range of >100 ps. If continuously tuning is too hard, we can also try discrete tuning – switching between several channels with different amounts of time delays, e.g. switching between for states: 25 ps, 50 ps, 75 ps and 100 ps. In this case, subwavelength gratings (SWG) could be a good candidate for implementing onto silicon waveguide [110]. Furthermore, 2D optical waveguide mesh networks with reconfigurable structures are also capable to provide discrete tunable time delays [85].

(b) Tunable coupler: A tunable coupler with adjustable coupling ratio is needed to switch ON/OFF of each MZI and adjust the amplitude of the generated passbands. Integrated tunable couplers with adjustable coupling ratio from 100:0 to 50:50 might be possible to be achieved by multimode interference couplers (MMI coupler) [111] and directional couplers, both through thermal tuning of heaters. Furthermore, a discrete ON/OFF switch between 0:100 and 50:50 may also work, such that we can enable/disable each of the MZIs for RF passbands reconfiguration purpose.

(c) Dispersive medium: Materials with large dispersion in a relative small size are desired to replace the DCF used in current system. Chirped fiber Bragg grating (CFBG) could be a good candidate to provide decent amount of time delays over a wide wavelength range, with a relative small size (several centimeters fiber). If a large amount of dispersion is required, cascading several CFBG at the same wavelength range may provide enough dispersion. However, the quality of the signal will be degraded since the signal is reflected back through several CFBGs. Another possible solution is to use special designed photonic crystal waveguide as the dispersion medium to replace the long DCF, up to 70 ps wavelength dependent time delay is achieved in a 1.5 mm long photonic crystal waveguide [18]. Although both of these two possible solutions are currently not integratable on silicon based waveguides, the overall size of the system can still be significantly reduced.

(d) 2D Waveguide mesh structure: Last, as shown in Figure 6.1, an integrated reconfigurable 2D waveguide mesh structure that consists of multiple MZIs is desired in the future, similar to the scheme demonstrated in [85]. Parallel cascade can serial cascade can be used at the same time to build 2-dimentional MZI mesh structure [87], which would further improve the reconfigurability with more possible passband combinations. By switching ON or OFF some of the MZIs, the possible number of simultaneous passbands can be significantly increased, and the functionality can be greatly expanded. In this way, the proposed RF multiband filter can potentially work as a powerful programmable processor which can provide a variety of functionalizes for RF signal processing [87]. Furthermore, this 2D waveguide mesh structure is also a promising solution for replacing tunable delay lines in the MZI, with different configurations of the 2D waveguide mesh, different amounts of path difference of the MZI can be achieved.

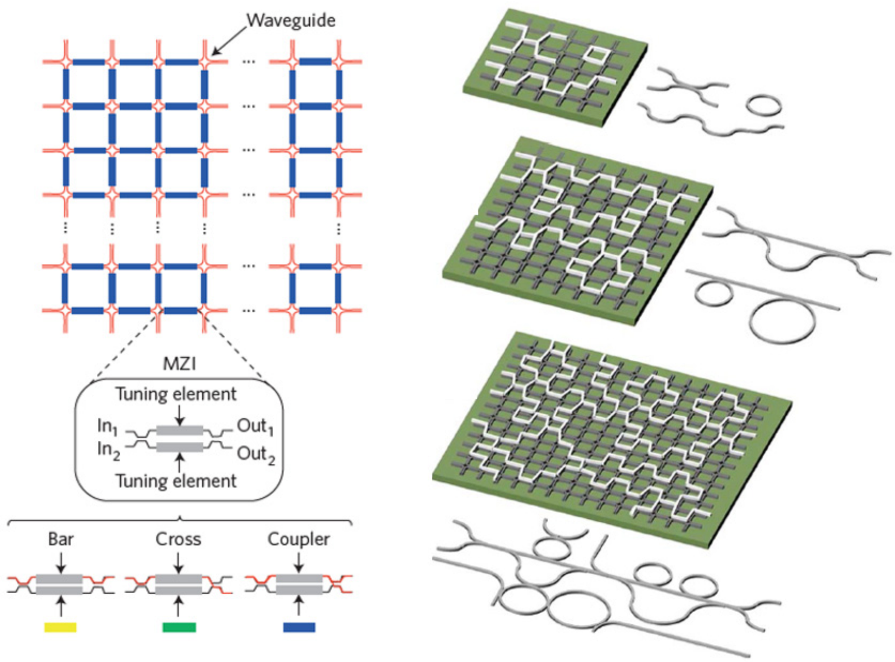

Figure 6.1. Integrated 2D waveguide mesh structure with the capability to be reconfigured into different schemes, demonstrated in [85,87].

6.2 Conclusions

In this dissertation, we developed and experimentally demonstrated several microwave photonics based RF signal processing techniques. Since RF filters are the most essential and widely used components in RF systems, we started with MWP filter designs and successfully developed several unique MWP filters. First, by taking advantage of the ultra-fast electro-optics Pockels effect, a MWP notch filter with gigahertz center frequency tuning speed was demonstrated. The ultrafast notch filter was used as a RF switch with a response time of ~100 ps, which was thousands time faster than existing RF switches. Then a switchable MWP dual-band filter was developed which can be optically controlled by a pump laser, also resulting gigahertz reconfigurable speed and hundreds picosecond level response time. With the help of ultrafast optical techniques, these RF filters significantly improved the tuning speed to gigahertz level, which was extremely useful for high-speed and dynamic applications. Later on, we moved on to the development of RF multiband filters for wideband signal processing, several FIR based tunable and reconfigurable MWP multiband filters were demonstrated. The maximum simultaneous passband number was increased to 13, which was the first experimental demonstration of a RF multiband filter with such a large number of passband. We also proposed a general methodology for MWP multiband implementation, which could dramatically increase the simultaneous passband number. Furthermore, all the generated passbands were both tunable and reconfigurable, providing exceptional operation flexibility for dynamic systems. Last, we applied the developed powerful MWP filters to wideband and dynamic signal processing applications, and successfully demonstrated arbitrary RF spectrum shaping and channel equalization functions. A RF spectral shaper was proposed with the capability to manipulate the frequency components over a wide range of frequency, which was extremely powerful and desired for arbitrary RF signal processing. Based on the developed techniques, ultimately a universal RF programmable processor is expected through integrated photonics techniques.

The signal processing capability for dynamic and wideband applications is significantly enhanced with the developed microwave photonic techniques above, many of which were first demonstrations. During the past two decades, microwave photonic signal processing already shows its great potential over conventional electronic solutions, and will keep bringing unique features to RF system design. With the rapid development of integrated photonics and its increasingly implementation in practical application, we believe microwave photonics will play a more important role in a number of fields.

REFERENCE

[1] José Capmany, José Mora, Ivana Gasulla, Juan Sancho, Juan Lloret, and Salvador Sales. "Microwave photonic signal processing." Journal of Lightwave Technology 31, no. 4 (2013): 571-586.

[2] Jianping Yao. "Microwave photonics." Journal of Lightwave Technology 27, no. 3 (2009): 314-335.

[3] Robert A. Minasian. "Photonic signal processing of microwave signals." IEEE Transactions on Microwave Theory and Techniques54, no. 2 (2006): 832-846.

[4] Robert A. Minasian, E. H. W. Chan, and X. Yi. "Microwave photonic signal processing." Optics Express 21, no. 19 (2013): 22918-22936.

[5] José Capmany, and Dalma Novak. "Microwave photonics combines two worlds." Nature photonics 1, no. 6 (2007): 319-330.

[6] David Marpaung, Chris Roeloffzen, René Heideman, Arne Leinse, Salvador Sales, and José Capmany. " Integrated microwave photonics." Laser & Photonics Reviews 7, no. 4 (2013): 506-538.

[7] Jianping Yao. "Photonics to the rescue: A fresh look at microwave photonic filters." IEEE Microwave Magazine 16, no. 8 (2015): 46-60.

[8] José Capmany, Beatriz Ortega, and Daniel Pastor. "A tutorial on microwave photonic filters." Journal of Lightwave Technology 24, no. 1 (2006): 201-229.

[9] Weiwei Zhang, and Robert A. Minasian. "Switchable and tunable microwave photonic Brillouin-based filter." Photonics Journal, IEEE 4, no. 5 (2012): 1443-1455.

[10] David Marpaung, Blair Morrison, Ravi Pant, and Benjamin J. Eggleton. "Frequency agile microwave photonic notch filter with anomalously high stopband rejection." Optics letters 38, no. 21 (2013): 4300-4303.

[11] Alayn Loayssa, José Capmany, Mikel Sagues, and José Mora. "Demonstration of incoherent microwave photonic filters with all-optical complex coefficients." Photonics Technology Letters, IEEE 18, no. 16 (2006): 1744-1746.

[12] David Marpaung, Blair Morrison, Ravi Pant, Chris Roeloffzen, Arne Leinse, Marcel Hoekman, Rene Heideman, and Benjamin J. Eggleton. "Si3N4 ring resonator-based microwave photonic notch filter with an ultrahigh peak rejection." Optics express 21, no. 20 (2013): 23286-23294.

[13] Mahmoud S. Rasras, Kun-Yii Tu, Douglas M. Gill, Young-Kai Chen, Alice E. White, Sanjay S. Patel, Andrew Pomerene et al. "Demonstration of a tunable microwave-photonic notch filter using low-loss silicon ring resonators."Journal of Lightwave Technology 27, no. 12 (2009): 2105-2110

[14] Dengke Zhang, Xue Feng, Xiangdong Li, Kaiyu Cui, Fang Liu, and Yidong Huang. "Tunable and Reconfigurable Bandstop Microwave Photonic Filter Based on Integrated Microrings and Mach–Zehnder Interferometer." Journal of Lightwave Technology 31, no. 23 (2013): 3668-3675.

[15] Jianji Dong, Li Liu, Dingshan Gao, Yuan Yu, Aoling Zheng, Ting Yang, and Xinliang Zhang. "Compact notch microwave photonic filters using on-chip integrated microring resonators." Photonics Journal, IEEE 5, no. 2 (2013): 5500307-5500307.

[16] Erwin HW Chan, and Robert A. Minasian. "Widely tunable, high-FSR, coherence-free microwave photonic notch filter." Journal of Lightwave Technology 26, no. 8 (2008): 922-927.

[17] Tae-Young Kim, Choong Keun Oh, Sun-Jong Kim, and Chang-Soo Park. "Tunable photonic microwave notch filter with negative coefficient based on polarization modulation." Photonics Technology Letters, IEEE 19, no. 12 (2007): 907-909.

[18] Juan Sancho, Jerome Bourderionnet, Juan Lloret, Sylvain Combrié, Ivana Gasulla, Stephane Xavier, Salvador Sales et al. "Integrable microwave filter based on a photonic crystal delay line." Nature communications 3 (2012): 1075.

[19] Daniel Pastor, Jose Capmany, and Beatriz Ortega. "Broad-band tunable microwave transversal notch filter based on tunable uniform fiber Bragg gratings as slicing filters." Photonics Technology Letters, IEEE 13, no. 7 (2001): 726-728.

[20] Huan Jiang, He Wen, Xiaoping Zheng, Zhigang Liu, Kai Wang, Hanyi Zhang, and Yili Guo. "Improved optical single-sideband generation using the self-modulation birefringence difference in semiconductor optical amplifiers." Optics letters 32, no. 17 (2007): 2580-2582.

[21] Mable P. Fok, Chester Shu, and Wing-Wa Tang. "A cascadable approach to produce widely selectable spectral spacing in birefringent comb filters."Photonics Technology Letters, IEEE 18, no. 18 (2006): 1937-1939

[22] Jia Ge, Hanlin Feng, and Mable P. Fok. "High-speed wavelength tunable DPSK demodulation using a phase modulator based loop mirror filter."Optics Letters 39, no. 12 (2014): 3500-3503.

[23] M. P. Fok, K. L. Lee, and C. Shu. "Waveband-switchable SOA ring laser constructed with a phase modulator loop mirror filter." IEEE photonics technology letters 17, no. 7 (2005): 1393-1395.

[24] K. Kubota, J. Noda, and O. Mikami, "Traveling wave optical modulator using a directional coupler LiNbO3 waveguide." Quantum Electronics, IEEE Journal of 16, no. 7 (1980): 754-760.

[25] Pat Hindle. "The state of RF/Microwave switches." Microwave Journal 53, no. 11 (2010): 20-36.

[26] Gabriel M. Rebeiz. RF MEMS: theory, design, and technology. John Wiley & Sons, 2004.

[27] Understanding RF/Microwave solid state switches and their applications, Application Note, Agilent Technologies Agilent (May, 2010). Available at: http://cp.literature.agilent.com/litweb/pdf/5989-7618EN.pdf.

[28] Peter Bacon, Drew Fischer, and Ruan Lourens. "Overview of RF Switch Technology and Applications." Microwave Journal 57, no. 7 (2014).

[29] Tao Yang, and Gabriel M. Rebeiz. "Three-pole 1.3–2.4-GHz diplexer and 1.1–2.45-GHz dual-band filter with common resonator topology and flexible tuning capabilities." IEEE Transactions on Microwave Theory and Techniques 61, no. 10 (2013): 3613-3624.

[30] Roberto Gómez-García, and Andrew C. Guyette. "Reconfigurable multi-band microwave filters." IEEE Transactions on Microwave Theory and Techniques 63, no. 4 (2015): 1294-1307.

[31] Yi-Chieh Lin, Tzyy-Sheng Horng, and Hui-Hsiang Huang. "Synthesizing a multiband LTCC bandpass filter with specified transmission-and reflection-zero frequencies." IEEE Transactions on Microwave Theory and Techniques 62, no. 12 (2014): 3351-3361.

[32] Ko-Wen Hsu, Jui-Hsiang Lin, and Wen-Hua Tu. "Compact sext-band bandpass filter with sharp rejection response." IEEE Microwave and Wireless Components Letters 24, no. 9 (2014): 593-595.

[33] Chan-Keong Chio, Sio-Weng Ting, and Kam-Weng Tam. "Novel reconfigurable multiple-band quasi-elliptic bandpass filter using defected ground structure." In Microwave Symposium Digest (IMS), 2013 IEEE MTT-S International, pp. 1-4. IEEE, 2013.

[34] Gabriel M. Rebeiz, Kamran Entesari, Isak C. Reines, Sang-June Park, Mohammed A. El-Tanani, Alex Grichener, and Andrew R. Brown. "Tuning in to RF MEMS." IEEE microwave magazine 10, no. 6 (2009).

[35] Qing Wang, and Jianping Yao. "Multitap photonic microwave filters with arbitrary positive and negative coefficients using a polarization modulator and an optical polarizer." IEEE Photonics Technology Letters 20, no. 2 (2008): 78-80.

[36] Yamei Zhang, and Shilong Pan. "Tunable multitap microwave photonic filter with all complex coefficients." Optics letters 38, no. 5 (2013): 802-804.

[37] Ehsan Hamidi, Daniel E. Leaird, and Andrew M. Weiner. "Tunable programmable microwave photonic filters based on an optical frequency comb." IEEE Transactions on Microwave Theory and Techniques 58, no. 11 (2010): 3269-3278.

[38] José Mora, Beatriz Ortega, Antonio Díez, José Luis Cruz, Miguel V. Andrés, José Capmany, and Daniel Pastor. "Photonic microwave tunable single-bandpass filter based on a Mach-Zehnder interferometer." Journal of lightwave technology 24, no. 7 (2006): 2500.

[39] V. R. Supradeepa, Christopher M. Long, Rui Wu, Fahmida Ferdous, Ehsan Hamidi, Daniel E. Leaird, and Andrew M. Weiner. "Comb-based radiofrequency photonic filters with rapid tunability and high selectivity." Nature Photonics 6, no. 3 (2012): 186-194.

[40] José Mora, Lawrence R. Chen, and José Capmany. "Single-bandpass microwave photonic filter with tuning and reconfiguration capabilities." Journal of Lightwave Technology 26, no. 15 (2008): 2663-2670.

[41] Yang Jiang, Perry Ping Shum, Peng Zu, Junqiang Zhou, Guangfu Bai, Jing Xu, Zhuya Zhou, Hengwen Li, and Shunyan Wang. "A selectable multiband bandpass microwave photonic filter." IEEE Photonics Journal 5, no. 3 (2013): 5500509-5500509.

[42] Lilin Yi, Wei Wei, Yves Jaouën, Mengyue Shi, Bing Han, Michel Morvan, and Weisheng Hu. "Polarization-independent rectangular microwave photonic filter based on stimulated Brillouin scattering." Journal of Lightwave Technology 34, no. 2 (2016): 669-675.

[43] Ruichen Tao, Xinhuan Feng, Yuan Cao, Zhaohui Li, and Bai-ou Guan. "Widely tunable single bandpass microwave photonic filter based on phase modulation and stimulated Brillouin scattering." IEEE Photonics Technology Letters 24, no. 13 (2012): 1097.

[44] Amol Choudhary, Iman Aryanfar, Shayan Shahnia, Blair Morrison, Khu Vu, Stephen Madden, Barry Luther-Davies, David Marpaung, and Benjamin J. Eggleton. "Tailoring of the Brillouin gain for on-chip widely tunable and reconfigurable broadband microwave photonic filters." Optics letters 41, no. 3 (2016): 436-439.

[45] Andrew J. Metcalf, Hyoung-Jun Kim, Daniel E. Leaird, Jose A. Jaramillo-Villegas, Keith A. McKinzie, Vikrant Lal, Amir Hosseini, Gloria E. Hoefler, Fred Kish, and Andrew M. Weiner. "Integrated line-by-line optical pulse shaper for high-fidelity and rapidly reconfigurable RF-filtering." Optics express 24, no. 21 (2016): 23925-23940.

[46] Xiaoxiao Xue, Xiaoping Zheng, Hanyi Zhang, and Bingkun Zhou. "Highly reconfigurable microwave photonic single-bandpass filter with complex continuous-time impulse responses." Optics express20, no. 24 (2012): 26929-26934.

[47] A. R. Charaplyvy, R. W. Tkach, L. L. Buhl, and R. C. Alferness. "Phase modulation to amplitude modulation conversion of CW laser light in optical fibres." Electronics Letters 22, no. 8 (1986): 409-411.

[48] Jia Ge, Hanlin Feng, Guy Scott, and Mable P. Fok. "High-speed tunable microwave photonic notch filter based on phase modulator incorporated Lyot filter." Optics letters 40, no. 1 (2015): 48-51.

[49] Adrián J. Torregrosa, Haroldo Maestre, Andrés L. Recas, José Antonio Pereda, Juan Capmany, and Carlos R. Fernández-Pousa. "Tunability of the multiple-bandpass response of cascaded single-source and continuous-sample microwave photonic filters." Optics Communications 283, no. 7 (2010): 1320-1325.

[50] Ryan Toole, and Mable P. Fok. "Photonic implementation of a neuronal algorithm applicable towards angle of arrival detection and localization." Optics express 23, no. 12 (2015): 16133-16141.

[51] Songnian Fu, Minxue Wang, Wen-De Zhong, P. Shum, Yang Jing Wen, Jian Wu, and Jintong Lin. "SOA nonlinear polarization rotation with linear polarization maintenance: Characterization and applications." IEEE Journal of Selected Topics in Quantum Electronics 14, no. 3 (2008): 816-825.

[52] K. L. Lee, M. P. Fok, S. M. Wan, and C. Shu. "Optically controlled Sagnac loop comb filter." Optics express 12, no. 25 (2004): 6335-6340.

[53] W. Mathlouthi, F. Vacondio, P. Lemieux, and Leslie A. Rusch. "SOA gain recovery wavelength dependence: simulation and measurement using a single-color pump-probe technique." Optics express 16, no. 25 (2008): 20656-20665.

[54] Jia Ge, and Mable P. Fok. "Frequency band selectable microwave photonic multiband bandpass filter based on Lyot filter." In Lasers and Electro-Optics (CLEO), 2015 Conference on, pp. 1-2. IEEE, 2015.

[55] Long Huang, Dalei Chen, Fangzheng Zhang, Peng Xiang, Tingting Zhang, Peng Wang, Linlin Lu, Tao Pu, and Xiangfei Chen. "Microwave photonic filter with multiple independently tunable passbands based on a broadband optical source." Optics express 23, no. 20 (2015): 25539-25552.

[56] Jia Ge, and Mable P. Fok. "Passband switchable microwave photonic multiband filter." Scientific reports 5 (2015).

[57] Jia Ge, Aneek E. James, Alexander K. Mathews, and Mable P. Fok. "Simultaneous 12-passband microwave photonic multiband filter with reconfigurable passband frequency." In Optical Fiber Communication Conference, pp. W1G-2. Optical Society of America, 2016.

[58] Gernot Hueber, and Robert Bogdan Staszewski, eds. Multi-mode/Multi-band RF transceivers for wireless communications: Advanced techniques, Architectures, and Trends. John Wiley & Sons, 2011.

[59] Andreas F Molisch. Wireless communications. Vol. 34. John Wiley & Sons, 2012.

[60] Joseph Mitola Iii. "Cognitive radio for flexible mobile multimedia communications." Mobile Networks and Applications 6, no. 5 (2001): 435-441.

[61] Yo-Shen Lin, Chien-Chang Liu, Ko-Mai Li, and Chun Hsiung Chen. "Design of an LTCC tri-band transceiver module for GPRS mobile applications." IEEE Transactions on Microwave Theory and Techniques 52, no. 12 (2004): 2718-2724.

[62] Chong-Yi Liou, and Shau-Gang Mao. "Triple-band marchand balun filter using coupled-line admmittance inverter technique." IEEE Transactions on Microwave Theory and Techniques 61, no. 11 (2013): 3846-3852.

[63] Shih-Cheng Lin. "Microstrip dual/quad-band filters with coupled lines and quasi-lumped impedance inverters based on parallel-path transmission." IEEE Transactions on Microwave Theory and Techniques 59, no. 8 (2011): 1937-1946.

[64] C-F. Chen, T-Y. Huang, and R-B. Wu. "Design of dual-and triple-passband filters using alternately cascaded multiband resonators." IEEE Transactions on Microwave Theory and Techniques 54, no. 9 (2006): 3550-3558.

[65] Sha Luo, Lei Zhu, and Sheng Sun. "Compact dual-mode triple-band bandpass filters using three pairs of degenerate modes in a ring resonator." IEEE Transactions on Microwave Theory and Techniques 59, no. 5 (2011): 1222-1229.

[66] Andrew C Guyette. "Intrinsically switched varactor-tuned filters and filter banks." IEEE Transactions on Microwave Theory and Techniques 60, no. 4 (2012): 1044-1056.

[67] José Capmany, Beatriz Ortega, Daniel Pastor, and Salvador Sales. "Discrete-time optical processing of microwave signals." Journal of Lightwave Technology 23, no. 2 (2005): 702-723.

[68] Jia Ge, Hanlin Feng, Guy Scott, and Mable P. Fok. "High-speed tunable microwave photonic notch filter based on phase modulator incorporated loop mirror filter." In Optical Fiber Communications Conference and Exhibition (OFC), 2015, pp. 1-3. IEEE, 2015.

[69] Yonatan Stern, Kun Zhong, Thomas Schneider, Ru Zhang, Yossef Ben-Ezra, Moshe Tur, and Avi Zadok. "Tunable sharp and highly selective microwave-photonic band-pass filters based on stimulated Brillouin scattering." Photonics Research 2, no. 4 (2014): B18-B25.

[70] David Marpaung, Blair Morrison, Mattia Pagani, Ravi Pant, Duk-Yong Choi, Barry Luther-Davies, Steve J. Madden, and Benjamin J. Eggleton. "Low-power, chip-based stimulated Brillouin scattering microwave photonic filter with ultrahigh selectivity." Optica 2, no. 2 (2015): 76-83.

[71] Liang Gao, Jiejun Zhang, Xiangfei Chen, and Jianping Yao. "Microwave photonic filter with two independently tunable passbands using a phase modulator and an equivalent phase-shifted fiber Bragg grating." IEEE Transactions on Microwave Theory and Techniques 62, no. 2 (2014): 380-387.

[72] David B. Hunter, and Robert A. Minasian. "Tunable microwave fiber-optic bandpass filters." IEEE Photonics technology letters 11, no. 7 (1999): 874-876.

[73] José Capmany, Daniel Pastor, Alfonso Martinez, Beatriz Ortega, and Salvador Sales. "Microwave photonic filters with negative coefficients based on phase inversion in an electro-optic modulator." Optics letters 28, no. 16 (2003): 1415-1417.

[74] J. Capmany, J. Mora, B. Ortega, and D. Pastor. "High-Q microwave photonic filter with a tuned modulator." Optics letters 30, no. 17 (2005): 2299-2301.

[75] Minhyup Song, Christopher M. Long, Rui Wu, Dongsun Seo, Daniel E. Leaird, and Andrew M. Weiner. "Reconfigurable and tunable flat-top microwave photonic filters utilizing optical frequency combs." IEEE Photonics Technology Letters 23, no. 21 (2011): 1618-1620.

[76] Xiaoxiao Xue, Xiaoping Zheng, Hanyi Zhang, and Bingkun Zhou. "Tunable chirped microwave photonic filter employing a dispersive Mach–Zehnder structure." Optics letters 36, no. 17 (2011): 3518-3520.

[77] Thomas XH Huang, Xiaoke Yi, and Robert A. Minasian. "Single passband microwave photonic filter using continuous-time impulse response." Optics express 19, no. 7 (2011): 6231-6242.

[78] Xiaoxiao Xue, Yi Xuan, Hyoung-Jun Kim, Jian Wang, Daniel E. Leaird, Minghao Qi, and Andrew M. Weiner. "Programmable single-bandpass photonic RF filter based on Kerr comb from a microring." Journal of Lightwave Technology 32, no. 20 (2014): 3557-3565.

[79] Xiaoxiao Xue, Hyoung-Jun Kim, Yi Xuan, Jian Wang, Daniel E. Leaird, Minghao Qi, and Andrew M. Weiner. "First demonstration of a tunable single-bandpass photonic radiofrequency filter based on optical frequency comb from a microring." In Optical Fiber Communications Conference and Exhibition (OFC), 2014, pp. 1-3. IEEE, 2014.

[80] Hao Chen, Zuowei Xu, Hongyan Fu, Shiwei Zhang, Congxian Wu, Hao Wu, Huiying Xu, and Zhiping Cai. "Switchable and tunable microwave frequency multiplication based on a dual-passband microwave photonic filter." Optics express 23, no. 8 (2015): 9835-9843.

[81] Ofir Aharon, and I. Abdulhalim. "Liquid crystal Lyot tunable filter with extended free spectral range." Optics Express 17, no. 14 (2009): 11426-11433.

[82] Jia Ge, and Mable P. Fok. "Frequency band selectable microwave photonic multiband bandpass filter based on Lyot filter." In Lasers and Electro-Optics (CLEO), 2015 Conference on, pp. 1-2. IEEE, 2015.

[83] H. J. S. Dorren, Daan Lenstra, Yong Liu, Martin T. Hill, and G-D. Khoe. "Nonlinear polarization rotation in semiconductor optical amplifiers: Theory and application to all-

optical flip-flop memories." IEEE Journal of Quantum Electronics 39, no. 1 (2003): 141-148.

[84] Jia Ge, and Mable P. Fok. "Optically Controlled Fast Reconfigurable Microwave Photonic Dual-Band Filter Based on Nonlinear Polarization Rotation." IEEE Transactions on Microwave Theory and Techniques 65, no. 1 (2017): 253-259.

[85] Leimeng Zhuang, Chris GH Roeloffzen, Marcel Hoekman, Klaus-J. Boller, and Arthur J. Lowery. "Programmable photonic signal processor chip for radiofrequency applications." Optica 2, no. 10 (2015): 854-859.

[86] Binbin Guan, Stevan S. Djordjevic, Nicolas K. Fontaine, Linjie Zhou, Salah Ibrahim, Ryan P. Scott, David J. Geisler, Zhi Ding, and SJ Ben Yoo. "CMOS compatible reconfigurable silicon photonic lattice filters using cascaded unit cells for RF-photonic processing." IEEE Journal of Selected Topics in Quantum Electronics 20, no. 4 (2014): 359-368.

[87] José Capmany, Ivana Gasulla, and Daniel Pérez. "Microwave photonics: The programmable processor." Nature Photonics 10, no. 1 (2016): 6.

[88] Jianping Yao. "Microwave photonics: Arbitrary waveform generation." Nature Photonics 4, no. 2 (2010): 79-80.

[89] Antoine Monmayrant, Sébastien Weber, and Béatrice Chatel. "A newcomer's guide to ultrashort pulse shaping and characterization." Journal of Physics B: Atomic, Molecular and Optical Physics 43, no. 10 (2010): 103001.

[90] Fahmida Ferdous, Houxun Miao, Daniel E. Leaird, Kartik Srinivasan, Jian Wang, Lei Chen, Leo Tom Varghese, and Andrew M. Weiner. "Spectral line-by-line pulse shaping of on-chip microresonator frequency combs." Nature Photonics 5, no. 12 (2011): 770-776.

[91] Maroof H. Khan, Hao Shen, Yi Xuan, Lin Zhao, Shijun Xiao, Daniel E. Leaird, Andrew M. Weiner, and Minghao Qi. "Ultrabroad-bandwidth arbitrary radiofrequency waveform generation with a silicon photonic chip-based spectral shaper." Nature Photonics 4, no. 2 (2010): 117-122.

[92] Bing Xia, and Lawrence R. Chen. "Arbitrary optical waveform generation using 2D ring resonator arrays." Optics express 14, no. 15 (2006): 6619-6627.

[93] Chao Wang, and Jianping Yao. "Phase-coded millimeter-wave waveform generation using a spatially discrete chirped fiber Bragg grating." IEEE Photonics Technology Letters 24, no. 17 (2012): 1493-1495.

[94] Qian Ma, and Mingbo Ma. "Broadband amplifier gain slope equalization filter." Session 1AP (2008): 17.

[95] Huan Wang, Bo Yan, Zhigang Wang, and Rui-Min Xu. "A broadband microwave gain equalizer." Progress In Electromagnetics Research Letters 33 (2012): 63-72.

[96] Lei Han. "A Reconfigurable Microwave Equalizer With Different Maximum Attenuations Based on RF MEMS Switches." IEEE Sensors Journal 16, no. 1 (2016): 17-18.

[97] Xiaoqi Zhu, Feiya Chen, Huanfa Peng, and Zhangyuan Chen. "Novel programmable microwave photonic filter with arbitrary filtering shape and linear phase." Optics Express 25, no. 8 (2017): 9232-9243.

[98] Jia Ge, and Mable P. Fok. "Continuously tunable and reconfigurable microwave photonic multiband filter based on cascaded MZIs." In IEEE Photonics Conference, WA1, Orlando, FL (2017).

[99] Javier S. Fandiño, Pascual Muñoz, David Doménech, and José Capmany. "A monolithic integrated photonic microwave filter." Nature Photonics 11, no. 2 (2017): 124-129.

[100] Graham T. Reed, G. Mashanovich, F. Y. Gardes, and D. J. Thomson. "Silicon optical modulators." Nature photonics 4, no. 8 (2010): 518-526.

[101] Siming Chen, Wei Li, Jiang Wu, Qi Jiang, Mingchu Tang, Samuel Shutts, Stella N. Elliott et al. "Electrically pumped continuous-wave III–V quantum dot lasers on silicon." Nature Photonics 10 (2016): 307-311.

[102] Léopold Virot, Paul Crozat, Jean-Marc Fédéli, Jean-Michel Hartmann, Delphine Marris-Morini, Eric Cassan, Frédéric Boeuf, and Laurent Vivien. "Germanium avalanche receiver for low power interconnects." Nature communications 5 (2014): 4957.

[103] Xia Chen, Chao Li, and Hon K. Tsang. "Device engineering for silicon photonics." NPG Asia Materials 3, no. 1 (2011): 34-40.

[104] Junjia Wang, Reza Ashrafi, Rhys Adams, Ivan Glesk, Ivana Gasulla, José Capmany, and Lawrence R. Chen. "Subwavelength grating enabled on-chip ultra-compact optical true time delay line." Scientific reports 6 (2016): 30235.

[105] D. J. Thomson, F. Y. Gardes, Y. Hu, G. Mashanovich, M. Fournier, P. Grosse, J. M. Fedeli, and G. T. Reed. "High contrast 40Gbit/s optical modulation in silicon." Optics express 19, no. 12 (2011): 11507-11516.

[106] Zhaotang Su, Qingzhong Deng, Zexuan Zhang, Xingjun Wang, and Zhiping Zhou. "High Extinction Ratio and Low Driver Electro-Refrative Phase Modulator with Double Graphene Layers." In Asia Communications and Photonics Conference, pp. ASu5B-5. Optical Society of America, 2015.

[107] Nathan Youngblood, Yoska Anugrah, Rui Ma, Steven J. Koester, and Mo Li. "Multifunctional graphene optical modulator and photodetector integrated on silicon waveguides." Nano letters 14, no. 5 (2014): 2741-2746.

[108] Qi Jiang, Siming Chen, Mingchu Tang, Jiang Wu, Alywn Seeds, and Huiyun Liu. "Monolithically grown superluminescent diodes on germanium and silicon substrates." In CLEO: Science and Innovations, pp. SM3G-6. Optical Society of America, 2015.

[109] Lukas Chrostowski, and Michael Hochberg. Silicon photonics design: from devices to systems. Cambridge University Press, 2015.

[110] Junjia Wang, Ivan Glesk, and Lawrence R. Chen. "Subwavelength grating devices in silicon photonics." Science Bulletin 61, no. 11 (2016): 879-888.

[111] G. Singh, R.P.Yadav, and V.Janyani, "Multimode Interference (MMI) coupler based All Optical Switch: Design, Applications & Performance Analysis", International Journal of Recent Trends in Engineering, Vol 1, No. 3, 115-119 (2009).

[112] Daniel Pérez, Ivana Gasulla, and José Capmany. "Software-defined reconfigurable microwave photonics processor." Optics express 23, no. 11 (2015): 14640-14654.

[113] Tianyu Jia, Jing Ye, and Zewen Liu. "A RF-MEMS based dual-band tunable filter with independently controllable passbands." In Solid-State and Integrated Circuit Technology (ICSICT), 2014 12th IEEE International Conference on, pp. 1-3. IEEE, 2014.

[114] Pawel Rulikowski, and John Barrett. "Adaptive arbitrary pulse shaper." IEEE Microwave and wireless components letters 18, no. 5 (2008): 356-358.

[115] M. P. Fok, and Jia Ge, "Tunable Multiband Microwave Photonic Filters," Photonics 4 (Multidisciplinary Digital Publishing Institute), no. 4 (2017): 45.

APPENDICES A

PUBLICATIONS DURING STUDY

Journal papers:

[J1] Jia Ge and M. P. Fok, "Optically controlled fast reconfigurable microwave photonic dual-band filter based on nonlinear polarization rotation," IEEE Transactions on Microwave Theory and Techniques, vol. 65, no. 1, pp. 253-259, Jan. 2017.

[J2] Jia Ge, A. E. James, L. Xu, Y. Chen, K. Kwok, and M. P. Fok, "Bidirectional Soft Silicone Curvature Sensor based on Off-centered Embedded Fiber Bragg Grating," IEEE Photonics Technology Letters, vol. 28, no. 20, pp. 2237-2240, Oct. 2016.

[J3] Jia Ge and M. P. Fok, "Ultra high-speed radio frequency switch based on photonics," Scientific Reports, vol. 5, p. 17263, Nov. 2015.

[J4] Jia Ge and M. P. Fok, "Passband switchable microwave photonic multiband filter," Scientific Reports, vol. 5, p. 15882, Nov. 2015.

[J5] Jia Ge, H. Feng, G. Scott, and M. P. Fok, "High-speed tunable microwave photonic notch filter based on phase modulator incorporated Lyot filter," Optics Letters, vol. 40, no. 1, pp. 48-51, Jan. 2015.

[J6] Jia Ge, H. Feng, and M. P. Fok, "High-speed wavelength tunable DPSK demodulation using a phase modulator based loop mirror filter," Optics Letters, vol. 39, no. 12, pp. 3500-3503, June 2014.

[J7] Jia Ge, H. Feng, Z. Tse, Y. Chen, and M. P. Fok, "Spiral-Structured Fiber Bragg Grating for Contact Force Sensing through Direct Power Measurement," Optics Express, vol. 22, no. 9, pp. 10439-10445, Apr. 2014.

[J8] M. P. Fok and Jia Ge, "Tunable Multiband Microwave Photonic Filters," Photonics, vol. 4, no. 4, p. 45, Nov. 2017 (Invited Review).

[J9] L. Xu, Jia Ge, J. Patel, and M. P. Fok, "Dual-layer orthogonal fiber Bragg grating mesh based soft sensor for 3-dimensional shape sensing," Optics Express, vol. 25, no. 20, pp. 24727-24734, Sep. 2017.

[J10] H. Feng, Jia Ge, S. Xiao, and M. P. Fok, "Suppression of Rayleigh backscattering noise using cascaded-SOA and microwave photonic filter for 10 Gb/s loop-back WDM-PON," Optics Express, vol. 22, p. 11770, May 2014.

[J11] Y. Chen, Jia Ge, K.W. Kwok, K.R. Nilsson, M. P. Fok, and Z. T. Tse, "MRI-conditional catheter sensor for contact force and temperature monitoring during cardiac electrophysiological procedures," Journal of Cardiovascular Magnetic Resonance, vol. 16, p. 150, Jan. 2013.

[J12] L. Xu, L. Feuerman, Jia Ge, K. R. Nilsson, Z. T. Tse, and M. P. Fok, "Temperature Insensitive Contact Force Sensing in Bi-directional Catheter Using Fiber Bragg Grating Pair," IEEE Sensors Journal, vol. 17, no. 16, pp. 5118-5122, July 2017.

[J13] Y. Chen, K. W. Kwok, Jia Ge, K. R. Nilsson, M. P. Fok and Z. T. Tse, "Augmented Reality for Improving Catheterization in Magnetic Resonance Imaging-Guided Cardiac Electrophysiology Therapy," Journal of Medical Devices, vol. 8, p. 020917, Apr. 2014.

[J14] L. Xu, M. I. Miller, Jia Ge, K. R. Nilsson, Z. T. Tse, and M. P. Fok, "Temperature Insensitive Fiber Optics Contact Force Sensor for Steerable Catheters," IEEE Sensors Journal, vol. 16, pp. 4771-4775, June 2016.

[J15] H. Feng, M. P. Fok, S. Xiao, Jia Ge, et al, "A Reconfigurable High-Order UWB Signals Generation Scheme Using RSOA-MZI Structure," IEEE Photonics Journal, vol. 6, no. 2, p. 7900307, Apr. 2014.

[J16] H. Feng, S. Xiao, Q. Zhou, Jia Ge and M. P. Fok, "Rayleigh backscattering noise suppression based on real-time heterodyne receiver for loop-back WDM-PON," Optics Express, vol. 22, pp. 22673-22679, Sep. 2014.

Conference proceedings:

[C1] Jia Ge and M. P. Fok, "Continuously tunable and reconfigurable microwave photonic multiband filter based on cascaded MZIs," in IEEE Photonics Conference (IPC 2017), p. WA1, Orlando, FL, USA, Oct. 2017.

[C2] Jia Ge, A. E. James, A. K. Mathews, and M. P. Fok, "Simultaneous 12-passband microwave photonic multiband filter with reconfigurable passband frequency," in Optical Fiber Communication Conference (OFC 2016), p. W1G.2, Anaheim, CA, USA, Mar. 2016.

[C3] Jia Ge, A. K. Mathews, A. E. James, and M. P. Fok, "Optically controlled microwave photonic dual-band filter with ultrafast reconfigurable capability," in Conference on Lasers and Electro-Optics (CLEO 2016), p. STh1F.6, San Jose, CA, USA, June 2016.

[C4] Jia Ge, H. Feng, G. Scott and M. P. Fok, "High-speed tunable microwave photonic notch filter based on phase modulator incorporated loop mirror filter," in Optical Fiber Communication Conference (OFC 2015), p. W2A.61, Los Angeles, CA, USA, Mar. 2015.

[C5] Jia Ge and M. P. Fok, "Frequency Band Selectable Microwave Photonic Multiband Bandpass Filter based on Lyot filter," in Conference on Lasers and Electro-Optics (CLEO 2015), p. STh3F.2, San Jose, USA, May 2015.

[C6] M. P. Fok, Jia Ge, R. Toole, R. Lin, et al, "Wideband Dynamic Microwave Photonic Systems: From Photonics to Neuromorphic," in Asia Communications and Photonics Conference, p. ATh3H.1, Nov. 2016 (Invited).

[C7] Q. Zhou, Jia Ge, and M. P. Fok, "Fast Dynamic In-band RF Self-Interference Cancellation for Enabling Efficient Spectral Usage", in Optical Fiber Communication Conference (OFC 2017), p. W4B.5, Mar. 2017.

[C8] L. Xu, Jia Ge, Jay Patel, and M. P. Fok, "3-Dimensional Soft Shape Sensor based on Dual-layer Orthogonal Fiber Bragg Grating Mesh", in Optical Fiber Communication Conference (OFC 2017), p. Th3H.2, Mar. 2017.

[C9] H. Feng, Jia Ge, S. Xiao and M. P. Fok, "Mitigating Rayleigh Backscattering Noise in WDM-PON by Using Cascaded SOAs and Microwave Photonic Filter," in Conference on Lasers and Electro-Optics (CLEO 2014), p. STu1J.5, San Jose, CA, USA, June 2014.

[C10] Y. Chen, Jia Ge, K. Kwok, K. R. Nilsson, M. P. Fok, and Z. T. Tse, "MRI-conditional Catheter Sensor for Contact Force and Temperature Monitoring during Cardiac Electrophysiological Procedures," in SCMR 17th Annual Scientific Session, New Orleans, LA, USA, Jan. 2014.

[C11] M. P. Fok, Q. Zhou, Jia Ge, and R. Toole, "Self-Adaptive Wideband Co-Site Co-Channel Interference Mitigation Based on Photonics and Neuromorphic Processing," in the 4th Photonics Global Conference (ICMAT 2015), p. ICMAT15-A-4219, July 2015 (Invited).

[C12] R. Lin, L. Perea, T. P. Do, Jia Ge, L. Xu, and M. P. Fok, "Bio-Inspired Optical Microwave Phase Lock Loop based on Nonlinear Effects in Semiconductor Optical Amplifier", in Optical Fiber Communication Conference (OFC 2017), p. Th2A.41, Mar. 2017.

APPENDICES B

MATLAB CODE FOR CALCULATING FREE SPECTRAL RANGE AND PASSBAND CENTER FREQUENCY

```
clear;

wa=1530:0.00001:1550;
f=1:0.1:20;
f1=zeros(length(f));
bi=6.333e-4;
l1=80;
l2=60;
l3=40;
l4=20;

b2=1.86e-25;
ld=10.2e3;
c=3e8;

fi1=2*pi*(bi*l1)./(wa/1000000000);
fi2=2*pi*(bi*l2)./(wa/1000000000);
fi3=2*pi*(bi*l3)./(wa/1000000000);
fi4=2*pi*(bi*l4)./(wa/1000000000);


y1=0.5*(1-cos(fi1));
y2=0.5*(1-cos(fi2));
y3=0.5*(1-cos(fi3));
y4=0.5*(1-cos(fi4));

y=1*y1+1*y2+1*y3+1*y4;
ylog=log(y);

comb_spacing=(1530/1000000000)^2/(bi*l1)*1e12;

disp(comb_spacing);

figure;
plot(wa,ylog);


f0=(bi*l1)/(b2*ld*c)/(1000000000)/10;%add another /10
f1(round(f0))=1;
%figure;
disp(f0);

%plot(f,f1);
```

APPENDICES C

MATLAB CODE FOR SIMULATING HIGH-ORDER LYOT LOOP FILTER

```
clear;
clc;
Q0=pi/2 ;% angle 2 for second order modulation
Einx=1*cos(Q0); %input E1 power 1
Einy=1*sin(Q0);
Ein1=[1;0];%?

wave=1550:0.00005:1555;
wa=wave/1000000000;%wavelength

B1=0.0074;% delta N
B2=0.00033;% delta N
k_cr=0.5;%couplering ratio
Q1=0*pi/4+30*pi/180;% PC 1 before PM and PMF
Q2=0*pi/4+0*pi/180;% PC 2 , between  PMF and PM
Q3=0*pi/4+30*pi/180;% PC 3 in the loop, between  2PMF
l1=50*10^(-3);   %hbf length
l2=53;
OP=2;

fi1=pi*B1*l1./wa;  %phase difference 1
fi2=pi*B2*l2./wa;  %phase difference 2

J_P1=[1 0; 0 0];
J_P2=[1 0; 0 0]; %Polarizer

%J_CP=[sqrt(1-k_cr) 1i*sqrt(k_cr);1i*sqrt(k_cr) sqrt(1-k_cr)]; %coupler J
% Jhbf=[exp(-j*fi1) 0;0 exp(j*fi1)];  %hbf J
J_HBF1=zeros(2,2,length(fi1));%HBF 1,define 1000 2x2 jones mattrix, and give the value
one by one.
for k=1:length(fi1)
    J_HBF1(:,:,k)=[exp(-1i*fi1(k)) 0;0 exp(1i*fi1(k))];
%1£°ÓÃ1iÀ´±íÊ¾ÐéÊý£¬¾¡Á¿²»ÓÃj£¬ÒÔÃâ»ìÏý¡£
    %2£°Õâ¾äÒâË¼¾ÍÊÇJhbfÇ°Á½Î¬¾ÍÊÇ[exp(-1i*fi1(k)) 0;0
exp(1i*fi1(k))]£¬µÚÈýÎ¬µÄindexÊÇk¡£
    %Jhbf(:,:,k)ÀïÃæ(:)Ã°ºÅ´ú±íÈÎÒâ£¬²»ÏÞ¶¨index¡£
end
J_HBF2=zeros(2,2,length(fi2));%Ê×ÏÈ¶¨ÒåÒ»¸öÈýÎ¬ÏòÁ¿£¬ÀïÃæÈ«²¿Îª0
for k=1:length(fi2)
    J_HBF2(:,:,k)=[exp(-1i*fi2(k)) 0;0 exp(1i*fi2(k))];
%1£°ÓÃ1iÀ´±íÊ¾ÐéÊý£¬¾¡Á¿²»ÓÃj£¬ÒÔÃâ»ìÏý¡£
    %2£°Õâ¾äÒâË¼¾ÍÊÇJhbfÇ°Á½Î¬¾ÍÊÇ[exp(-1i*fi1(k)) 0;0
exp(1i*fi1(k))]£¬µÚÈýÎ¬µÄindexÊÇk¡£
    %Jhbf(:,:,k)ÀïÃæ(:)Ã°ºÅ´ú±íÈÎÒâ£¬²»ÏÞ¶¨index¡£
end

J_PC1n=[cos(Q1) -sin(Q1); sin(Q1) cos(Q1)];%PC J may not be right
J_PC1p=[cos(-Q1) sin(-Q1); -sin(-Q1) cos(-Q1)];
J_PC2n=[cos(Q2) -sin(Q2); sin(Q2) cos(Q2)];
J_PC2p=[cos(-Q2) sin(-Q2); -sin(-Q2) cos(-Q2)];
```

```
J_PC3n=[cos(Q3) -sin(Q3); sin(Q3) cos(Q3)];
J_PC3p=[cos(-Q3) sin(-Q3); -sin(-Q3) cos(-Q3)];
%Jpc2=[cos(Q2) -sin(Q2);sin(Q2) cos(Q2)];%PC J Q2!

%EoutLyot=J_P2*J_PC1p*J_HBF1.*J_PC2p*J_HBF2.*J_PC3n*J_HBF2.*J_PC2n*J_HBF1.*J_PC1n*J_P1
*Ein1;

E_P_PC1=J_PC1n*J_P2*Ein1;%start

E_P_PC1_HBF1=zeros(2,length(fi1));%Ê×ÏÈ¶¨ÒåÒ»¸ö2Î¬ÏòÁ¿£¬ÀïÃæÈ«²¿Îª0 after HBF1,2x301
 for k=1:length(fi1)
    E_P_PC1_HBF1(:,k)=J_HBF1(:,:,k)*E_P_PC1; %1£ºÓÃ1iÀ´±íÊ¾ÐéÊý£¬¾¡Á¿²»ÓÃj£¬ÒÔÃâ»ìÏý¡£
     %2£ºÕâ¾äÒâË¼¾ÍÊÇJhbfÇ°Á½Î¬¾ÍÊÇ[exp(-1i*fi1(k)) 0;0
exp(1i*fi1(k))]£¬µÚÈýÎ¬µÄindexÊÇk¡£
     %Jhbf(:,:,k)ÀïÃæ(:)Ã°ºÅ´ú±íÈÎÒâ£¬²»ÏÞ¶¨index¡£
 end

E_P_PC1_HBF1_PC2=J_PC2n*E_P_PC1_HBF1;%2x1000

%E_P_PC1_HBF1_PC2_HBF2=zeros(2,length(fi1));%Ê×ÏÈ¶¨ÒåÒ»¸ö2Î¬ÏòÁ¿£¬ÀïÃæÈ«²¿Îª0 after
HBF1,2x301
for k=1:length(fi1)
    E_P_PC1_HBF1_PC2_HBF2(:,k)=J_HBF2(:,:,k)*E_P_PC1_HBF1_PC2(:,k);
%1£ºÓÃ1iÀ´±íÊ¾ÐéÊý£¬¾¡Á¿²»ÓÃj£¬ÒÔÃâ»ìÏý¡£
     %2£ºÕâ¾äÒâË¼¾ÍÊÇJhbfÇ°Á½Î¬¾ÍÊÇ[exp(-1i*fi1(k)) 0;0
exp(1i*fi1(k))]£¬µÚÈýÎ¬µÄindexÊÇk¡£
     %Jhbf(:,:,k)ÀïÃæ(:)Ã°ºÅ´ú±íÈÎÒâ£¬²»ÏÞ¶¨index¡£
end

E_P_PC1_HBF1_PC2_HBF2_PC3=J_PC3n*E_P_PC1_HBF1_PC2_HBF2;

%E_P_PC1_HBF1_PC2_HBF2_PC3_HBF2=zeros(2,length(fi1));%Ê×ÏÈ¶¨ÒåÒ»¸ö2Î¬ÏòÁ¿£¬ÀïÃæÈ«²¿Îª0
after HBF1,2x301
for k=1:length(fi1)
    E_P_PC1_HBF1_PC2_HBF2_PC3_HBF2(:,k)=J_HBF2(:,:,k)*E_P_PC1_HBF1_PC2_HBF2_PC3(:,k);
%1£ºÓÃ1iÀ´±íÊ¾ÐéÊý£¬¾¡Á¿²»ÓÃj£¬ÒÔÃâ»ìÏý¡£
     %2£ºÕâ¾äÒâË¼¾ÍÊÇJhbfÇ°Á½Î¬¾ÍÊÇ[exp(-1i*fi1(k)) 0;0
exp(1i*fi1(k))]£¬µÚÈýÎ¬µÄindexÊÇk¡£
     %Jhbf(:,:,k)ÀïÃæ(:)Ã°ºÅ´ú±íÈÎÒâ£¬²»ÏÞ¶¨index¡£
end
E_P_PC1_HBF1_PC2_HBF2_PC3_HBF2_PC2=J_PC2p*E_P_PC1_HBF1_PC2_HBF2_PC3_HBF2;

%E_P_PC1_HBF1_PC2_HBF2_PC3_HBF2_PC2_HBF1=zeros(2,length(fi1));%Ê×ÏÈ¶¨ÒåÒ»¸ö2Î¬ÏòÁ¿£¬Àï
ÃæÈ«²¿Îª0 after HBF1,2x301
for k=1:length(fi1)

E_P_PC1_HBF1_PC2_HBF2_PC3_HBF2_PC2_HBF1(:,k)=J_HBF1(:,:,k)*E_P_PC1_HBF1_PC2_HBF2_PC3_H
BF2_PC2(:,k); %1£ºÓÃ1iÀ´±íÊ¾ÐéÊý£¬¾¡Á¿²»ÓÃj£¬ÒÔÃâ»ìÏý¡£
     %2£ºÕâ¾äÒâË¼¾ÍÊÇJhbfÇ°Á½Î¬¾ÍÊÇ[exp(-1i*fi1(k)) 0;0
exp(1i*fi1(k))]£¬µÚÈýÎ¬µÄindexÊÇk¡£
     %Jhbf(:,:,k)ÀïÃæ(:)Ã°ºÅ´ú±íÈÎÒâ£¬²»ÏÞ¶¨index¡£
end

E_P_PC1_HBF1_PC2_HBF2_PC3_HBF2_PC2_HBF1_PC1_P2=J_P2*J_PC1p*E_P_PC1_HBF1_PC2_HBF2_PC3_H
BF2_PC2_HBF1;

E4outx=E_P_PC1_HBF1_PC2_HBF2_PC3_HBF2_PC2_HBF1_PC1_P2(1,:);
E4outy=E_P_PC1_HBF1_PC2_HBF2_PC3_HBF2_PC2_HBF1_PC1_P2(2,:);
P4out=abs((E4outx.^2+E4outy.^2));%Pout
×î°óµÃµ½E2µÄÊä³öÄÜÁ¿dBÖµ£¬ÔÚ²¨³¤·¶Î§ÄÚÑ¡ÔñÊ²¨+E4outy.^2

LG2out=10*log10(P4out);
figure;
```

```
plot(wa,P4out);
%E3!E3!E3!E3!

%E3_CP=sqrt(1-k_cr)*Ein1;
%E3_CP_PC1=J_PC1p*E3_CP;% 2x1

%
% E3_CP_PC1_HBF1=zeros(2,length(fi1));%Ê×ÏÈ¶¨ÒåÒ»¸ö2Î¬ÏòÁ¿£¬ÀïÃæÈ«²¿Îª0 after
HBF1,2x301
% for k=1:length(fi1)
%     E3_CP_PC1_HBF1(:,k)=J_HBF1(:,:,k)*E3_CP_PC1;
%1£ºÓÃ1iÃ´±íÊ¾ÐéÊý£¬¾¡Á¿²»ÓÃj£¬ÒÔÃâ»ìÏý¡£
%     %2£ºÕâ¾äÒâË¼¾ÍÊÇJhbfÇ°Á½Î¬¾ÍÊÇ[exp(-1i*fi1(k)) 0;0
exp(1i*fi1(k))]£¬µÚÈýÎ¬µÄindexÊÇk¡£
%     %Jhbf(:,:,k)ÀïÃæ(:)Ã°ºÅ´ú±íÈÎÒâ£¬²»ÏÞ¶¨index¡£
% end
% %Eout4=J_PC*Eout3;%2x301
% %Eout=zeros(2,length(fi2));%Ê×ÏÈ¶¨ÒåÒ»¸ö2Î¬ÏòÁ¿£¬ÀïÃæÈ«²¿Îª0  after
HBF2,2x2x301*2x301,µÚ¶þ¸ö301ÐèÒªÓÃk
% E3_CP_PC1_HBF1_PC3=J_PC3p*E3_CP_PC1_HBF1;
% E3_CP_PC1_HBF1_PC3_HBF2=zeros(2,length(fi2));%E4fan
% for k=1:length(fi2)
%     E3_CP_PC1_HBF1_PC3_HBF2(:,k)=J_HBF2(:,:,k)*E3_CP_PC1_HBF1_PC3(:,k);
%1£ºÓÃ1iÃ´±íÊ¾ÐéÊý£¬¾¡Á¿²»ÓÃj£¬ÒÔÃâ»ìÏý¡£
%     %2£ºÕâ¾äÒâË¼¾ÍÊÇJhbfÇ°Á½Î¬¾ÍÊÇ[exp(-1i*fi1(k)) 0;0
exp(1i*fi1(k))]£¬µÚÈýÎ¬µÄindexÊÇk¡£
%     %Jhbf(:,:,k)ÀïÃæ(:)Ã°ºÅ´ú±íÈÎÒâ£¬²»ÏÞ¶¨index¡£
% end
%
% E3_CP_PC1_HBF1_PC3_HBF2_PC2=J_PC2p*E3_CP_PC1_HBF1_PC3_HBF2;
%
% %E4·´ ·Öxy
% E4outx=E3_CP_PC1_HBF1_PC3_HBF2_PC2(1,:);
% E4outy=E3_CP_PC1_HBF1_PC3_HBF2_PC2(2,:);
% P4out=abs((E4outx.^2+E4outy.^2));%Pout
×î°óµÃµ½E2µÄÊä³öÄÜÁ¿dBÖµ£¬ÔÚ²¨³¤·¶Î§ÄÚÑ¡ÔñÂË²¨
%
% %E4!E4!E4!E4!
% E4_CP=1i*sqrt(k_cr)*Ein1;
% E4_CP_PC2=J_PC2n*E4_CP;% 2x1
%
% E4_CP_PC2_HBF2=zeros(2,length(fi1));%Ê×ÏÈ¶¨ÒåÒ»¸ö2Î¬ÏòÁ¿£¬ÀïÃæÈ«²¿Îª0 after
HBF1,2x301
% for k=1:length(fi1)
%     E4_CP_PC2_HBF2(:,k)=J_HBF2(:,:,k)*E4_CP_PC2;
%1£ºÓÃ1iÃ´±íÊ¾ÐéÊý£¬¾¡Á¿²»ÓÃj£¬ÒÔÃâ»ìÏý¡£
%     %2£ºÕâ¾äÒâË¼¾ÍÊÇJhbfÇ°Á½Î¬¾ÍÊÇ[exp(-1i*fi1(k)) 0;0
exp(1i*fi1(k))]£¬µÚÈýÎ¬µÄindexÊÇk¡£
%     %Jhbf(:,:,k)ÀïÃæ(:)Ã°ºÅ´ú±íÈÎÒâ£¬²»ÏÞ¶¨index¡£
% end
% %Eout4=J_PC*Eout3;%2x301
% %Eout=zeros(2,length(fi2));%Ê×ÏÈ¶¨ÒåÒ»¸ö2Î¬ÏòÁ¿£¬ÀïÃæÈ«²¿Îª0  after
HBF2,2x2x301*2x301,µÚ¶þ¸ö301ÐèÒªÓÃk
% E4_CP_PC2_HBF2_PC3=J_PC3n*E4_CP_PC2_HBF2;
% E4_CP_PC2_HBF2_PC3_HBF1=zeros(2,length(fi2));%E4fan
% for k=1:length(fi2)
%     E4_CP_PC2_HBF2_PC3_HBF1(:,k)=J_HBF1(:,:,k)*E4_CP_PC2_HBF2_PC3(:,k);
%1£ºÓÃ1iÃ´±íÊ¾ÐéÊý£¬¾¡Á¿²»ÓÃj£¬ÒÔÃâ»ìÏý¡£
%     %2£ºÕâ¾äÒâË¼¾ÍÊÇJhbfÇ°Á½Î¬¾ÍÊÇ[exp(-1i*fi1(k)) 0;0
exp(1i*fi1(k))]£¬µÚÈýÎ¬µÄindexÊÇk¡£
%     %Jhbf(:,:,k)ÀïÃæ(:)Ã°ºÅ´ú±íÈÎÒâ£¬²»ÏÞ¶¨index¡£
% end
%
```

```
% E4_CP_PC2_HBF1_PC3_HBF1_PC1=J_PC1n*E4_CP_PC2_HBF2_PC3_HBF1;
%
% %E3·´ ·Öxy
% E3outx=E4_CP_PC2_HBF1_PC3_HBF1_PC1(1,:);
% E3outy=E4_CP_PC2_HBF1_PC3_HBF1_PC1(2,:);
% P3out=abs((E3outx.^2+E3outy.^2));%Pout
×î°óµÃµ½E2µÄÊä³öÄÜÁ¿dBÖµ£¬ÔÚ²¨³¤·¶Î§ÄÚÑ¡ÔñÂË²¨


%final coupling

%Eoutx=1i*sqrt(k_cr)*E3outx+sqrt(1-k_cr)*E4outx;
%Eouty=1i*sqrt(k_cr)*E3outy+sqrt(1-k_cr)*E4outy;
%Pout3=(abs(Eoutx)).^2+(abs(Eouty)).^2;

%plot(wa,Pout3);
%2
%Erightx=[E3outx;E4outx];
%Erighty=[E3outy;E4outy];
%Eleftx=J_CP*Erightx;
%Eleftxx=Eleftx(2,:);
%Elefty=J_CP*Erighty;
%Eleftyy=Elefty(2,:);
%Etest=1i*sqrt(k_cr)*E4_CP_PC2_HBF2_PC3_HBF1_PC1+sqrt(1-
k_cr)*E3_CP_PC1_HBF1_PC3_HBF2_PC2;
%Etestx=Etest(1,:);
%Etesty=Etest(2,:);
%Ptest=abs((Etestx.^2+Etesty.^2));

%P2out=abs((Eleftxx.^2+Eleftyy.^2));



%T1=(1-2*k)^2+4*k*(1-k)*sin(Q1)*sin(Q1).*cos(fi1).*cos(fi1);
%T2=(cos(fi1+fi2).*cos(Q2).*sin(Q1)+sin(Q1).*cos(Q2).*cos(fi1-fi2)).^2;  %
Õâ¸öT2ÊÇÓ¦¸ÃµÃµ½µÄ½á¹û£¬ÎÒÏëÓÃ¾ØÕóµÄ·½Ê½³Ë³öÀ´£¬ÒòÎªÐèÒª¸Ä±äÀïÃæµÄ²ÎÊý,no k_cr?
%LL2=10*log10(T2);

%LG3out=10*log10(P3out);
%LG4out=10*log10(P4out);

%LG2out=10*log10(Pout3);
%LGtest=10*log10(Ptest);
%figure;
%plot(wa,LL2);
%figure;
%plot(wa,LG2out);
```